

University of Kentucky

UKnowledge

Theses and Dissertations--Plant Pathology

Plant Pathology


2021

NEGATIVE REGULATORY FACTORS IN TOMBUSVIRUS REPLICATION: KNOWN PROTEINS, NOVEL ROLES

Paulina Alatríste González

University of Kentucky, palatris@gmail.com

Author ORCID Identifier:

 <https://orcid.org/0000-0003-1525-791X>

Digital Object Identifier: <https://doi.org/10.13023/etd.2021.080>

[Right click to open a feedback form in a new tab to let us know how this document benefits you.](#)

Recommended Citation

Alatríste González, Paulina, "NEGATIVE REGULATORY FACTORS IN TOMBUSVIRUS REPLICATION: KNOWN PROTEINS, NOVEL ROLES" (2021). *Theses and Dissertations--Plant Pathology*. 32.
https://uknowledge.uky.edu/plantpath_etds/32

This Doctoral Dissertation is brought to you for free and open access by the Plant Pathology at UKnowledge. It has been accepted for inclusion in Theses and Dissertations--Plant Pathology by an authorized administrator of UKnowledge. For more information, please contact UKnowledge@lsv.uky.edu.

STUDENT AGREEMENT:

I represent that my thesis or dissertation and abstract are my original work. Proper attribution has been given to all outside sources. I understand that I am solely responsible for obtaining any needed copyright permissions. I have obtained needed written permission statement(s) from the owner(s) of each third-party copyrighted matter to be included in my work, allowing electronic distribution (if such use is not permitted by the fair use doctrine) which will be submitted to UKnowledge as Additional File.

I hereby grant to The University of Kentucky and its agents the irrevocable, non-exclusive, and royalty-free license to archive and make accessible my work in whole or in part in all forms of media, now or hereafter known. I agree that the document mentioned above may be made available immediately for worldwide access unless an embargo applies.

I retain all other ownership rights to the copyright of my work. I also retain the right to use in future works (such as articles or books) all or part of my work. I understand that I am free to register the copyright to my work.

REVIEW, APPROVAL AND ACCEPTANCE

The document mentioned above has been reviewed and accepted by the student's advisor, on behalf of the advisory committee, and by the Director of Graduate Studies (DGS), on behalf of the program; we verify that this is the final, approved version of the student's thesis including all changes required by the advisory committee. The undersigned agree to abide by the statements above.

Paulina Alariste González, Student

Dr. Peter D. Nagy, Major Professor

Dr. Rick Bennett, Director of Graduate Studies

NEGATIVE REGULATORY FACTORS IN TOMBUSVIRUS REPLICATION:
KNOWN PROTEINS, NOVEL ROLES

DISSERTATION

A dissertation submitted in partial fulfillment of the
requirements for the degree of Doctor of Philosophy in the
College of Agriculture, Food and Environment
at the University of Kentucky

By
Paulina Alatraste González
Lexington, Kentucky
Director: Dr. Peter D. Nagy, Professor of Plant Pathology
Lexington, Kentucky
2021

Copyright © Paulina Alatraste González 2021
<https://orcid.org/0000-0003-1525-791X>

ABSTRACT OF DISSERTATION

NEGATIVE REGULATORY FACTORS IN TOMBUSVIRUS REPLICATION: KNOWN PROTEINS, NOVEL ROLES

Although host cells are a rather rich source for co-opted host factors, lipids and metabolites, positive stranded RNA viruses vastly rewire cellular pathways and remodel cellular membranes to support viral replication. To accomplish such major changes, these viruses depend on the availability of different host factors and the ability to readily assemble viral replication organelles (VROs). Genome-wide screens and proteomics approaches with Tomato Bushy Stunt Virus (TBSV) in a yeast model host indicated that tombusviruses rely on the cellular cytoskeleton to reorganize the cellular environment of their hosts. Using temperature-sensitive (ts) mutants of beta and gamma-tubulin proteins and pharmacological inhibitors, I demonstrated that the dynamic microtubular network restricts TBSV replication.

Moreover, changes in the structure of microtubules greatly interfere with the actin structure as well, leading to problems in the subversion of selected host factors into replicase complexes and the enrichment of sterols at replication sites. In addition to the efficient recruitment of co-opted host factors, lipids and metabolites to the sites of viral replication, tombusviruses promote the biogenesis and accumulation of host factors that facilitate the production of energy required to fuel replication.

I discovered that Centromeric Histone H3 (CENH3), an essential chromatin-associated protein, has a non-canonical role during virus replication, as a regulator of the biosynthesis of several glycolytic enzymes that are necessary to generate ATP within the viral replication compartment. This function is achieved by the binding of this protein with components of the viral replication machinery such as the RNA chaperone p33 and the viral repRNA, a function that is initially inhibitory but that is circumvented by the virus to reach optimal replication.

Altogether, the studies with the microtubule cytoskeleton and CENH3 revealed an emerging picture for (+)RNA tombusviruses, suggesting that the extensive rewiring of metabolic pathways and remodeling of cellular membranes that support viral replication, requires the activities of particular kinds of cell-intrinsic restriction factors (CIRFs). These types of factors, which I called negative regulatory CIRFs, have an intrinsic inhibitory

function but are exploited by the virus to achieve robust replication at the expense of certain viral resources.

KEYWORDS: Positive strand RNA virus, microtubule cytoskeleton, CENH3, host cell rewiring, negative regulatory CIRFs.

Paulina Alatríste González

May 6, 2021

Date

NEGATIVE REGULATORY FACTORS IN TOMBUSVIRUS REPLICATION:
KNOWN PROTEINS, NOVEL ROLES

By

Paulina Alariste González

Peter D. Nagy, Ph.D.

Director of Dissertation

Rick Bennett, Ph.D.

Director of Graduate Studies

May 6, 2021

Date

DEDICATION

*To María Luisa, Román and Diana,
for believing in me before I believed in myself.*

ACKNOWLEDGEMENTS

The following dissertation would not have been possible without the help and support of many individuals. I would like to begin by expressing my deep gratitude to my advisor Dr. Peter Nagy, for giving me the opportunity to do my Ph.D. studies in his lab at the University of Kentucky, Department of Plant Pathology. His guidance, motivation, insights and advice were really valuable and allowed me to grow as a person and scientist.

I am extremely grateful to my doctoral committee members, Dr. Lisa Vaillancourt and Dr. Becky Dutch for their valuable and constructive suggestions during the planning and development of this research work. Thank you also for being such a great inspiration and remarkable women scientists. My deepest appreciation and sincere thanks to another member of my doctoral committee, Dr. Michael Goodin, for all the words of encouragement, laughs, coffee and lessons along the way. I celebrate his life with this work, may he rest easy in grace and love. Thank you to my outside examiner Dr. Jan Smalle.

I would like to express my great appreciation for past and current members of the Nagy lab, thank you for all your assistance and the fun we had working together. Special thanks to Dr. Judit Pogany and Dr. Ching-Kai Chuang for their constant encouragement and their sincere friendship.

I gratefully acknowledge the continuous help and guidance of the Department Chair Dr. Christopher Schardl, Director of Graduate Studies Dr. Rick Bennet and the Department of Plant Pathology Office Staff.

The completion of my Ph.D studies would not have been possible without the support, nurturing and love of Jannine Baker, Craig Locke and Melissa Molho. Thank you for being my home away from home. Many thanks to my dear friend Fabian Calvario, for being a ray of sunshine even on my darkest days.

I cannot begin to express my thanks to Wyatt Sarbacker, for being the one who supports me, loves me, helps me, listens to everything I say and does not judge me. My true best friend.

Finally, my deepest love and gratitude to my mom, dad and sister for being the biggest source of inspiration, encouragement and unconditional love. Everything I am you helped me to be. This is for you.

TABLE OF CONTENTS

ACKNOWLEDGEMENTS	iii
LIST OF TABLES	vii
LIST OF FIGURES	viii
Chapter 1. INTRODUCTION.....	1
1.1 Tombusviruses	1
1.2 Remodeling the host cell to fit viral functions	3
1.3 Viral replication is regulated by cell-intrinsic restriction factors	6
Chapter 2. INTEGRATED NETWORK ANALYSIS OF TOMBUSVIRUS HOST FACTORS INTERACTIONS	8
2.1 Introduction.....	8
2.2 Systematic identification of host factors via high-throughput genome-wide screens in yeast	10
2.3 Protein-protein interaction networks for the analysis of high-throughput interaction data.....	11
2.4 PPI networks reveal hubs among TBSV antiviral restriction factors.	13
2.5 Expanding the TBSV host factor PPI network analysis to understand cellular remodeling during infection.....	14
2.6 Discussion.....	17
Chapter 3. TUBULIN MUTANTS REVEAL AN INHIBITORY ROLE FOR THE DYNAMIC MICROTUBULE NETWORK IN TOMBUSVIRUS REPLICATION	37
3.1 Introduction.....	37
3.2 Materials and Methods.....	40
3.3 Results.....	52
3.4 Discussion.....	63
Chapter 4. EPIGENETIC REPROGRAMMING OF THE HOST BY RECRUITMENT OF THE CENTROMERIC HISTONE 3 BY A CYTOSOLIC RNA VIRUS.....	97
4.1 Introduction.....	97
4.2 Materials and Methods.....	100

4.3 Results.....	115
4.4 Discussion.....	126
Chapter 5. CONCLUSIONS AND PERSPECTIVES	155
5.1 Conclusions.....	155
5.2 Perspectives.....	159
REFERENCES	165
VITA.....	184

LIST OF TABLES

Table 2.1 List of yeast CIRFs identified for tombusviruses based on high throughput yeast screens.....	20
Table 2.2 List of genes used for the second network analysis.....	24
Table 3.1 List of primers used in this study.....	67
Table 3.2 Co-purified host proteins with p33 from tub2 ^{ts} yeast	68
Table 4.1 List of primers used in this study.....	130

LIST OF FIGURES

Figure 2.1. Physical and genetic protein interaction network of CIRFs and pro-viral host factors in yeast.	30
Figure 2.2. Physical and genetic protein interaction network including XRN1, ACT1, and CSE4 CIRFs.....	32
Figure 2.3. Physical and genetic protein interaction network of characterized host factors affecting TBSV replication.	34
Figure 2.4. Physical protein-protein interaction network of characterized host factors affecting TBSV replication.	36
Figure 3.1. Temperature-sensitive mutations of beta- and gamma-tubulins increase TBSV repRNA accumulation in yeast.	70
Figure 3.2. Microtubules restrict tombusvirus repRNA replication when it takes place at different subcellular locations in yeast.	72
Figure 3.3. Pharmacological inhibitors of microtubules enhance TBSV RNA accumulation in yeast and <i>N. benthamiana</i> protoplasts.....	74
Fig 3.4 A beta-tubulin mutation affects viral RNA synthesis in yeast and in vitro.	76
Figure 3.5. Microtubules localize at the vicinity of tombusvirus replication sites in yeast.	78
Figure 3.6. Microtubules localize at the vicinity of tombusvirus replication sites in plant.	80
Figure 3.7. The tub2 ^{ts} mutant facilitates the enrichment of sterols at the sites of tombusvirus replication in yeast.	82
Figure 3.8. Rapid interaction between p33 replication protein and Scs2p VAP protein in tub2 ^{ts} yeast.	84
Figure 3.9. Enhanced co-purification of cellular ORP protein with the tombusvirus p33 replication protein from tub2 ^{ts} yeast.	86
Figure 3.10. The effect of Nocodazole on TBSV repRNA replication in the absence of selected ORPs in yeast.	88
Figure 3.11. Reduced co-purification of cellular restriction factors with the tombusvirus p33 replication protein from tub2 ^{ts} yeast.	90
Figure 3.12. Knock down of Tub5 or TubG1 interferes the formation of actin filaments and cables in plants.	92
Figure 3.13. The microtubule cytoskeleton is important for the biogenesis of tombusvirus VROs.....	94
Figure 3.14. Silencing of Tub5 and TubG1 in <i>N.benthamiana</i> plants reduces TBSV RNA accumulation.	96
Figure 4.1 The essential centromeric histone variant CenH3 is a restriction factor of	

tombusvirus replication in yeast and plants.	134
Figure 4.2 Re-distribution of nuclear CenH3 to the sites of viral replication in plants..	136
Figure 4.3 Re-distribution of nuclear CenH3 to the sites of viral replication in yeast. ..	138
Figure 4.4 CenH3 has an RNA chaperone activity and inhibits tombusvirus replication in vitro.	140
Figure 4.5 The highly conserved HFD of Cse4p is involved in viral RNA binding and RNA chaperone activity.	142
Figure 4.6 CenH3 interacts with TBSV p33 replication protein.	144
Figure 4.7 TBSV reprograms host gene expression via CenH3 in yeasts and plants.	146
Figure 4.8 Reprogramming of glycolytic and fermentation enzymes expression by TBSV via CenH3 affects ATP accumulation within VROs in plants.....	148
Figure 4.9 Reprogramming of glycolytic and fermentation enzymes expression by TBSV via CenH3 affects ATP accumulation within VROs in yeast.	150
Figure 4.10 A portion of the viral (+)RNA distributes into the nucleus of plant cells. ..	152
Figure 4.11 RepRNA-hp is replication competent in the presence of p33 and p92 ^{pol}	154

Chapter 1

INTRODUCTION

1.1 Tombusviruses

As the prototype genus in the large Tombusviridae family [1], tombusviruses are among the most deeply studied plus-stranded ((+)RNA) plant viruses [2]. As with any other viruses, they rely extensively on the host cells during the infection process. In order to replicate, tombusviruses reprogram the host cell metabolism to support the infection and escape or suppress host defense mechanisms. Virus-infected cells are subject to a series of major changes during infection [3] and tombusviruses achieve this by subverting many host-proteins involved in different cellular pathways such as RNA transcription, lipid synthesis, protein modification, cell cycle, vesicle-mediated transport and translation [3-5].

Tomato Bushy Stunt Virus (TBSV), the type species of the tombusvirus genus has a single stranded messenger-sensed (+)RNA genome that is approximately 4.8 kb in length [2] and encodes five open reading frames (ORFs) [1]. The 5'- proximally encoded ORFs, p33 and p92, are translated directly from the genome and both are essential for viral RNA replication [6, 7]. The p33 sequence overlaps with the N-terminus of p92 and has RNA chaperone activity involved in the recruiting of the tombusvirus (+)RNA to the cytosolic surface of peroxisomal membranes [8-11]. p92, is the readthrough product of p33 ORF and acts as an RNA-dependent RNA polymerase (RdRp). In addition, the binding of p92 with

p33 helps in the assembly of the membrane-bound functional viral replicase complex (VRC) [9, 12-15].

Expression of the 3'-proximal ORFs (i.e., p41, p22, and p19) requires transcription of additional viral mRNAs, termed subgenomic (sg) mRNAs [16]. sg mRNA2 (the shortest) is produced first and templates the translation of overlapping ORFs p22 and p19 [17]. p22 is required for cell-to-cell movement within the plant whereas p19 is a suppressor of virus-induced gene silencing [18-20]. The larger sg mRNA1 is transcribed later in the infection and directs translation of p41, the coat protein (CP) [21] .

Tombusviruses are commonly associated with subviral molecules derived entirely from the genomic RNA and are known as defective interfering (DI) RNAs [1]. They are usually composed of three or four short noncontiguous segments and do not code for proteins, but they can be easily amplified when viral replication proteins are provided in trans. DI RNAs have become a major tool for the study of tombusvirus replication [1, 13, 15, 22].

Development of yeast as a surrogate host for tombusviruses makes them excellent model viruses for the study of fundamental aspects of (+)RNA virus replication and recombination. TBSV essential replicase proteins are needed for studies in yeast. The RNA chaperone p33, the RNA dependent RNA polymerase p92, and a viral replicon RNA (repRNA) are all expressed from plasmids to launch viral replication [23].

A good number of genome and proteome-wide screens, using yeast strain libraries, protein microarrays or mass spectrometry-based proteomics, have helped to identify host genes affecting TBSV replication and influencing viral RNA recombination [4, 24-30].

Moreover, the development of powerful cell-free *in vitro* assays based on yeast extracts has given many new insights into the viral replication process [22, 31, 32].

1.2 Remodeling the host cell to fit viral functions

The viral infection process of any virus comprises a major re-wiring of cellular pathways and remodeling of the cellular environment that renders the cell suitable for replication [33]. For instance, in spite of the modest genome framework of most plant viruses, the interaction with their hosts is a rather complex and dynamic process, involving numerous interactions among viral-coded and host-coded proteins, proteins and viral nucleic acids, and proteins and host membranes (lipids) [5]. Dissecting and explaining the types of interactions between viruses and their hosts is at the frontier of virus research and over the past decade there has been an increase in the number of studies about the interplay between plant viruses and their hosts.

Perhaps one of the most prominent examples of major cellular rearrangements induced by plant viruses is the formation of specialized membranous replication organelles. These “replication factories” are generated from a variety of endomembranes, mitochondria, chloroplasts, endoplasmic reticulum (ER), peroxisomes and vacuoles. The membrane modifications generally involve the formation of spherules, vesicles, and/or multivesicular bodies, which communicate with the surrounding cytosol through a narrow channel [34, 35]. In the case of TBSV, replication occurs within large membranous viral replication organelles (VROs), which contain many vesicle-like spherule structures formed

by the invagination of cellular membranes. These invaginations are ~60-70 nm and have narrow openings towards the cytosol [34-37].

The assembly of the VROs is orchestrated by the virus accessory replication proteins (i.e. p33 for TBSV) but its biogenesis and function also depend on the subversion of numerous cellular proteins and metabolic pathways [5, 36, 38, 39]. Moreover, there is evidence supporting the idea that specific lipid composition is crucial for the establishment of VROs and that viruses use diverse strategies to create the optimal structure [40, 41]. Within this concept, membrane contact sites (MCS) have been recognized as host cellular structures used by plant viruses for replication and movement, possibly having a role in linking these two processes or involved in other crucial steps of plant virus infection [42]. The role of tombusvirus-induced membrane contact sites (MCS) for the supply of lipids required for the formation and maintenance of VROs has been studied in detail [43-47] and has provided insights of the importance of lipid composition in these compartments.

Remodeling of host membranes into specialized structures is a conserved mechanism for all (+)RNA viruses including human viruses such as Zika virus, SARS-coronavirus, hepatitis C virus (HCV), dengue virus and poliovirus [35, 48]. The formation and properties of animal virus-induced membrane alterations have many similarities with what is observed for plant viruses. This illustrates the universal character of some essential viral replication processes.

Another example of virus induced tailoring of the cell is the hijacking of the cytoskeleton network. Actin filaments and microtubules are two cytoskeleton components that are important for the maintenance of proper cell functionality and are often disrupted during viral infections [49-51]. Viruses induce rearrangements of the cytoskeletal

architecture and dynamics to either utilize them as tracks or to prevent them from becoming barriers for replication. Virus particles also co-opt motor proteins for the movement of viral components and host factors to different subcellular sites [52-54]. Because microfilaments and microtubules have a role in the positioning of the endomembrane system and the movement of many cellular constituents [49], viral induced reshaping of the cytoskeleton network often comprises a repositioning of organelles and membranes as well as a disruption on the trafficking of host pro-viral and antiviral factors. Simultaneously, the roles of actin filaments and microtubules have been characterized for a relatively small number of animal virus families during several steps of the infection process including binding and cell surface surfing [55, 56], internalization [57, 58], intracellular and cell-to-cell movement [59-62], genome replication [63, 64] and egress [65-67].

Disruption of the actin network dynamics, which normally fluctuate between rapid assembly and disassembly, facilitates TBSV VRC formation due to an efficient recruitment of sterols into the replication compartments. This is due to the inhibition of the cofilin actin depolymerization factor through the direct binding of p33 replication protein. The p33-cofilin interaction blocks the cofilin/ADF-driven severing of existing actin filaments, stabilizing them and prohibiting the emergence of new actin filaments [68]. Actin filaments have also been seen running throughout TBSV and Carnation Italian ringspot virus (CIRV) large VROs in plants. It has been demonstrated that the actin network is an important cellular component where the replicase preassembly and VRC assembly processes can occur efficiently [68, 69].

Previous screenings with a library of temperature-sensitive yeast mutants [25] identified β -tubulin 2 (TUB2) and γ -tubulin 4 (TUB4) as factors that affect TBSV

replication in yeast. Since microtubules play an important role in the formation of MCS and intracellular trafficking a more in-depth study was performed to understand its role during tombusvirus replication and will be discussed in Chapter 3.

1.3 Viral replication is regulated by cell-intrinsic restriction factors

The cell deploys several antiviral mechanisms to limit viral infections creating a constant evolutionary battle with viruses. The result of this battle has been the development of several layers of host defense responses and the emergence of novel suppressor mechanisms/effectors by viruses [70].

Among the different antiviral strategies used against plant viruses, intrinsic antiviral immunity (an example of innate resistance) stands as a first line of defense. This immunity is conferred by restriction factors that are mostly preexistent in certain cell types, although these factors can be further induced by viral infection. Cell-intrinsic restriction factors (CIRFs) recognize specific viral components and block many stages of the (+)RNA virus life cycle, such as translation, viral replication organelle [62] assembly, recruitment of the viral RNA and replication [71-74].

The extensive genome-wide screens based on yeast libraries performed with TBSV has allowed the recognition of ~73 yeast genes acting as CIRFs against viral infection. Identified CIRFs against tombusviruses can be grouped into several different known cellular functions and subcellular localizations, which indicates that the whole plant cell responds to viral infection [75].

Notwithstanding that several of the characterized CIRFs act directly against TBSV, some of them act more as negative regulators of replication, specifically when tombusviruses are able to circumvent their inhibitory function and make use of them in a way that benefits its replication. Such is the case of the cellular actin depolymerizing factor cofilin. This host factor disassembles the actin filaments, balancing the dynamic nature of the actin network [76-78]. Overexpression of cofilin suppresses TBSV replication. The inhibition comes from two different mechanisms. First, the direct interaction between p33 and cofilin could be partially sequestering these proteins and restricting its involvement in VRC formation and the other steps of replication. Second, the dynamic actin rearrangement induced by cofilin also seems to inhibit the efficient recruitment of host factors to the VRCs and consequently overall replication [68]. But, as discussed above, it has also been demonstrated that TBSV p33-cofilin binding blocks the severing of actin filaments which stabilizes the actin network and facilitates the recruitment of other host factors [68]. Thus, actin structure, specifically the polymerization of new filaments, is a major restriction factor of replication but TBSV is able to modulate this process and obstruct the formation of new filaments which in turn benefits replication.

Another example of a CIRF whose inhibitory role is circumvented by TBSV is the Centromeric Histone H3 (CENH3). The novel antiviral role of this protein and its involvement in the epigenetic reprogramming of the host during TBSV replication will be discussed more deeply in Chapter 4.

Chapter 2

INTEGRATED NETWORK ANALYSIS OF TOMBUSVIRUS HOST FACTORS INTERACTIONS

(Part of this chapter was published in *Frontiers in Plant Science Journal*, in August 2014, Vol. 5, doi: 10.3389/fpls.2014.00383)

2.1 Introduction

These days, it is a well-established idea that, in spite of the modest genome framework of most plant viruses, the interaction with their hosts is a rather complex and dynamic process, involving numerous interactions among viral-coded and host-coded proteins, proteins and viral nucleic acids, and proteins and host membranes (lipids) [5]. Hence, it is not surprising that dissecting and explaining the types of interactions between viruses and their hosts is at the frontier of virus research.

In the last decade there has been an explosion in our knowledge about the interplay between plant viruses and their hosts at a molecular level, particularly for tombusviruses. (+)RNA plant tombusviruses such as Tomato bushy stunt virus (TBSV) and Carnation Italian ringspot virus emerged as useful model systems for the study of virus-host interactions [2]. These viruses have a monopartite (+)RNA genome that replicate in high levels which facilitates the purification of viral proteins and RNA/host protein complexes from infected cells. In addition, similar to other plant and animal (+)RNA viruses, TBSV and CIRV replication occurs within large viral replication organelles (VROs) where vesicle-like spherule structures are formed by the invagination of cellular membranes [9,

37]. Despite their simple genome organization and a limited coding capacity, tombusviruses not only exploit their hosts by remodeling intracellular membranes but also by disrupting metabolic pathways, recruiting host factors and escaping host antiviral responses.

One of the most advantageous features of using tombusviruses as model systems is the development of *Saccharomyces cerevisiae* as a surrogate host, which enables high-throughput studies to identify cellular factors involved in tombusvirus replication [79]. Yeast emerged as a valuable tool and is especially useful to define the roles of viral proteins and host factors during the infection process of some viruses [3, 23, 80, 81]. This is due to the small size of its genome (~6,000 genes), reduced level of redundancy, lack of introns in the majority of its genes and the availability of different toolboxes and libraries for the controlled expression of selected genes. Furthermore, around 75% of yeast genes have characterized functions and ~60% of its genes have orthologs in humans and/or in plants, making it the preferable host for genome-wide studies and suitable for the validation of identified host factors as well as the dissection of their functions. It is clear now that host factors are involved in all steps of (+)RNA virus replication from translation to viral movement and egress. Therefore, this complex interplay between TBSV and conserved cellular factors (unlikely to be unique), can influence future studies with many (+)RNA viruses. These studies are expected to uncover comparable interactions with co-opted cellular proteins and lipids that are required for (+)RNA virus replication.

The list of host factors that affect tombusvirus replication has grown considerably in the past few years and, although there have been great efforts to characterize several of these factors, we need different approaches to analyze the current data. This chapter focuses

on the interactions between identified host factors and how integrated network analysis can benefit our understanding of viral replication in the context of host cell biology. The findings made through this type of analysis could help guide the virus-host interactions research by providing new insights of the host cell systems.

2.2 Systematic identification of host factors via high-throughput genome-wide screens in yeast

The most extensive genome-wide screens based on yeast libraries have been performed with TBSV. Collections of yeast strains or libraries such as the yTHC Yeast tet promoter Hughes Collection (essential gene knockdown library), the protein over-expression library, YKO gene deletion library and the temperature-sensitive library of essential genes were used for high-throughput screenings of host factors involved in TBSV replication and recombination [24, 25, 27-30, 69]. The result of these screenings was ~350 identified host proteins that could affect TBSV replication.

In addition to the gene expression screenings, a yeast membrane-based two-hybrid assay (MYTH) with yeast cDNA libraries and a global proteomic-based screen with a yeast protein array facilitated the identification of different sets of host factors interacting with the viral replication proteins p33 and p92^{pol} and the viral RNA [82-84]. In combination, the proteomic-based and genomic-based screens led to the identification of ~500 yeast genes potentially involved in tombusvirus replication.

A similar approach with yeast-based genome-wide screens was used to study host factors that could affect the unrelated Brome mosaic virus (BMV). BMV belongs to the alphavirus supergroups whereas TBSV is a member of the flavivirus supergroup. The screens were conducted using the yTHC [85] and YKO libraries [26], a GFP-tagged protein expression collection [86] and a proteomic approach with purified yeast proteins [84, 87]. Altogether, these high-throughput screens and some additional low-throughput ones enabled the identification of ~150 genes affecting BMV replication in yeast. Interestingly, a comparison between the set of host genes identified for BMV with the set identified for TBSV revealed just a few overlaps. This highlights how the versatility of (+)RNA virus genome organization could influence the types of virus-host interactions established.

Recently, plant specific host factors affecting TBSV replication were identified in a yeast MYTH screening using a library of *Arabidopsis thaliana* cDNA as well as plant homologs of some of the genes found in previous screenings (Molho, M. et.al unpublished). Overall, the tombusvirus-yeast system is one of the best-characterized models in virus-host interaction. From the ~500 host factors that have been found to influence TBSV replication or recombination, ~100 of them have been extensively characterized [4, 5, 39, 88, 89], leading to a better understanding of the types of cellular processes and resources that the virus utilizes for its replication.

2.3 Protein-protein interaction networks for the analysis of high-throughput interaction data

The advent of technological advances in proteomics as well as decades of research in cell and molecular biology, biochemistry and structural biology have resulted in a remarkable

accumulation of data on the function, molecular properties and interactions of individual proteins. This is particularly true for the budding yeast *S. cerevisiae* where a myriad of comprehensive studies has been performed [90-93].

Because the amount of “omics” data increases considerably every year, the strategies to obtain systems-level interpretations on these datasets have become an active area of research. Biological network analysis is a powerful tool to analyze the data generated for a single or multiple organism(s), providing a mostly unbiased framework. Because protein interactions are fundamental for orchestrating essentially all biological processes, protein-protein interaction (PPIs) networks are of particular interest amid the different types of molecular networks [94, 95]. PPI networks simplify the visualization of the complex set of interactions that takes place inside a cell. They usually consist of graphs with nodes that represent proteins and edges indicating interactions between two connecting proteins.

A PPI network analysis starts typically with the identification of a set of genes or proteins of interest and is followed by the search and retrieval of binary interactions between the input genes/proteins from a curated PPI database. A network can then be assembled based on the interactions and analyzed [96]. Two complementary approaches commonly used for the analysis of PPI networks are topology analysis, which focuses on the whole network constitution to identify important nodes (hubs) and module analysis, that separates a dense network into small tightly connected modules in order to recognize the more active ones (active “hotspots”) [96-98] .

2.4 PPI networks reveal hubs among TBSV antiviral restriction factors.

The data generated from the yeast-based genome-wide screenings for TBSV resulted in a suitable list of proteins of interest that could be used to perform a network analysis. In an initial approach, aimed to gain insights into the function of antiviral factors, I used a set of ~73 previously identified cell-intrinsic restriction factors (CIRFs) (Table 2.1) and other previously identified and characterized pro-viral host factors to assemble protein networks. Additionally, three other datasets used in this initial study were (i) the viral RNA/replication proteins-host protein interactions (based on a yeast protein array) [82, 84] (ii) mass spectrometry analysis of the viral replicase [99] and (iii) MYTH two-hybrid assay with yeast cDNA libraries [83].

Network assembly was performed as follows: the function and the systematic name of each gene/protein in Figure 2.1-2.2 and Table 2.1 were obtained from the *Saccharomyces* genome database (SGD) [100], in order to find interactions among the positive pro-viral factors and the inhibitory factors obtained from previous genome-wide screens with TBSV. Results were deposited in a plain text format file that was used afterwards as input to a program written in the R programming language (R Core Team, 2014) that generates a PDF file with a network depicting the found interactions. Parameters such as type of interaction (physical, genetic or both) and confidence (number of experiments that support the interaction) were considered in the program.

The protein networks (Figure 2.1-2.2) obtained in this initial study, published in [75], revealed several interesting observations. First, three network hubs (yeast proteins with the highest connectivity in the network map) were identified and included the well-

characterized Xrn1p 5'–3' exoribonuclease, and the Act1p actin protein and Cse4p centromere protein which are less-characterized as anti-TBSV proteins (at the time of publication) (Figure 2.1, marked with arrows and Figure 2.2). These possible key hub proteins with high connectivity might target important viral components or host factors to inhibit TBSV replication. The PPI network also revealed an interplay between the pro-viral Hsp70 cellular chaperone and antiviral co-chaperones (Figure 2.1), as well as the ribosomal or ribosome associated factors whose antiviral activities have not yet been characterized in further details. Interestingly, the protein network map excluded 8 CIRFs. These factors might work as single antiviral factors, or their interactome was not yet well characterized, thus leading to their omission from the protein network map (Figure 2.1).

2.5 Expanding the TBSV host factor PPI network analysis to understand cellular remodeling during infection

Since the initial network analysis with identified host factors involved in TBSV replication and recombination, there have been efforts to characterize the functions of more host factors and a need emerged to have a broader picture of the systematic changes that the virus induces in the infected cells. The idea is that analyzing the interactions between the host factors will give us a different perspective of the types of processes that the virus hijacks and re-purposes as well as how these same processes overlap and connect with each other to allow the robust replication that we observe for TBSV. Essentially, proteins function in concert with other proteins and are part of multiprotein complexes or members of particular cellular pathways. So, taking advantage of the available PPI databases and

information available, I performed a network analysis with a different set of proteins to include previously identified and well-characterized host factors.

The new analysis included 107 genes (Table 2.2) which function during TBSV replication. They have been explored in detail and, in most cases, published. Similar to the previous network analysis for CIRFs, the workflow used was as follows: the function and the systematic name of each gene/protein in Figure 2.3, Figure 2.4 and Table 2.2 were obtained from the SGD database [100]. Then each gene/protein was analyzed using the BioGRID interaction database [101] in order to find interactions among each of the host factors (genetic, physical or both). This time, results were deposited in an Excel file that was used afterwards as input to the Cytoscape software platform [102] for visualization of the network.

When using all of the 107 proteins and all of the types of interactions found, the resulting network has 941 edges representing 941 unique interactions between the host factors used in the analysis (Figure 2.3). Genetic interactions were included in this network because they identify functional relationships between genes that do not necessarily arise from the direct physical interaction of their protein products. Genetic interactions occur when mutations in two or more genes combine and the outcome is an unexpected phenotype. These types of interactions can be negative, i.e., when two combined mutations (not lethal individually) produce cell death, or positive when mutations in the genes produce a phenotype that is not as severe as expected [103].

The network revealed six modules that correspond with the identified general function of the proteins during TBSV replication. The six groups in decreasing number of nodes are: i) VRO and viral replication complex (VRC) biogenesis (23 proteins), ii) lipid

metabolism and MCS formation (22 proteins), iii) antiviral function (19 proteins), iv) endomembrane system and transport vesicles (16 proteins), v) cellular metabolism and energy (12 proteins) and vi) VRC function or activity (12 proteins). Each of the six modules connect with each of the other five modules highlighting that within the cell exists a functional correlation between all the different groups of proteins. At the same time, this also suggests that host factors are involved in more than one of the viral replication steps. For all of the modules a few internal hubs can be recognized but Act1, Rsp5, Rpn11 and Sec22 are the overall network hubs with 67, 49, 48 and 47 connections respectively. Actin is a ubiquitous, conserved cytoskeletal element critical for many cellular processes [49] so it is not surprising that this protein is the main hub in the network. E3 ubiquitin ligase Rsp5 is an antiviral factor against TBSV that interacts with several important pro-viral factors like glycolytic and fermentation pathway enzymes CDC19 and PDC5. Rpn11 is a metalloprotease subunit of the 19S regulatory particle, part of 26S proteasome lid, while Sec22 is a SNARE protein involved in anterograde and retrograde transport between the ER and Golgi. Interestingly, Act1, Rpn11 and Sec22 hub proteins are part of the same VRO and VRC biogenesis functional module.

Genetic interactions help us to understand the relationship between genotype and phenotype, but unfortunately their scope during viral replication is still not well understood. Consequently, I assembled a network whose edges represent physical interactions only (Figure 2.4). There are two remarkable differences between the physical interactions network and the one assembled with all the types of interactions. The first difference is that 11 of the 107 genes were missing from the network (Figure 2.4, bottom left). This means that on the date this analysis was performed there was no data suggesting

a physical connection between these proteins and the rest of the protein group. Second, the hubs for this network are different from those identified in the previously assembled network. Rpn11 metalloprotease became the main hub with 37 physical interactions, followed by Ssa1 chaperone with 25 and Cse4 histone variant with 20. Although they are not major hubs in the physical interactions network, Rsp5, Act1, and Sec22 kept considerable numbers of interactions, 14, 10 and 10 respectively.

Interestingly, Cse4 reappeared as a hub in this network as in our initial network analysis (Figure 2.1-2.2). This indicates that it is relevant to keep track of our analyses in order to compare them and recognize significant changes and/or similarities. By doing this we might be able to identify relevant host factors that could have been previously missed.

2.6 Discussion

Systematic genome-wide screens using yeast as a model host have allowed the identification of more than 500 host factors affecting tombusvirus replication and a significant portion of them have been mechanistically/functionally characterized to determine their roles during the infection cycle. As the number of characterized host factors increases, the paradigm should shift from the study of individual proteins to large-scale, collective studies of multiple proteins. If we think of cells as molecular machines, the behavior of the underlying system governing cellular processes is quite different from merely the sum of the interactions of its various parts.

A critical step towards unraveling the complex molecular relationships in living systems is the mapping of protein-to-protein physical interactions. Since the yeast *S.*

cerevisiae currently has one of the best characterized interactomes, utilizing all the available data and maps of identified host factors involved in TBSV replication could become a powerful tool to understand viral infection at both cellular and systems levels.

In this chapter I reviewed two distinct network analyses performed with host factors identified in yeast screenings with TBSV. In both of these studies interesting findings were observed, particularly the unexpected recognition of proteins with high connectivity in the network maps or “hubs”. For example, at the time of publication of the first analysis [75] extensive work had been performed to characterize Xrn1p 5’–3’ exoribonuclease [104] but although Act1 and Cse4 were initially classified as CIRFs, they were still not well characterized. The network analysis uncovered a different biological aspect of these proteins as interactors of multiple other host factors making them of interest for further detailed studies. Indeed, Act1, the single essential gene for actin, was characterized in the following years [25, 68] and it is now established that subversion of the actin network by TBSV is a key step for the virus to gain access to cellular resources required for virus replication.

An intriguing observation in both network analyses, was the appearance of Cse4 protein as a network hub. This protein is a Histone H3-like variant which replaces conventional H3 in the nucleosome core of centromeric chromatin [105]. It is essential for centromere identity and function [106]. It was not clear how Cse4 could act as a CIRF against viral replication but because of its distinctive canonical function and its high connectivity with other antiviral and pro-viral factors, we decided to study this protein in detail. The results of this study are summarized in Chapter 4.

The assembly of TBSV host factors PPI networks have influenced how we perceive the viral infection process and has enabled the study of unconventional host factors. This type of analysis should be performed regularly, particularly because the advent of new technologies has allowed a constant update of interactome data for several organisms. As more plant genome sequences become available and functionally characterized, the network analysis can then be made with plant genes and proteins. Also, the curation of more databases and the development of user-friendly network analysis software and tools will contribute to the automation of PPI network construction and interpretation.

Table 2.1 List of yeast CIRFs identified for tombusviruses based on high throughput yeast screens.

Name	Function	Localization	Plant ortholog
ACT1	Actin	Cytoskeleton	AT3G12110/ACT11
AFG2	60S ribosomal biogenesis	Preribosome	–
APM2*	Vesicle mediated transport	Vesicle transport	–
AQY1	Spore-specific water channel	pm	AT1G01620/PIP1C
ARP7	Chromatin remodeling, transcription regulation, DNA processing	SWI/SNF complex	–
ARP9	Chromatin remodeling, transcription regulation, DNA processing	SWI/SNF complex	–
BUD21*	Component of small ribosomal subunit	Small ribosome	–
CCA1	Nucleotidyltransferase	mit, cyt, nuc	–
CDC21	Pyrimidine biosynthesis	Nucleus	AT4G34570/THY-2
CDC33	CAP-dependent mRNA translation initiation	Nucleus, cytoplasm	AT4G18040/EIF4E
CDC53	Involved in protein catabolic processes	Ubiquitin ligase complex (SCF)	AT1G26830/CUL3A
CNS1*	Chaperons/co-chaperons, protein folding	cyt	AT1G04130/TPR2
COF1*	Severs actin filaments	Cytoskeleton	AT2G31200/ADF6
CPR1*	Chaperons/co-chaperons, protein folding	nuc, mit,	AT4G38740/ROC1
CPR7*	Chaperons/co-chaperons, protein folding	cyt	–

Table 2.1 (continued)

CSE4	Chromatin accessibility and Pol II- binding regions	Nucleosome	-
DCP2	Decapping enzyme, and transcription initiation	Nucleus, cytoplasm	AT5G13570/DCP2
DDR48*	DNA damage responsive protein	cyt	-
DEG1*	Pseudouridine synthase	Nucleus, cytoplasm	AT1G34150
ESS1*	Protein folding, chromatin silencing	nuc, cyt	AT2G18040
GPI19	Glycosylphosphatidylinositol synthesis	ER	-
GPI8	Glycosylphosphatidylinositol tranferase function	ER	AT1G08750
GRC3	Possibly involved in rRNA processing	nuc	-
HAA1	Transcriptional activator	Nucleus, cytoplasm	-
HAS1*	RNA helicase, biogenesis of 40S, 60S ribosome subunits	nuc	AT5G65900
MCD4	Glycosylphosphatidylinositol synthesis	ER	-
MED7	Part of the Pol II mediator complex	nuc	AT5G03220
MPS3	Nuclear envelope/pore complex protein	Nuclear pore	-
MRPL32	Mitochondrial ribosomal protein	mit	-
MYO2	Actin based cargo transport	Cytoskeleton	AT5G43900/MYA2
NDC1	Subunit of the nuclear pore complex	Nuclear pore	-

Table 2.1 (continued)

NMT1	Myristoyl transferase	cyt	AT5G57020/ATNMT1
NOG1	60S ribosomal biogenesis	Preribosome	AT1G50920
NOG2	60S ribosomal biogenesis and nuclear export	Preribosome	AT1G52980/ATNUG2
NOP2	Processing and maturation of 27S pre-rRNA	Preribosome	AT5G55920/OLI2
NOP53	60S ribosomal biogenesis	nuc	AT2G40430
NSE4	DNA replication and repair	nuc	–
NSL1	MIND kinetochore complex	nuc	–
NSR1*	Required for pre-rRNA processing	mit, cyt, nuc	AT1G48920/ATNUC-L1
NUG1	Nuclear export of the 60S ribosome	nuc	AT3G07050/NSN1
OTU2*	Predicted cystein protease	cyt	AT3G62940
POL1	Required for DNA synthesis	nuc, mit	AT5G67100/ICU2
PRI1	Required for DNA synthesis	nuc	AT5G41880/POLA3
PRP31	Splicing factor	nuc	AT1G60170/EMB1220
PRP4	Splicing factor	snRNPcomplex	AT2G41500/LIS
PRP5	Prespliceosome formation	mit, cyt, nuc	–
PUS4*	Pseudouridine synthase	mit, nuc	–
RFA1	DNA repair and replication	cyt, nuc	AT2G06510/ATRPA1A
RNY1*	Vacuolar RNase, relocalizes to the cytosol upon stress	Vacuole, cytosol	AT2G02990/RNS1
RPL15A	Required for processing of pre-rRNA	Large ribosome	AT4G16720
RPL17A	Component of the 60S ribosomal subunit	Large ribosome	AT1G67430

Table 2.1 (continued)

RPL1B	Component of the 60S ribosomal subunit	Large ribosome	AT5G22440
RPL7A	Required for processing of pre-rRNA	Large ribosome	AT3G13580
RPT2	Proteasome component	nuc, proteasome	AT4G29040/RPT2a
RSP5*	Ubiquitination	cyt, nuc, Golgi, pm	–
SEC26	Secretory pathway proteins	(COPI) coated vesicles	AT4G31480
SEC31	Secretory pathway proteins	(COPII) coated vesicles	AT3G63460/SEC31B
SEC4*	Secretory pathway proteins	Actin cap, mit, vesicles, pm	AT3G09900/ATRABE1E
SHE4	Myosin function regulator	Cytoskeleton	–
SHO1	Transmembrane osmosensor	pm	–
SKP1	Part of the ubiquitin ligase complex (SCF)	nuc, cyt	AT5G42190/ASK2
SLX9	Pre-ribosomal RNA processing	Preribosome	–
SNU114	Splicing factor	nuc	–
STI1*	Chaperons/co-chaperons, protein folding	cyt	AT4G12400/HOP3
SUB1	Transcriptional coactivator	nuc	–
TAF2	Pol II transcription initiation	TFIID complex nucleus	–
TUB4	Nucleates microtubules	Cytoskeleton	AT3G61650/TUBG1
URA6	Pyrimidine biosynthesis	nuc, cyt	AT5G26667/PYR6
UTP7*	Processing of pre-18S rRNA	nuc	AT3G10530
XRN1	RNase, involved in ribosomal RNA maturation	Nucleus, cytoplasm	–

Table 2.1 (continued)

YPT1	Secretory pathway proteins	ER to Golgi vesicles, COPII coated vesicles, cyt vesicles, mit	AT1G02130/ATRAB1B
------	----------------------------	--	-------------------

mit, mitochondria; cyt, cytoplasm; nuc, nucleus; pm, plasma membrane.

* CIRFs that have direct physical interactions with viral components (RNA or replication proteins) based on prior proteomics screens.

Table 2.2 List of genes used for the second network analysis.

Yeast gene (plant or animal gene)	Function	Interaction
ACT1 (ACT1)	Actin filaments	-
ADH1 (AtADH1)	Fermentation	p33
ARP2	Actin branching	-
ARP3	Actin branching	-
ATG11 (Atg11)	Autophagy	p33
BRO1 (Bro1, ALIX)	ESCRT accessory	p33
CCC2	Copper pump	-
CDC19 (PK1)	Glycolysis	p33
CDC34	E2 conjugating enzyme	Ub-p33
CHO2	Phospholipid synthesis	-
CNS1 (Ttc4)	TPR co-chaperone	p33
COF1 (Adf2)	Actin depolymerization	p33
CPR1 (CypA)	Cyclophilin	p33
CPR6 (Cyp40)	Cyclophilin	p33

CPR7 (Cyp40)	Cyclophilin	p33
--------------	-------------	-----

Table 2.2 (continued)

CRM1 (Xpo1)	Exportin	p33/RNA
CSE4 (CENH3)	Centromeric histone	p33/RNA
DBP2 (RH20 and p68)	DEAD-box helicase	p33/RNA
DBP3 (RH5 and DDX3)	DEAD-box helicase	p33/RNA
DED1 (RH20 and DDX3)	DEAD-box helicase	p33/RNA
DEG1	Pseudourylation	RNA
DID4/VPS2	ESCRT-III	p33
DSL1	DSL1 complex	p33
EFM4	Translation elongation	-
ENO2	Glycolysis	p33
ERG4	Ergosterol synthesis	-
ERG9 (SQS)	Ergosterol synthesis	-
ERG25 (SMO1/2)	Ergosterol synthesis	-
ESS1	Parvulin	p33
FAL1 (RH2 and eIF4AIII)	DEAD-box helicase	p33/RNA
FAS2	Fatty acid synthesis	-
FBA1	Glycolysis	p33
FIS1 (Fis1)	Mitochondria division	p33
GEF1	Proton chloride exchanger	-
HES1/OSH5 (ORP)	MSC, sterol transfer	p33
INO2	Phospholipid synthesis	-
INO4	Phospholipid synthesis	-
MET22 (AHL, Sal1)	Affects Xrn1	-
MYO2	Actin motor protein	-
NCR1	RNA transport	RNA

NGL2	Endoribonuclease	-
------	------------------	---

Table 2.2 (continued)

NME1	Endoribonuclease, MRP complex	-
OPI1	Phospholipid synthesis	-
OSH3 (ORP)	MSC, sterol transfer	p33
OSH6 (ORP)	MSC, sterol transfer	p33
OSH7 (ORP)	MSC, sterol transfer	p33
PAH1	Phospholipid synthesis	-
PDC1	Fermentation	p33
PDC5	Fermentation	-
PEP8/VPS26 (Vps26)	Retromer complex	p33
PEX19 (Pex19)	Peroxisome biogenesis	p33
PGK1	Glycolysis	p33
PIK1	PI4K	-
PKC1 (Pkc1 in animals)	Protein kinase	p33
PMR1(ECA3/LCA1 --SERCA)	Ca/Mn ion pump	-
PRP40	WW-domain	p33
RAD6 (Ubc2)	E2 conjugating enzyme	Ub-p33
RPN11 (Rpn11)	Ub de-ubiquitinase	p33
RSP5 (Ubc8)	E3 Ub-ligase, WW domain	p92
SAC1 (Sac1a/b)	PI4 phosphatase, MCS	p33
SAR1 (AtSar1)	COPII vesicles formation	-
SCH9 (S6K)	Protein kinase	-
SCS2 (VAP27-2)	MCS formation	p33
SCS22	MCS formation	p33
SEC20	ER SNARE	p33

SEC22	DSL1 complex	p33
SEC39	DSL1 complex	p33

Table 2.2 (continued)

SNF7 (CHMP-III)	ESCRT-III	-
SNM1	Endoribonuclease, MRP complex	-
SRM1	Exportin GTPase	-
SSA1 (Hsp70-1)	Hsp70 chaperone	p33/p92
SSA2 (Hsp70-1)	Hsp70 chaperone	p33/p92
SSA3 (Hsp70)	Hsp70 chaperone	p33/p92
SSA4 (Hsp70)	Hsp70 chaperone	p33/p92
STI1 (HOP1)	TPR co-chaperone	p36-CIRV
STP22/VPS23 (Vps23, Tsg101)	ESCRT-I	Ub-p33
STT4	PI4K	-
TDH2 (GAPDH)	Glycolysis	p33/p92
TDH3 (GAPDH)	Glycolysis	p33/p92
TEF1 (eEF1A)	Translation elongation	p33/RNA
TEF2 (aEF1A)	Translation elongation	p33/RNA
TEF4 (eEF1B)	Translation elongation	p33/RNA
TOR1	TOR kinase	-
TOR2	TOR kinase	-
TUB2	Alpha tubulin	-
TUB4	Tubulin nucleation	-
UFE1 (Syp81, syntaxin 18)	ER SNARE	p33
USE1	ER SNARE	p33
VPS4	ESCRT AAA ATPase	p33/RNA
VPS5 (SNX1/2)	Retromer formation	p33
VPS15	VPS34 complex	-

VPS17 (missing in plants)	Retromer formation	-
VPS20	ESCRT-III	p33

Table 2.2 (continued)

VPS21 (Rab5)	Early endosome formation	p33
VPS24	ESCRT-III	p33
VPS29 (Vps29)	Retromer complex	p33
VPS30	VPS34 complex	-
VPS34 (Vps34)	PI3K	p33
VPS35 (Vps35)	Retromer complex	p33
VPS38	VPS34 complex	-
WWM1	WW-domain	p33
XRN1 (Xrn4)	5' to 3' exonuclease	RNA
YMR1	PI3 phosphatase	-
YPT1 (RabD1/D2, Rab1)	COPII vesicles	p33
YPT7 (Rab7)	Retromer and late endosome	p33
YPT52 (Rab5)	Early endosome formation	p33
YPT53 (Rab5)	Early endosome formation	p33

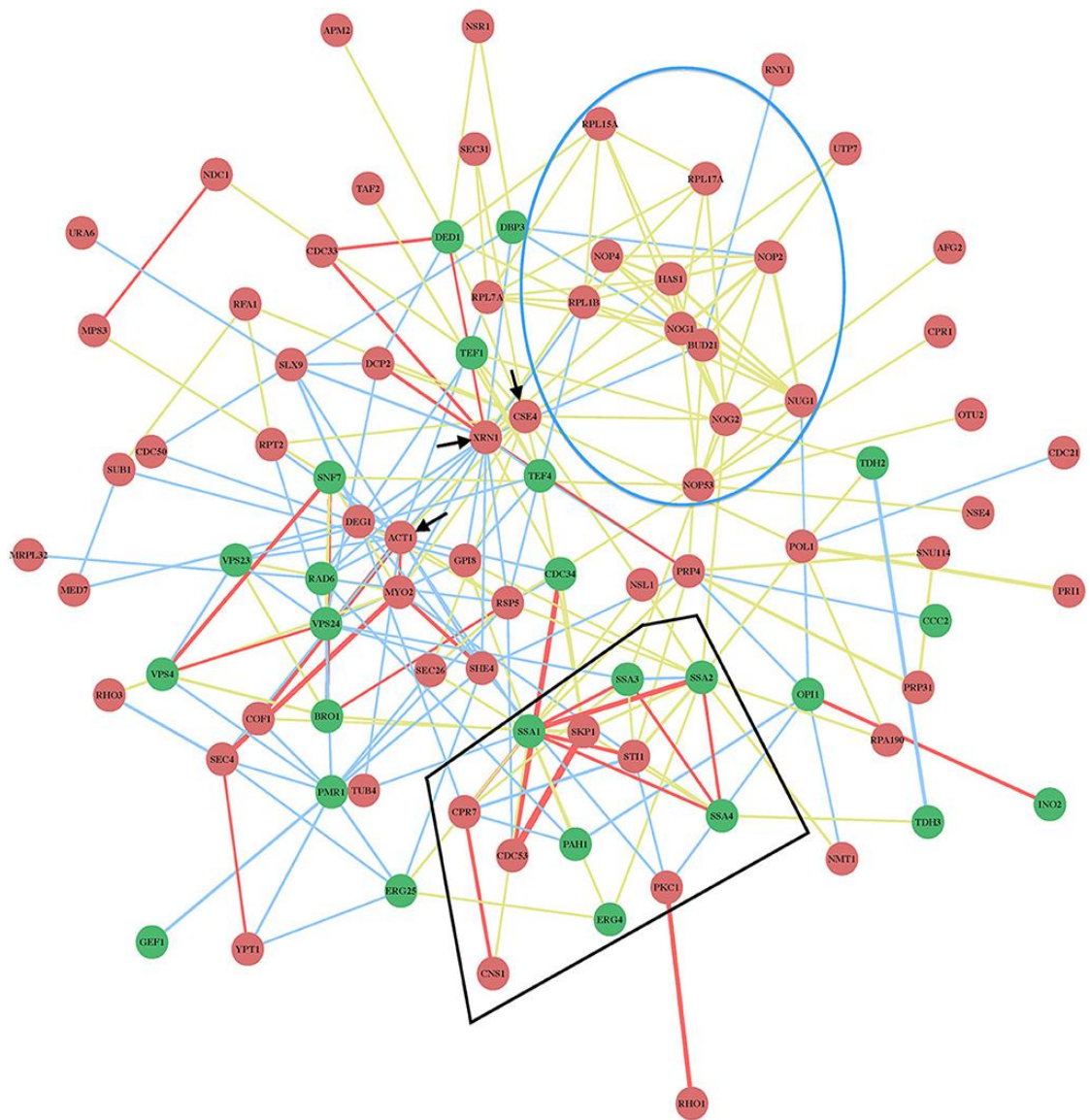


Figure 2.1

Figure 2.1. Physical and genetic protein interaction network of CIRFs and pro-viral host factors in yeast.

Functions of the genes are listed in Table 2.1. Red nodes indicate inhibitory CIRFs (i.e., viral replication increases when the gene is deleted or down-regulated); green nodes show positive pro-viral host factors (viral replication decreases when the gene is deleted or down-regulated); yellow lines indicate physical interactions; blue lines mark genetic interactions; red lines show both physical and genetic interactions. The thicker the line between two nodes, the greater the confidence of the interaction is, indicating that there are more experimental data supporting the existence of the particular interaction. The blue circle encloses the largest group of related inhibitory factors with similar functions in biogenesis, processing, and maturation of ribosomal structure. The black polygon indicates cellular factors, such as the TPR-domain co-chaperones, interacting with the Hsp70 (Ssa1-4) chaperone system. The black arrows mark the three proteins with the largest number of connections, namely *XRNI*, *ACT1* and *CSE4* with 20, 17, and 14 connections respectively. Note that *ARP7*, *ARP9*, *CCAI*, *DDR48*, *HAA1*, *MCD4*, *PRP5*, and *PUS4* genes (Table 2.1) are not included in the network map because they are not connected to the listed factors based on known interactions.,

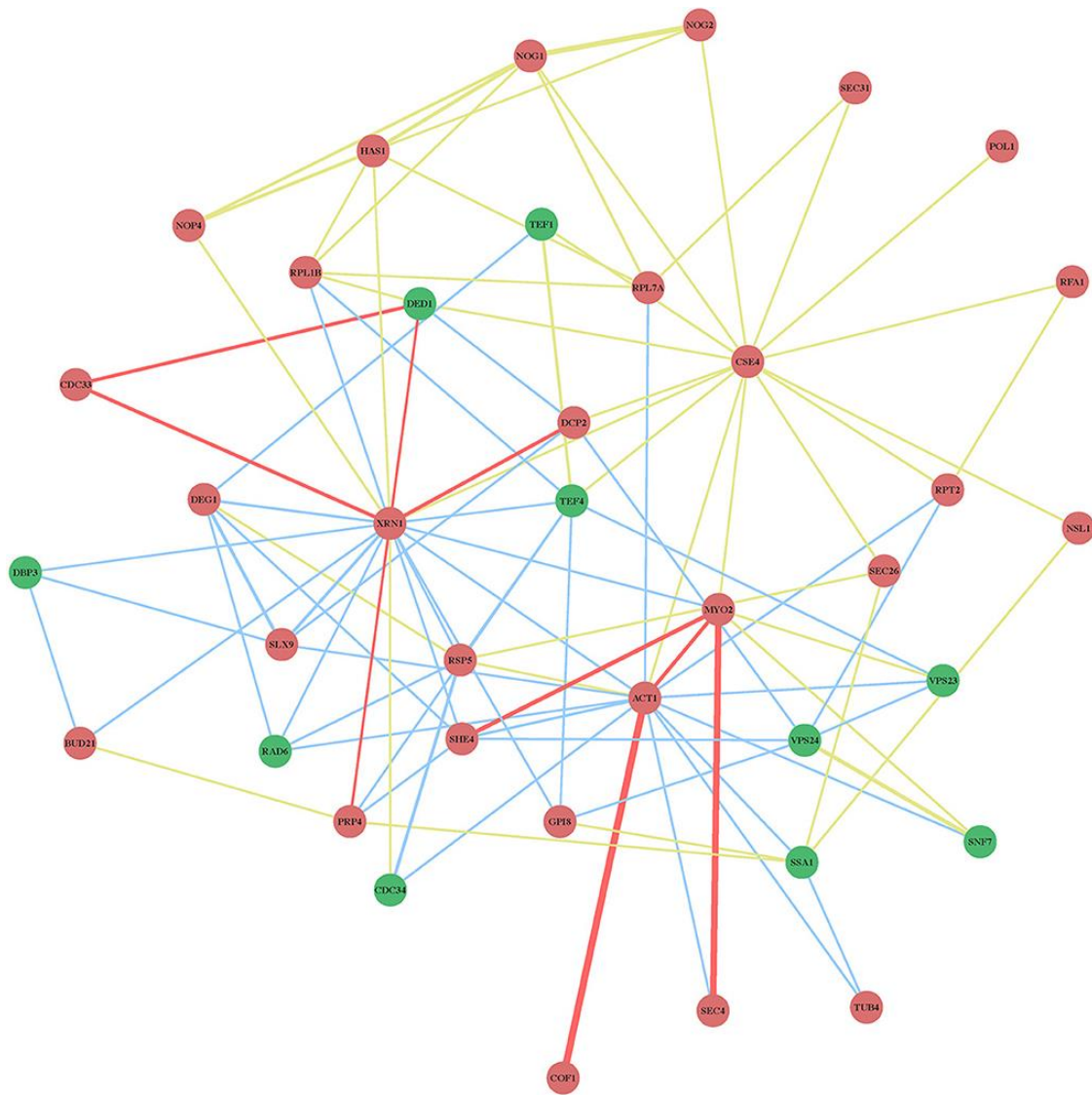


Figure 2.2. Physical and genetic protein interaction network including *XRN1*, *ACT1*, and *CSE4* CIRFs.

The network was assembled with the known interactors of CIRFs *XRN1*, *ACT1* and *CSE4*, the three host factors with the largest number of connections in Figure 2.1. Functions of the genes are listed in Table 2.1. Evidence of interaction with *XRN1*, *ACT1* or *CSE4* has not been identified for all the genes in Table 2.1 hence the resulting network is smaller than the one in Figure 2.1. Red nodes indicate inhibitory CIRFs; green nodes show positive proviral host factors; yellow lines indicate physical interactions; blue lines mark genetic interactions; red lines show both physical and genetic interactions.

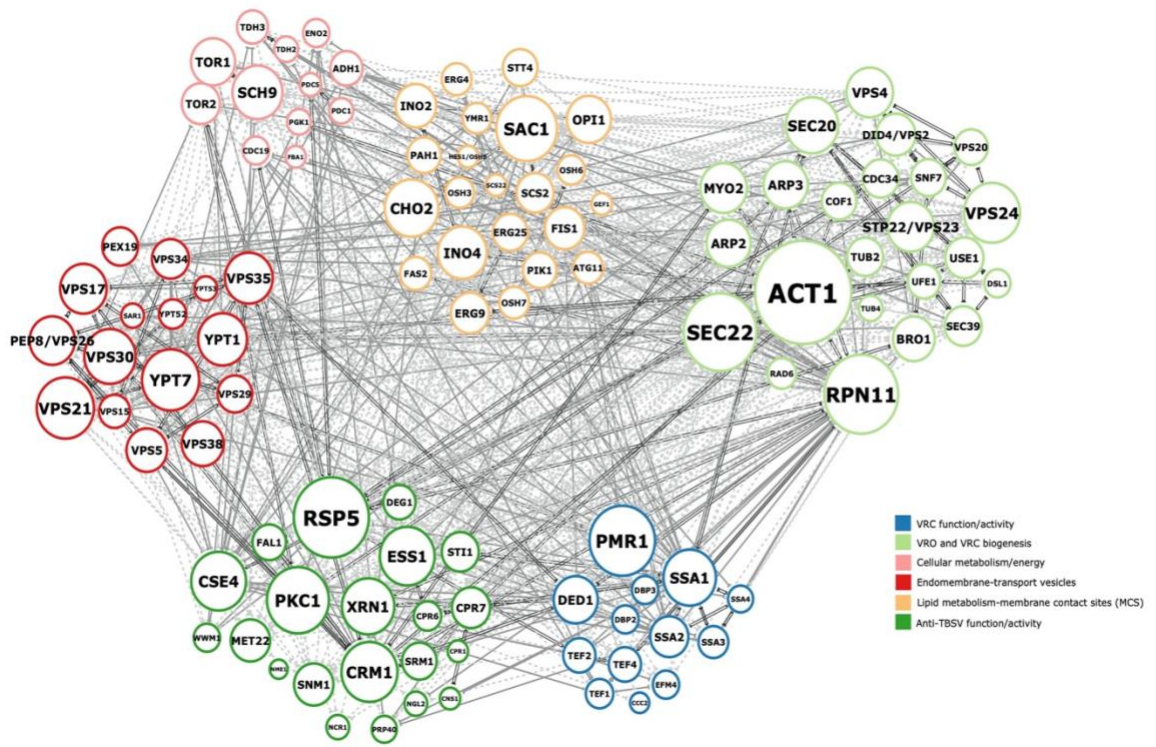


Figure 2.3

Figure 2.3. Physical and genetic protein interaction network of characterized host factors affecting TBSV replication.

Functions of the genes are listed in Table 2.2 as well as previously identified direct interactions of the host factors with viral replication proteins p33, p92 or the viral RNA for reference. The 6 functional modules are indicated with different node border colors. The VRO and VRC biogenesis functional group appears to be an active “hotspot” with the largest number of proteins (23 of 107) involved in these processes. Solid lines indicate physical interactions; dashed lines mark genetic interactions; double lines show both physical and genetic interactions. The size of the nodes represents the degree of connectivity of the nodes: the bigger the node, the larger the number of connections. Act1, Rsp5, Rpn11 and Sec22 are the overall network hubs with 67, 49, 48 and 47 connections respectively.

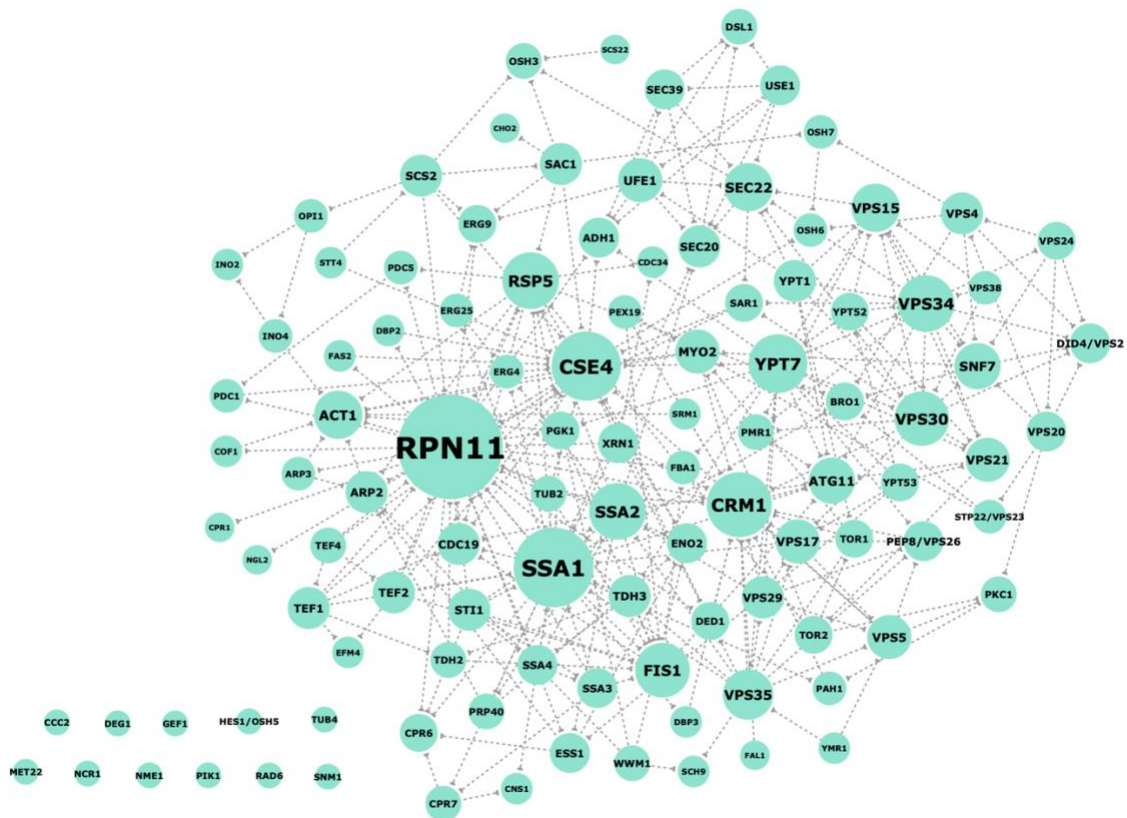


Figure 2.4

Figure 2.4. Physical protein-protein interaction network of characterized host factors affecting TBSV replication.

Functions of the genes are listed in Table 2.2 as well as previously identified direct interactions of the host factors with viral replication proteins p33, p92 or the viral RNA for reference. This network excludes genetic interactions, so edges represent a direct physical interaction between two host factors. The size of the nodes represents the degree of connectivity of the nodes: the bigger the node size, the larger the number of connections. Physical interactions have not been identified for 11 host factors, but they are still represented in the network as “floating” nodes with no edges. Rpn11 metalloprotease is the main hub with 37 physical interactions followed by Ssa1 chaperone with 25 and Cse4 histone variant with 20.

Chapter 3

TUBULIN MUTANTS REVEAL AN INHIBITORY ROLE FOR THE DYNAMIC MICROTUBULE NETWORK IN TOMBUSVIRUS REPLICATION

3.1 Introduction

Plus-stranded (+)RNA viruses, which include many important pathogens of plants, animals and humans, subvert a number of host-coded proteins and lipids to facilitate the replication process [3, 5, 36, 107-109]. These viruses also remodel host membranes and alter host cellular pathways to take advantage of host resources and to avoid recognition by host antiviral defenses. Characterization of an increasing number of host factors involved in (+)RNA virus replication has already revealed intriguing and complex interactions between various viruses and their hosts. Functional studies with selected host proteins have identified a plethora of activities performed by these host proteins during RNA virus infections [5, 36, 40, 89, 108-112]. In spite of the intensive efforts, our current cataloging of host factors is still far from complete and our current knowledge on the role of the identified host factors is incomplete.

One of the advanced viral systems to study virus-host interactions is tomato bushy stunt virus (TBSV), a small (+)RNA virus, which can replicate in the model host *Saccharomyces cerevisiae* [2, 13, 23, 80, 113]. TBSV replication requires two viral-coded proteins, namely p33 and p92^{pol} replication proteins. Although these proteins have overlapping sequences, they have different functions. p33, which has RNA chaperone

activity, has been shown to recruit the TBSV (+)RNA to the cytosolic surface of peroxisomal membranes, the sites of replication [8-11]. The p92^{pol} has RNA-dependent RNA polymerase (RdRp) activity and binds to p33 to assemble the membrane-bound functional viral replicase complex (VRC) [9, 12-15, 114].

The activities of TBSV replication proteins, however, are affected by numerous host proteins [3, 5, 44, 81, 110-112, 115-117]. Indeed, over 500 host genes/proteins that affect TBSV replication and/or recombination, have already been identified by using multiple genome-wide screens of yeast and global proteomic approaches [24, 27-30, 83, 118]. Moreover, the tombusvirus VRC contains several host proteins [82, 84, 99], including heat shock protein 70 (Hsp70), glyceraldehyde-3-phosphate dehydrogenase (GAPDH), eukaryotic elongation factor 1A (eEF1A), eEF1B γ , the DDX3-like Ded1, eIF4AIII-like RH2, DDX5-like RH5 DEAD-box RNA helicases, and the ESCRT (endosomal sorting complexes required for transport) family of host proteins [38, 81, 84, 89, 99, 119-121]. These proteins are required for VRC assembly or affect viral RNA synthesis [3, 5, 84, 119, 121-123]. The TBSV replication process also depends on phospholipids, phosphoinositides and sterols, which are actively recruited to, or synthesized at, the sites of viral replication [44, 117, 124-128].

The tombusvirus-yeast system offers the opportunity to explore how viruses can manipulate molecular and cellular processes to achieve robust replication. Moreover, we can also learn how a simple eukaryotic cell responds to the challenge of the viral exploitation of cellular resources. The effects of host genes and cellular pathways on virus replication and recombination can be discovered by studying yeast mutants [5, 39, 89]. In this chapter, I explore the effect of the cytoskeleton, specifically the microtubules in tombusvirus

replication. These studies were initiated based on previous genome-wide screenings and protein over-expression screens in yeast, which have led to the identification of beta-tubulin (Tub2), and gamma-tubulin (Tub4), as well as microtubule associated-proteins, such as Spc34, Spc97, Spc105, and Stu2 as host factors affecting viral replication [24, 25]. In addition, proteome-wide screens for p33-interacting cellular proteins identified NAP1, which is a histone chaperone involved in regulation of microtubule dynamics during mitosis [82].

In yeast and plant cells, the cytoskeleton is composed of two major types of elements: microfilaments (actin), and microtubules [129, 130]. The cytoskeleton has been shown to have roles in several steps of the infectious cycles for a number of viruses. The microtubule cytoskeleton consists of very dynamic filaments that connect various parts of the cell. Microtubules are rigid, long and hollow cylinders, approximately 25 nm in diameter, made of tubulin subunits. They typically have one end attached to a microtubule-organizing center, such as the spindle pole body (SPB) in yeast or the centrosome in mammalian cells [131-135]. Microtubules help determining the positions of diverse membrane-enclosed organelles and direct intracellular traffic acting as “highways”. They also are one of the most important constituents of the DNA segregating machine in eukaryotic cells. Microtubules are composed of three different tubulin subunits. γ -tubulin and other capping proteins that function as nucleating platforms initiate microtubule assembly. Subsequent addition of α and β tubulin heterodimers in a GTP-dependent manner allows the polymer to grow [136-138]. They are highly dynamic structures, oscillating between three different stages: polymerization, depolymerization and stable (due to posttranslational modification) where they remain in pause. Rapid polymerization-

depolymerization steps, termed dynamic instability, plays a key role in determining the organization of microtubules into arrays shaping the microtubule network in cells [135].

In this work, using temperature-sensitive (ts) Tub2p and Tub4p yeast mutants at semi-permissive temperature, I found an increased level of TBSV RNA accumulation in yeast cells. The *in vitro* activity of the tombusvirus replicase prepared from yeast expressing *tub2^{ts}* was also higher than the activity of the wt replicase. Pharmacological inhibition of dynamic function in yeast or in plant cells also led to increased TBSV replication. I demonstrated that the dynamic microtubules restrict the ability of TBSV to recruit pro-viral host proteins and sterols to the viral replication sites. Altogether, I found that the cellular dynamic microtubules restrict TBSV replication.

3.2 Materials and Methods

Yeast strains and expression plasmids. *Saccharomyces cerevisiae* strain BY4741 (*MATa*, *his3Δ1*, *leu2Δ0*, *met15Δ0*, *ura3Δ0*) and *alf1Δ* (YKO library) were obtained from Open Biosystems. The temperature-sensitive (ts) yeast strains *tub2-443* (*tub2^{ts}*), *tub4-Y445D* and *tub4-ΔDSY* were a generous gift from C. Boone (University of Toronto) [139]. Yeast strains MGY1 (*MATa*, *leu2Δ1*, *trp1Δ63*, *his4-917*, *URA3/ura3-52*, *tub2-His₆*), which contains a His₆ tag at the C terminus of Tub2p, and the MGY1 mutant strain MGY1-C354S (*MATa*, *leu2Δ1*, *trp1Δ63*, *his4-917*, *URA3/ura3-52*, *tub2-His₆-C354S*) were requested from Richard H. Himes lab (Kansas University) and generously donated [140, 141]. Strains SEY6210 (*MATa ura3-52 his3Δ200 lys2-801 leu2-3,112 trp1Δ901 suc2Δ9*), JRY6266 (SEY6210 *osh3Δ::LYS2 osh5Δ::LEU2 osh6Δ::LEU2 osh7Δ::HIS3*) and JRY6232

(SEY6210 *osh5Δ::LEU2 osh6Δ::LEU2 osh7Δ::HIS3*) were obtained from Dr. Christopher T. Beh (Simon Fraser University) [142]. Deletion strains, BY4741 *pex3Δ* and *tub2^{ts} pex3Δ* were obtained by transformation and consequent homologous recombination of a fragment containing a nourseothricin resistance marker gene, previously PCR-amplified with primers #4719/#4720 (see table 3.1), using the Euroscarf plasmid pF6a-natNT2 [143] linearized with *SpeI*. The above primers carry 42 (forward primer) and 41 (reverse primer) nucleotides, matching sequences upstream and downstream of *PEX3* gene, including start and stop codons. Correct integration of the nourseothricin marker gene was confirmed with primers #4721/#2215. Primer #4721 targets an upstream region of the *PEX3* gene and #2215 matches a sequence of the nourseothricin resistance cassette.

The following yeast expression plasmids have been previously described: HpGBK-CUP1-Hisp-33/ADH1-DI-72 (*HIS3* selection), UpYES-NT-Cpr1 (*URA3* selection) [83], LpGAD-CUP1-His-p92 (*LEU* selection) [13]. UpESC-GAL10-DI72/GAL1-His-p33 (*URA3* selection), TpGAD-CUP1-His-92 (*TRP1* selection), UpYC2/NT-C-OSH6 (*URA3* selection) [43]. HpGBK-CUP1-His-p33/GAL1-DI-72 (*HIS3* selection), HpGBK-CUP1-Flag-p33/GAL1-DI-72 (*HIS3* selection), LpGAD-CUP1-His-p92 (*LEU2* selection), LpGAD-CUP1-Flag-p92 (*LEU2* selection) [38]. HpESC-GAL1-Hisp36/GAL10-DI-72 (*HIS3* selection) [32], UpYC-DI-72 (*URA3* selection) [23], UpYC-His-CypA (*URA3* selection) [144], UpYES-RH30 [88]. LpESC-CUP1-Flag-CIRVp95 to be described elsewhere (*LEU2* selection, J. Pogany and P.D. Nagy, unpublished). UpYES-NT-Cpr7 (*URA3* selection) plasmid was made by former lab member Venugopal Mendu by the PCR amplification of yeast Cpr7 ORF with primers #3152/#3196 from *S. cerevisiae* cDNA. The

fragment was inserted into UpYES-NT (Invitrogen) vector, after digestion of both the fragment and vector with restriction enzymes *Bam*HI and *Xho*I.

The following plasmids were used for confocal laser microscopy and described previously: LpGAD-CUP1-GFP-p33 (*LEU2* selection) and UpYES-GAL1-RFP-p33 (*URA3* selection) [145], LpGAD-Pho86-CFP (*LEU2* selection) [9], LpGAD-pex13-RFP (*LEU2* selection) [38], HpESC-HisYFP-p33-GAL1/DI-72-GAL10 (*HIS3* selection) [8], HpESC-VenN-p33-DI72 (*HIS3* selection) and UpYC-VenC-SCS2 (*URA3* selection) [43]. pRS315-TUB1-GFP (*LEU2* selection) used to express C-terminal GFP tagged TUB1 under its native promoter was created by PCR amplification of *TUB1* ORF with primers #6243/#6244 and digestion with *Sal*I and *Nhe*I restriction enzymes. The *GFP* sequence was PCR amplified with primers #6624/6513 using the pGDG vector as a template (provided by Dr. M. Goodin) [146] followed by digestion with *Xba*I and *Sac*I. After ligation of *TUB1* and *GFP* fragments, the resulting *TUB1-GFP* product was inserted into pRS315 vector previously digested with *Sal*I and *Sac*I.

Plant expression plasmids. The plant expression plasmids pGD-T33-BFP, pGD-RFP-SKL, pGD-Cox4-RFP, pGD-p19 and pGD-C36-BFP have been described before [46]. VIGS plasmids were created as follows: The *Nicotiana tabacum* sequence for *TubG1* (γ -tubulin) and the *Arabidopsis thaliana* sequence for *Tub5* (β -tubulin) were used to do a blast in Sol Genomics database and obtain the predicted cDNA sequences. To generate the VIGS constructs, 5' or 3' fragments of the *NbTubG1* and *NbTub5* genes were PCR-amplified from *N. benthamiana* cDNA using primer pairs #5435/#5436, #5437/#5438,

#5591/#5592 and #5593/#5594. The fragments were inserted into the plasmid pTRV2 [147] to generate pTRV2-NbTubG-5', pTRV2-NbTubG1-3', pTRV2-NbTub5-5' and pTRV2-NbTub5-3'. Plasmid pTRV2-cRFP will be described elsewhere (M. Molho and P.D. Nagy, unpublished).

Yeast transformation and cultivation. Yeast strains were co-transformed with different combinations of plasmids using the lithium acetate (LiAc)–single-stranded DNA (ssDNA)–polyethylene glycol (PEG) method [148], and transformants were selected by complementation of auxotrophic markers by plating them on selective SC medium.

Analysis of tombusvirus replication in yeast. For CNV repRNA accumulation, yeast strains BY4741, *alf1*Δ, *tub2^{ts}*, *tub4*-Y445D, *tub4*-ΔDSY, MGY1, MGY1-C354S, BY4741 *pex3*Δ and *tub2^{ts} pex3*Δ were transformed with HpGBK-CUP1-Hisp-33/ADH1-DI-72 and LpGAD-CUP1-His-p92. In the case of the temperature sensitive mutants and BY4741 wild type strain two sets of cultures per strain were grown at 23 °C overnight in SC-LH⁻ (synthetic complete medium without leucine and histidine) medium containing 2% glucose and 100 μM BCS (bathocuproinedisulfonic acid). Then, a set of cultures was placed at 32 °C for 4 h the other set remained at 23 °C. After the 4 h, cells were centrifuged and washed thoroughly with clean SC-LH⁻ (2 % glucose) medium and pellets were re-suspended in the same medium containing 50 μM CuSO₄ to induce viral protein expression and repRNA replication. Cells were grown for additional 24 h at 23 °C or 32 °C, after which total RNA and protein were extracted. Additional BY4741 and *tub2^{ts}* cells grown as described above

were used for detection and comparison of viral (+) and (-) RNA (see details in *RNA analysis* section of these Materials and Methods). MGY1, MGY1-C354S strains were grown likewise but only one set of cultures was needed and maintained at 29 °C. The same growth conditions were used to compare repRNA accumulation between the BY4741 wild type yeast and the *alf1*Δ YKO strain. For CIRV repRNA accumulation cells were transformed with plasmids HpESC-GAL1-Hisp36/GAL10-DI-72 and LpESC-CUP1-Flag-CIRVp95 and grown as above with the exception that pellets were thoroughly washed with SC-LH⁻ medium (2% galactose) and re-suspended in SC-LH⁻ medium containing 2% galactose and 50 μM CuSO₄. Total RNA and protein were extracted after 30 h of viral induction.

Yeast microtubule disruption and cell cycle arrest. Three sets of cultures of BY4741 transformed with HpGBK-CUP1-Hisp-33/ADH1-DI-72 and LpGAD-CUP1-His-p92 were grown at 23 °C overnight in SC-LH⁻ medium with 2% glucose containing 100 μM BCS. Next morning cells were centrifuged and washed, followed by an OD adjustment of OD₆₀₀=0.2 by diluting with one of the following mixtures: 1) SC-LH⁻ medium (2% glucose) with 100 μM BCS and 1.5 μl/ml of a nocodazole stock (6.6 mM, dissolved in DMSO), to disrupt microtubules; 2) SC-LH⁻ medium (2% glucose) with 100 μM BCS and 40 mg/ml of hydroxyurea to arrest cell cycle; 3) SC-LH⁻ medium (2% glucose) with 100 μM BCS and 1.5 μl/ml of DMSO as control. After dilution, cells were grown for 1 h at 29 °C. An additional 1.5 μl/ml of nocodazole or DMSO were added to the corresponding cultures (for a final concentration of 20 μM). After another 2 h of grow at 29 °C all sets of cultures were centrifuged and washed to get rid of BCS and pellets were re-suspended in

the same mixtures as above but instead of BCS, CuSO₄ was added (50 μM final concentration). Cells were allowed to grow for ca. 12 h while OD was monitored at 3, 6, 9 and 12 h time points. Finally, RNA samples were extracted from all cultures.

Yeast strains SEY6210, JRY6266 and JRY6232 were transformed with plasmids UpESC-GAL10-DI72/GAL1-His-p33 and TpGAD-CUP1-His-92. Cells were initially grown at 23 °C in SC-UT⁻ medium (synthetic complete medium without uracil and tryptophan) with 2% galactose and 100 μM BCS overnight and next day changed to SC-UT⁻ medium with 2% galactose, 50 μM CuSO₄ and 35 μM (final concentration) of nocodazole or DMSO (for control samples). After 24 h cells were harvested, and RNA was extracted and analyzed as described below in *RNA analysis* section.

RNA stability assay. Yeast strains BY4741 and *tub2^{ts}* were transformed with plasmid pYC-DI-72 and grown 12 h overnight at 23°C in 3 ml of SC-U⁻ (synthetic complete medium without uracil) medium with 2% glucose. The next morning the cultures were centrifuged, washed twice with sterile miliQ water and re-suspended in SC-U⁻ medium with 2% galactose. After 6 h of growth at 23°C cells were washed again, and the pellet was re-suspended in SC-U⁻ medium with 2% glucose. Samples were collected at given time points mentioned in the legend of Figure 3.3 and total RNA was isolated and analyzed.

RNA analysis. Total RNA isolation and northern blot analysis were performed as described previously [13, 23] with a minor modification. Briefly, for extraction of total RNA, yeast cells were broken by shaking for 1 to 2 min at room temperature (rt) with equal volumes

of RNA extraction buffer (50 mM NaOAc [pH 5.2], 10 mM EDTA, and 1% sodium dodecyl sulfate [SDS]) and water-saturated phenol, and then incubated for 4 min at 65 °C. After a short incubation on ice and centrifugation for 10 min at 12,000 x g at 4 °C, the aqueous phase (~200 µl) was transferred to phenol-chloroform (~250 µl volume) mixed in 1:1 ratio, followed by vortexing, centrifugation (again at 4 °C for 10 min) and ethanol precipitation of the aqueous phase. The obtained RNA samples were separated on a 1.5% agarose gel and transferred to a Hybond-XL membrane (Amersham) before hybridization with a ³²P-labeled DI-72-specific or 18S rRNA probe [23]. Detection of (+)RNA or (-) RNA was made via a ³²P-labeled DI-72RIII/IV probe prepared with in vitro T7-based transcription using PCR-amplified DNA obtained on pGBK-CUP1-6xHisp33/GAL1-DI-72 [149] template, with primers #22 and #1165 for (+)RNA detection, and primers #18 and #1190 for (-)RNA detection. Viral RNA accumulation was normalized based on rRNA using the ImageQuant software and a Typhoon scanner (General Electric).

Protein analysis by western blot. For protein analysis, pelleted cells were resuspended in 200 µl of 0.1 M NaOH and incubated at rt for 15 min while shaking in an Eppendorf shaker. NaOH was aspirated after a short centrifugation and the pellets were re-suspended in 50 µl of 1X SDS/PAGE buffer with 5% β-mercaptoethanol. After another 15 min of shaking at rt, samples were incubated at 85 °C for 15 min. Finally, after a brief centrifugation at 12,000 x g, the supernatant was used for SDS/PAGE and western blot analysis as previously described [13, 25]. Antibodies used were anti-His (Sigma), anti-Flag (Sigma) and the secondary antibody alkaline-phosphatase-conjugated anti-mouse IgG (Sigma).

Microtubule disruption in protoplasts. Protoplasts were isolated from *Nicotiana benthamiana* callus by treatment with 1 g Cellulysin and 0.2 g Macerase (Calbiochem) as described before [150] and left at rt for 12 h overnight. Next morning samples were electroporated with 2 µg of a mixture of *N. benthamiana* and TBSV RNA previously isolated from an infected plant (9 days post-inoculation) using the phenol-chloroform method [151]. For this, 3 µl of a 6.6 mM nocodazole stock (dissolved in DMSO) was added to the electroporation cuvette (for a final concentration of 20 µM) along with the RNA, a few seconds prior to electroporation. For control treated cells, 3 µl of DMSO (instead of nocodazole) and RNA were added. After electroporation, samples were kept on ice for 30 min, then 1.7 ml of protoplast culture medium [152] was added to each sample and transferred into 35 × 10 mm petri dishes for incubation in the dark for 24 h at rt. Protoplasts were harvested by centrifugation with no breaks and RNA was isolated as described in the *RNA analysis* section with a modification. Protoplast samples were not incubated at 65 °C after breaking the cells.

Replicase purification and in vitro replication assay. Initially, BY4741 and *tub2^{ts}* yeast cells transformed with HpGBK-CUP1-Flag-p33/GAL1-DI-72 and LpGAD-CUP1-His-p92, were grown at 23 °C in 2 ml of SC-LH⁻ medium with 2% glucose containing 100 µM BCS. Later the volume was gradually increased from 2 ml to 50 ml by adding medium. The OD₆₀₀ was measured and when it reached a value between 1 and 2 the cultures were diluted as follows: 25 ml of culture with 25 ml of clean SC-LH⁻ medium containing 2% glucose and 100 µM BCS. After 2 h, cells were thoroughly washed, and the pellets re-suspended in 200 ml of SC-LH⁻ medium with 2% galactose and 50 µM CuSO₄ for and

additional 24 h growth at 23 °C. Finally, 2 g of cells were harvested and washed with 40 ml of 20 mM Tris-HCl pH 7.5. Purification of the viral replicase was performed as described before [153]. The activity of the purified replicase was tested by programming the replicase with 0.5 mg/ml repRNA (RI/RIII(-)RNA). The in vitro assays were performed at 25 °C for 3 h in the presence of ³²P-labeled UTP as described [13]. Then, the RNA was phenol/chloroform purified, precipitated by isopropanol-ammonium acetate and analyzed in 5% denaturing polyacrylamide gel containing 8 M urea.

In vitro tombusvirus replicase assay using yeast membrane-enriched fraction. For this assay cells were transformed and grown exactly as for replicase purification, and membrane-enriched fractions were obtained as follows: Yeast cells were centrifuged, and pellets were re-suspended in 1.5 volumes of extraction Buffer E [200 mM sorbitol, 50 mM Tris-HCl (pH 7.5), 15 mM MgCl₂, 10 mM KCl, 10 mM β-mercaptoethanol, 1% Ypic) followed by a break step with glass beads in a FastPrep homogenizer. In order to remove cell debris, obtained yeast extracts were first centrifuged at low speed (100 x g) for 5 min at 4°C. Then, the membrane-enriched fraction containing the viral replicase complex and the co-purified RNA template was obtained by centrifugation of the supernatant at high speed (21,000 x g) for 15 min at 4°C. The pellet considered the membranous fraction was washed with Buffer E (containing 1.2 M NaCl), centrifuged and re-suspended again in clean Buffer E. The in vitro assays were performed at 25 °C for 3 h in the presence of ³²P-labeled UTP as described [125] using normalized membrane fraction preparations. Then, the RNA was phenol/chloroform purified, precipitated by isopropanol-ammonium acetate and analyzed in 5% denaturing polyacrylamide gel containing 8 M urea.

VIGS-based knockdown of tubulin in *N. benthamiana* plants. The virus-induced gene silencing (VIGS) in *N. benthamiana* was done as described previously [147, 154]. After 11 days of VIGS treatment (pTRV1 together with pTRV2-NbTubG-5', pTRV2-NbTubG1-3', pTRV2-NbTub5-5', pTRV2-NbTub5-3' or pTRV2-cGFP) two distal leaves were sap inoculated with TBSV virions. Samples were collected 2 days post-infection from the infected leaves and 4 days post-infection from systemic leaves. Viral RNA accumulation was analyzed by northern blot after total RNA extraction.

The levels of *N. benthamiana TubG1* and *Tub5* mRNA was determined by RT-PCR with primers oligo-d(T) (for RT) and #5433/#5434, #5595/5596 respectively (for PCR). *Actin* mRNA was used as a control for amplification by RT-PCR using primers #3993/#3994.

Confocal laser scanning microscopy. Transformed BY4741 and *tub2^{ts}* yeast strains were grown 12 h overnight in the proper SC medium (according to the plasmid combination) with 2% glucose and 100 μ M BCS (only when needed). The next morning cells were centrifuged and washed (with sterile water) and pellets re-suspended in the same medium with 2% galactose and 50 μ M CuSO₄ to induce expression of the fluorescently tagged proteins. Samples were collected at the time points given in the main figure (or after 24 h where not stated) and analyzed by confocal microscopy as previously described [8].

Co-purification of yeast host proteins with Flag-p33 from cellular membranes. Cell growth and FLAG-p33 purification from cellular membranes using anti-FLAG M2 agarose was done as described previously [43]. Purified FLAG-p33 was analyzed by western blot using anti-flag antibody followed by anti-mouse antibody conjugated to alkaline phosphatase. Co-purified His6-tagged proteins were analyzed with anti-His antibody followed by anti-mouse antibody conjugated to alkaline phosphatase.

Filipin staining of sterols and microscopy. BY4741 and *tub2^{ts}* yeast strains were co-transformed with HpGBK-CUP1-Hisp-33/ADH1-DI-72 and LpGAD-CUP1-His-p92 or pESC-HIS3 (Agilent Technologies) and pGBK empty vectors as control. Cells were grown 12 h overnight in SC-LH⁻ medium with 2% glucose and 100 μ M BCS. The next morning after washing out BCS, pellets were re-suspended in SC-LH⁻ medium with 2% glucose and 50 μ M CuSO₄ to induce viral replication for the time points showed in main figure. Cells were then fixed with 37.5% formaldehyde for 1 h at rt, washed with 1 ml of 1X PBS and re-suspended in 500 μ l of 1X PBS containing 20 μ l of filipin solution (5 mg/ml in DMSO). After incubating in the dark with filipin overnight at 4 °C while rotating, samples were centrifuged to remove most of the liquid leaving ca. 20 μ l and re-suspended again. Then 2 μ l the cell suspensions were directly spotted onto microscope slides and examined in a UV light microscope (Zeiss) using a DAPI filter set.

Bimolecular fluorescence complementation (BiFC) assay in yeast. BY4741 and *tub2^{ts}* yeast strains were co-transformed with plasmids HpESC-VenN-p33-DI72, UpYC-VenC-

SCS2 and LpGAD-CUP1-His-p92 and grown 12 h overnight in SC-ULH⁻ (synthetic complete medium without uracil, leucine and histidine) medium containing 2% glucose and 100 μ M BCS. The next morning cells were centrifuged and washed (with sterile water) and pellets re-suspended in SC-ULH⁻ medium with 2% galactose and 50 μ M CuSO₄ to induce viral replication. Samples were collected at the time points given in the main figure and analyzed by confocal microscopy as previously described [8].

Confocal laser microscopic analysis of plant F-actin. Leaves of 8wk-old transgenic *N. benthamiana* plants expressing GFP-mTalin (mouse Talin) [155], which specifically binds to F-actin [156] (a gift from Dr. Michael M. Goodin at University of Kentucky), were treated for TubG1 and Tub5 VIGS as described above, but this time only pTRV2-NbTubG1-3' and pTRV2-NbTub5-3' were used for silencing and pTRV2-cRFP was used as control. After 11 d of VIGS treatment two distal leaves were mock inoculated or inoculated with TBSV or CIRV sap. Leaf epidermal cells were observed under confocal laser microscope (Olympus FV1000 microscope) 2 d after TBSV inoculation or 3 d after CIRV inoculation, for localization of GFP-mTalin.

A similar approach was used to detect plant F-actin in the presence of viral proteins after silencing of *TubG1* or *Tub5*. Again, VIGS-based knockdown of *TubG1* or *Tub5* was performed in GFP-mTalin transgenic plants as described above. After 11 d of VIGS treatment two distal leaves were agroinfiltrated with pGD-T33-BFP and pGD-RFP-SKL (peroxisomal marker) or pGD-C36-BFP and pGD-Cox4-RFP (mitochondrial marker). These same leaves were mock inoculated or inoculated with TBSV or CIRV sap 24 h later. Leaf epidermal cells were observed under confocal laser microscope (Olympus FV1000

microscope) 2 d after TBSV inoculation or 3 d after CIRV inoculation, for localization of GFP-mTalin, p33-BFP and RFP-SKL or GFP-mTalin, p36-BFP and Cox4-RFP.

3.3 Results

Mutations in tubulin genes affect TBSV replication in yeast. Previous high throughput screens have identified yeast proteins that are part of the microtubule network affecting TBSV replication [24, 25, 27]. To further test the role of microtubules and the cytoskeleton, I used haploid yeast expressing a single temperature-sensitive (ts) mutant of beta-tubulin gene (*TUB2*) [110] in TBSV replication studies. I observed ~3.5-fold increased TBSV repRNA accumulation at the semi-permissive temperature (32 °C, lanes 6-10, Figure 3.1B), whereas there was only ~1.5-fold increase at 23 °C (Figure 3.1A). Interestingly, C-terminal mutations in the γ -tubulin gene (*TUB4*) also increased TBSV repRNA accumulation by ~2.5-3.5-fold (Figure 3.1C). In case of these strains, similar to the *tub2^{ts}* mutant, cells arrest prior to anaphase and show an increased number of abnormally long and stable cytoplasmic microtubules at the semi-permissive temperature. None of these tubulin mutants showed elevated p33 levels (Figure 3.1D), suggesting that the effects of the tubulin gene mutations are not through enhanced p33 translation or altered stability.

An additional *TUB2* mutant yeast (*tub2*-C354S called MGY1-C354S), which forms a single cytoplasmic microtubule with a reduced dynamicity greater than 90% *in vivo* and *in vitro* [141] was also tested. Yeast expressing *tub2*-C354S shows an intrinsically stable microtubules, allowing us to test the effect of stable versus dynamic microtubules (as in wt yeast) on TBSV replication. Interestingly, similar to the *tub2^{ts}* mutant, *tub2*-C354S

supported a higher level of TBSV repRNA accumulation compared to the control MGY1 strain (Figure 3.1E), suggesting that a microtubule with enhanced stability could intensify viral replication. These results suggest that in contrast with the stable microtubules, the dynamic microtubules restrict TBSV replication in yeast.

To test the role of α -tubulin, which is represented by the redundant *TUB1* and *TUB3*, I used *alf1* Δ yeast in TBSV replication studies. Alf1p (homolog of mammalian cofactor B) is required for the formation of polymerization-competent tubulin heterodimers consisting of properly folded α -tubulin and β -tubulin [157]. As expected, *alf1* Δ yeast also supported ~2-fold higher level of TBSV repRNA (Figure 3.1F), further supporting the inhibitory role of dynamic microtubules in TBSV replication.

Mutations in tubulin also affect tombusvirus replication in the ER and mitochondria in yeast. To learn if microtubules affect tombusvirus replication only in the original peroxisomal location, whose membrane is used by TBSV to build VRCs, first I tested TBSV repRNA replication occurring in the endoplasmic reticulum (ER) membrane due to the deletion of yeast *PEX3* peroxisome biogenesis gene [8]. Expression of the *tub2*^{ts} mutant (as the only Tub2 protein) in *pex3* Δ yeast led to a ~2-fold increase in TBSV replication when compared to *pex3* Δ yeast expressing the wt copy of Tub2 (Figure 3.2A, lanes 1-4 versus 5-8). Overall, TBSV repRNA accumulated to a comparable level in *pex3* Δ yeast as in wt yeast as found previously [8], confirming that wt microtubules restrict TBSV replication as efficiently in the ER as in the peroxisomal membrane.

I also tested the effect of microtubules on the replication of a closely related tombusvirus, carnation Italian ringspot virus (CIRV), which replicates on the outer mitochondrial membrane [32, 158]. Yeast expressing the *tub2^{ts}* mutant supported higher CIRV accumulation by 3.5-fold (Figure 3.2B, lanes 10-12 versus 1-3), and yeast expressing one of the *tub4^{ts}* mutants supported higher CIRV accumulation by ~2-fold compared to wt BY4741 yeast (Figure 3.2B, lanes 7-9 versus 1-3). Altogether, these data suggest that tombusvirus replication is restricted by dynamic microtubules regardless of the subcellular locations of the VRCs.

Pharmacological disruption of microtubules promotes viral repRNA replication in yeast and plant cells. To explore the effect of microtubule dynamics on tombusvirus replication, I applied the depolymerizing agent nocodazole, which is known to affect microtubule polymerization by altering the dynamic instability of microtubules via increasing tubulin GTPase activity and lowering the elongation and shortening velocities, with an overall reduction of microtubule turnover rates [159]. To further test the role of microtubules in TBSV replication, BY4741 yeast cells were treated with nocodazole or DMSO for 14 h and TBSV repRNA accumulation was analyzed by northern blotting. Interestingly, nocodazole, unlike DMSO, treatment enhanced repRNA accumulation by ~2-fold (Figure 3.3A, lanes 4-6 versus 1-3), confirming that chemical disturbance of microtubule polymerization dynamics can promote viral replication. This pro-viral effect of nocodazole is not due to its effect on cell growth since treatment of yeast with hydroxyurea, which is a strong inhibitor of the cell-cycle [160] (Figure 3.3C), led to low repRNA accumulation when compared to the nocodazole treatment (Figure 3.3B, lanes 1-

3 versus 4-6). Therefore, I suggest that the effect of nocodazole treatment on TBSV accumulation is the result of diminished microtubule turnover rate and not an output of cell-cycle arrest.

To demonstrate a comparable role for the microtubule filaments on TBSV replication in plant cells, I tested the effect of nocodazole and oryzalin treatments in *N. benthamiana* protoplasts electroporated with the TBSV genomic RNA. Oryzalin functions as a microtubule depolymerizing agent, sequestering tubulin dimers and disrupting the structure of microtubules [161]. Additionally, oryzalin has been shown to induce changes in the morphology of the ER and Golgi leading to small membranous aggregates named “oryzalin bodies” [162]. I found that both nocodazole and oryzalin treatments increased TBSV genomic (g)RNA and subgenomic (sg)RNAs accumulation by close to ~2-fold when compared with DMSO treatment (Figure 3.3D-E). These results suggest that microtubules likely play similar restriction roles in TBSV replication in yeast and plant cells.

Mutations in tubulin affect VRC activity in yeast. To gain insights into the role of microtubules in TBSV replication, I tested if *tub2^{ts}* mutant influenced (-) or (+) strand RNA accumulation based on strand-specific probes in northern blots. I found that both (-) and (+) strand RNA accumulation increased by more than 3-fold in *tub2^{ts}* yeast at semi-permissive temperature (Figure 3.4C-D) and by ~2-fold at the permissive temperature (Figure 3.4A-B). The increased RNA accumulation was not due to enhanced viral repRNA stability based on similar degradation in wt and *tub2^{ts}* yeast (Figure 3.4E).

To characterize the viral replicase, I first isolated the membrane fraction from wt and *tub2^{ts}* yeast actively replicating the TBSV repRNA. After adjusting for comparable amounts of viral replicase (based on p33/p92 replication proteins), I tested the efficiency of in vitro repRNA synthesis. These experiments revealed that the membrane-enriched fraction from *tub2^{ts}* yeast produced ~2-fold more repRNA product than the replicase from the wt yeast (Figure 3.4G). These data suggest that the VRCs formed in *tub2^{ts}* yeast are more active than VRCs from wt yeast.

Second, the tombusvirus replicase from wt and *tub2^{ts}* yeast was affinity-purified. The endogenous (VRC-bound) repRNA is mostly lost during detergent-based solubilization of the cellular membranes and affinity-purification [12, 13]. Therefore, I programmed the purified replicase preparations, containing comparable levels of viral replication proteins, with the same amount of short (-)repRNA-derived template, called RI/RIII(-) [12, 13]. The in vitro replicase assay revealed ~2.5-fold higher activity for the affinity-purified replicase preparations from the *tub2^{ts}* yeast in comparison with the replicase preparations obtained from wt yeast (Figure 3.4H). Altogether, *in vitro* results with the tombusvirus replicase reveal the formation of more active VRCs in yeast expressing the *tub2^{ts}* mutant.

Localization of microtubules in the vicinity of Tombusvirus replication sites in yeast and plant cells. To study if microtubules are actively involved in the formation of tombusvirus replication organelles (VROs), which represent the sites of viral replication, I performed confocal laser microscopy on wt and *tub2^{ts}* mutant yeast cells. The VROs were detected with RFP-p33, while the microtubules were followed by GFP-tagged Tub1 alpha-

tubulin. Although I did observe several p33-containing punctate structures, which are VRO-like structures [12, 163, 164], in close vicinity of microtubules (Figure 3.5A-B), most of the p33-containing structures were not located in the vicinity of microtubules in wt or *tub2^{ts}* mutant yeasts at 6 or 16 h time points. Also, the distribution of microtubules was not altered in yeast expressing p33 replication protein, suggesting that tombusvirus does not visibly alter microtubule structures (not shown). In addition, mostly peroxisomal membrane distribution of p33 was observed, with a small fraction of p33 localized close to the ER in wt or *tub2^{ts}* mutant yeasts (Figure 3.5C-D). Overall, *tub2^{ts}* mutant yeast showed similar distribution and structures for p33 replication protein to those in wt yeast.

In plant cells transiently co-expressing RFP-tagged p33 replication protein and the GFP-tagged microtubule-binding domain (GFP-MBD) as a microtubule marker protein, microtubules were observed in the vicinity of the p33-containing large punctate structures (Figure 3.6A). Similarly, the CIRV p36 replication protein, which is localized to the mitochondrial outer membrane [32, 158], seems to be associated with microtubules (Figure 3.6B). Several microtubules seem to cross through the large VROs (Figures 3.6 and 3.7). However, changes in distribution or concentration of microtubules around the VROs were not observed. These observations suggest that microtubules might affect tombusvirus replication through contacts with VROs in plant cells. Therefore, I decided to perform functional studies on tombusvirus replication in cells in which the microtubules were altered as described below.

Rapid sterol re-distribution in *tub2^{ts}* mutant yeast supporting Tombusvirus replication. TBSV replication leads to retargeting of sterols from the plasma membrane to

the replication sites, which become highly sterol-enriched [43]. To test if sterols are more efficiently retargeted into VROs in *tub2^{ts}* mutant yeasts, which would lead to more efficient VRC assembly and enhanced replication, I analyzed the distribution of sterols in yeast cells. Filipin-based staining of sterols, which were visualized by fluorescent microscopy [43], revealed the rapid redistribution of sterols to internal sites in *tub2^{ts}* mutant yeasts as early as 30 min after induction of TBSV replication (Figure 3.7A), whereas 2 h were needed in wt yeast cells to observe sterol re-distribution. At later time points, both the wt and *tub2^{ts}* mutant yeasts showed re-distribution of sterols to internal sites in cells supporting tombusvirus replication (Figure 3.7B).

Enhanced recruitment of cellular ORP and VAP proteins by TBSV in *tub2^{ts}* mutant yeast. TBSV controls intracellular sterol transport through p33-driven subversion of VAP protein (such as yeast Scs2p or Vap27, which is a plant ortholog) and oxysterol binding proteins (OSBP-related or ORP, such as Osh3p, Osh5p, Osh6p and Osh7p) [43]. The cellular VAP and ORP proteins facilitate the formation of membrane contact sites (MCSs) between the ER and the peroxisomes. The MCSs are likely needed for the efficient transport of sterols to the peroxisomal membranes where VROs form [43].

To test if TBSV p33 could rapidly bind to Scs2p (the yeast VAP protein), I performed BiFC studies with the N-terminal half of YFP fused to p33 replication protein and the C-terminal half of YFP fused to Scs2p expressed in wt or *tub2^{ts}* mutant yeasts. Interestingly, I observed BiFC signals in 5% of *tub2^{ts}* mutant yeast at the 6 h time point, but not in wt yeast (Figure 3.8A). Also, the percentage of cells showing BiFC signals was ~3.5-fold higher in *tub2^{ts}* mutant yeast than in wt yeast at the 9 h time point (Figure 3.8B).

These data indicate that the interaction between p33 replication protein and the yeast Scs2p VAP protein occurs faster and more efficiently in *tub2^{ts}* mutant yeast than in wt yeast, suggesting more rapid formation of MCSs in *tub2^{ts}* mutant yeast. This could be beneficial for TBSV in building VROs [43], thus likely promoting TBSV RNA replication in *tub2^{ts}* mutant yeast.

To test if TBSV could efficiently co-opt a cellular ORP [43], p33 replication proteins were FLAG-affinity purified from detergent-solubilized membrane fractions, followed by western blotting to measure the co-purified yeast His₆-tagged Osh6p. I found ~2-fold increase in the amount of co-purified cellular Osh6p in *tub2^{ts}* yeast co-expressing p33/p92 and replicating TBSV repRNA (Figure 3.9A) or only expressing p33 (Figure 3.9B) in comparison with wt yeast at the permissive temperature. The more efficient co-purification of Osh6p in the *tub2^{ts}* mutant yeast suggests the enhanced or more stable formation of viral-induced MCSs. The efficient co-purification of an ORP also could explain the high enrichment of lipids (sterols) at internal sites (likely representing VROs) in the *tub2^{ts}* mutant yeast.

To further test if the more efficient hijacking of ORPs by the p33 replication protein is indeed the major mechanism for enhanced TBSV repRNA replication in *tub2^{ts}* yeast, I treated yeasts lacking critical ORPs for TBSV replication (either *osh5,6,7Δ* or *osh3,5,6,7Δ* yeast) with nocodazole to inhibit dynamic microtubule functions, followed by measuring TBSV repRNA replication. As previously shown [43], TBSV replicated poorly in either *osh5,6,7Δ* or *osh3,5,6,7Δ* yeasts (down to ~25-35% level, Figure 3.10). Interestingly, nocodazole treatment increased TBSV replication in both *osh5,6,7Δ* and *osh3,5,6,7Δ* yeasts, but these yeasts were still less efficient than the wt yeast treated with nocodazole

(Figure 3.10, lanes 10-12 and 16-18 versus 13-15). These data suggest that blocking microtubule function with nocodazole does causes more changes in yeast than only affecting the ability of TBSV to recruit ORP proteins to MCSs.

To test if recruitment of additional pro-viral host factors might be influenced by microtubules, a co-purification-based proteomic approach based on affinity-purified p33 and p92 replication proteins was used, which revealed that several co-opted host factors, such as Vap27-1 Scs2-like VAP protein from *Arabidopsis*, Cdc34 ubiquitin-conjugating enzyme, Tef1p (eEF1A) translation elongation factor, Pex19 peroxisome membrane biogenesis protein, and Vps4p AAA+ ATPase ESCRT factor, co-purified with the tombusvirus replicase ~40-90% more efficiently from *tub2^{ts}* yeast in comparison with wt yeast (Table 3.2). Other cellular pro-viral host factors, such as Tdh2p (GAPDH), DDX3-like Ded1p helicase, eIF4AIII-like RH2 helicase, Rpn11 deubiquitinase, and Vps23p ESCRT factor, co-purified with the replicase as efficiently from *tub2^{ts}* yeast as from wt yeast (Table 3.2). Based on these data, I suggest that *Tub2* mutation also facilitates the hijacking of some cellular pro-viral host factors by TBSV into the VRCs. The enhanced recruitment of these pro-viral factors likely promotes TBSV replication in *tub2^{ts}* mutant yeast.

Limited recruitment of cellular restriction factors into TBSV VROs in *tub2^{ts}* mutant yeast. TBSV replication is also affected by several cellular restriction factors, which are recruited into VROs [75, 89]. These restriction factors inhibit various steps in TBSV replication. Therefore, I wanted to know if the recruitment of selected restriction factors is affected by microtubules. The p33 replication proteins were affinity-purified from

detergent-solubilized membrane fractions, followed by western blotting to measure the co-purified His₆-tagged cyclophilins, namely the yeast Cyp40-like Cpr7 and Cpr1, and the orthologous human CypA [83, 144, 165]. The *Arabidopsis* RH30 DEAD-box helicase, which is a strong restriction factor when expressed in yeast or in *N. benthamiana* [88] was also tested. All these host restriction factors bind to the p33 and p92 replication proteins and inhibit their abilities to bind to the viral RNA [83, 144, 165]. A ~2-3-fold decrease was found in the amounts of co-purified cellular Cpr7 and Cpr1 cyclophilins, whereas CypA recruitment was reduced to close to undetectable level in *tub2^{ts}* yeast co-expressing p33/p92 and replicating TBSV repRNA (Figure 3.11A-C) in comparison with wt yeast at the semi-permissive temperatures (29°C and 32°C). The co-purification of the antiviral RH30 helicase with the replication proteins from *tub2^{ts}* yeast also showed reduced recruitment into VROs, but to a lesser extent than observed with the above cyclophilins. Altogether, the less efficient co-purification of all these restriction factors in the *tub2^{ts}* mutant yeast suggests the inefficient recruitment of these restriction factors into TBSV VROs. Altogether, the inefficient co-purification of these restriction factors could explain, at least partially, the more efficient replication of TBSV repRNA in the *tub2^{ts}* mutant yeasts with less dynamic microtubules at the semi-permissive temperatures. These results suggest that the microtubules are involved (directly and likely indirectly, see below) in recruitment of cellular restriction factors into tombusvirus VROs.

The effect of microtubules on TBSV VROs is connected with the altered actin filaments in plants with knocked down tubulin expression. The cytoskeleton plays remarkable roles in transportation of organelles and molecules in the crowded cytosolic

milieu. The microtubules frequently affect the structures of actin filaments and vice versa [130, 166, 167]. Because TBSV targets cofilin actin depolymerization protein to stabilize actin filaments and cables [68], I also examined what happens to TBSV association with the actin filaments in plants with tubulin knock downs. Remarkably, VIGS-based knock down of *TUB5* or *TUBG1* expression in *N. benthamiana* interfered with the formation of characteristic TBSV-induced actin filaments and cables (Figure 3.12B, D). In most cases, I observed only short actin filaments in TBSV-infected *TUB5* or *TUBG1* VIGS plants. This is in contrast with the thick actin filaments and cables in the TBSV-infected control plants (Figure 3.12B). The experiments using CIRV, which is even more prominent in stabilizing actin filaments and cables in wt plants [46], also showed a similar trend of poor formation of actin filaments in infected *TUB5* or *TUBG1* VIGS plants (Figure 3.12C). Co-expression of TBSV BFP-tagged p33 replication protein and RFP-SKL peroxisomal marker protein was then used to decorate the VROs in *TUB5* or *TUBG1* VIGS plants. In comparison with the TBSV-infected control plant cells showing the aggregation of several peroxisomes representing the VROs in the close vicinity of the actin filaments, TBSV infection induced lesser aggregation of peroxisomes in *TUB5* VIGS plants (Figure 3.13A). Interestingly, in *TUBG1* VIGS plants, I frequently observed the lack of aggregation of peroxisomes (i.e., p33-decorated VROs). These observations were further strengthened using CIRV-infected plants (Figure 3.13B). Nevertheless, the VROs were still associated with the actin filaments in *TUB5* or *TUBG1* VIGS plants, suggesting the active participation of actin filaments in VRO biogenesis [68]. Based on these findings, I propose that microtubules and the cytoskeleton overall is important for the biogenesis of tombusvirus induced VROs in plant cells.

Silencing of *TUBG1* expression in *N. benthamiana* reduced TBSV RNA accumulation moderately by ~20% in the inoculated leaves (Figure 3.14A). Silencing of *TUB5* expression had a more significant effect, leading to ~5-fold reduction in TBSV RNA accumulation in the inoculated leaves (Figure 3.14D). The upper, new leaves, which are systemically infected by TBSV in the corresponding leaves of the control plants, showed poorly detectable accumulation of TBSV RNA in *TUB5* or *TUBG1* VIGS plants (Figure 3.14B, 3.14E). This is likely due to the predicted roles of microtubules in virus movement, as demonstrated for multiple plant viruses [129]. Accordingly, disruption of the dynamic microtubules in plant leaves also resulted in major decrease in TBSV accumulation (Figure 3.14G).

3.4 Discussion

The dynamic cellular microtubule network restricts TBSV replication. High-throughput genome-wide screens with yeast mutant libraries have indicated a role of the cellular microtubules in tombusvirus replication [24, 25, 27, 29, 82]. In this work, I have shown that mutations in proteins associated with microtubules frequently led to increased TBSV repRNA accumulation in yeast, suggesting that the cellular cytoskeleton restricts TBSV replication in some ways. Accordingly, the mutations in the β -tubulin and γ -tubulin proteins or the Alf1p α -tubulin folding co-factor led to more efficient TBSV replication in yeast. Similarly, pharmacological inhibition of microtubules in yeast or plant cells resulted in higher levels of TBSV RNA accumulation.

The enhanced viral replication is likely due to the increased RNA replication activities of the tombusvirus VRCs as demonstrated *in vitro* (Figure 3.4). Because both (-)-strand and (+)-strand viral RNAs accumulated to higher levels in *tub2^{ts}* yeast and the affinity-purified tombusvirus replicase was more active *in vitro* when prepared from *tub2^{ts}* yeast, it is likely that either the VRC assembly is more robust or the activation of the p92^{pol} RdRp [114] is more efficient in *tub2^{ts}* yeast than in wt yeast. Interestingly, the microtubule network also affects TBSV replication when it takes place in the ER due to deletion of *PEX3* peroxisome biogenesis gene resulting in the absence of peroxisomes in the mutant yeast. Moreover, dynamic microtubules restricted CIRV replication which takes place on the outer membranes of mitochondria. Thus, the dynamic microtubules likely hinder some common steps in TBSV and CIRV replication and the viral restriction seems independent of the subcellular membranes forming the VROs (i.e., peroxisomes, ER or mitochondria).

The role of microtubules in recruitment of pro-viral and antiviral host factors into VROs. TBSV replication proteins do not seem to stably interact with the components of microtubules (based on previous proteomic screens, not shown) and distribution of microtubules and α -tubulin (Tub1p) looks similar in yeast or plant cells expressing or lacking the viral replication proteins. However, I found that the microtubules affect TBSV replication through influencing the recruitment of several host factors into VROs. For example, I observed enhanced redistribution of sterols in *tub2^{ts}* yeast in comparison with wt yeast expressing the viral replication proteins at an early time point, suggesting that mutation in β -tubulin facilitates the hijacking of sterols, which are needed for p33 functions and membrane structure within the tombusvirus VROs [45, 168, 169]. This conclusion is

further supported by the more efficient co-option of Vap27-1 (an Scs2 homolog in plants) as shown by co-purification with the p33 replication protein (Table 3.2) and BiFC studies indicating more robust and earlier interaction between Scs2p and p33 in *tub2^{ts}* yeast in comparison with wt yeast (Figure 3.8). More efficient co-purification of an ORP protein with p33 was detected from *tub2^{ts}* yeast in comparison with wt yeast (Figure 3.9).

Interestingly, the ER-resident Scs2/Vap27-1 and the ORP proteins are known to function in the formation of membrane contact sites (MCSs), where membranes are juxtaposed [170, 171]. Accordingly, microtubules are involved in localization of Vap27-1 at MCSs in plants [172]. The tombusvirus p33 replication protein directly interacts with ORPs and Scs2p/Vap27-1 and induces or stabilizes MCSs in yeast and plants, which likely facilitates channeling lipids to the viral replication sites [43, 47]. All these data are in agreement that TBSV could co-opt sterols more readily in *tub2^{ts}* yeast in comparison with wt yeast, indicating that the microtubule network affects VRO biogenesis.

In addition to the co-option of sterols, microtubules also affect the subversion of selected pro-viral host factors, including Cdc34 ubiquitin-conjugating enzyme, eEF1A, Pex19, and Vps4p AAA+ ATPase ESCRT factor, all of which are known to be involved in VRC assembly [43, 82, 84, 110, 120, 164, 173]. These host factors are more efficiently co-purified with p33 replication protein from *tub2^{ts}* yeast in comparison with wt yeast (Table 3.2). eEF1A is also involved in (-)RNA synthesis [84, 120], thus the more efficient subversion of eEF1A in *tub2^{ts}* yeast could be one of the reasons for the increased (-)RNA synthesis by the tombusvirus replicase. Based on these data, I propose that the dynamic microtubule-based cytoskeleton is important for the cell to restrict TBSV replication by (i) inhibiting the subversion of sterols and several pro-viral host factors for viral replication;

and (ii) facilitating the re-distribution of tombusvirus restriction factors into VROs, which must happen early during infection [89].

A model on the role of microtubules in tombusvirus replication. I propose that the dynamic cytoskeleton might hinder the ability of TBSV to subvert pro-viral host proteins or subcellular membranes due to the efficient transfer/movement of these factors via the cytoskeleton to their final (i.e., normal subcellular) destination in cells. In contrast, mutant cytoskeletal proteins could slow down these transport processes, giving more time for TBSV to hijack selected host proteins and membranes. Also, the more stable (less dynamic) cytoskeleton might help TBSV to build VROs around cytoskeleton hubs. Alternatively, the active/dynamic cytoskeleton restricts TBSV replication via facilitating antiviral responses and the delivery of cell-intrinsic restriction factors into tombusvirus VROs (Figure 3.11) [145]. These models are not mutually exclusive and could explain the enhanced TBSV replication in cells carrying mutant cytoskeleton or when the cytoskeleton is inhibited pharmacologically.

Table 3.1 List of primers used in Chapter 3

Primer #	Sequence
18	GTAATACGACTCACTATAGGAGAAAGCGAGTAAGACAG
22	GTAATACGACTCACTATAGGGCTGCATTTCTGCAATGTTCC
1165	AGCGAGTAAGACAGACTCTTCA
1190	GGGCTGCATTTCTGCAATG
2215	CTGCAGCGAGGAGCCGTAAT
3152	CGCGGATCCATGATTCAAGATCCCCTTGTA
3196	CCGCTCGAGTTAGGAGAAAACTTTGATAT
3993	GGAAGTAGCATAAGATGGCAGATGGAGAGG
3994	CCAGATCTTCTCCATATCATCCCAGTTGCTGAC
4719	AAGCAGAAGCACGAAACAAGGAGGCAAACCACTAAAAGGAT GCGTACGCTGCAGGTCGAC
4720	TATATATTCTGGTGTGAGTGTGAGTACTTATTCAGAGATTAAT CGATGAATTCGAGCTCG
4721	GGCTGTGTTCAAGTTCCCGTC
5433	ATTCTTGAAGATTTTGCTACTCAGG
5434	GCTGTAGCGATCATTGAGAGTTTC
5435	CGCCGAATTCCAGATCGGAATGGAGTTCTGGA
5436	CGCCACGCGTCATGCCTGAGCCAGTTCC
5437	CGCCGAATTCCAGGATACATGAATAACGACTTGGT
5438	CGCCACGCGTGCTTGTCTCTTTCTCAATTTATCGT
5591	CGCCGAATTCGCGGCAATGCGGTAAC
5592	CGCCACGCGTATCCTTGCAAGCAATCACAA
5593	CGCCGAATTCCAATACATTTCCCTCACAGTGC
5594	CGCCACGCGTTGAACATGGCTGTGAACTGCT
5595	TCACTTGGTGGAGGGACTGG

Table 3.1 (continued)

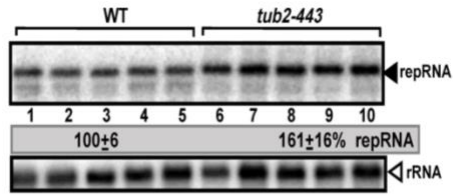
5596	AGAGGTCAATGGTGCAAAGC
6243	CGCGTCGACAGGAATAATTCATACGGCAAATTTCTTCAT
6244	CGCGCTAGCAAATTCCTCTTCCTCAGCGTATG
6513	CGCGGAGCTCTTACTGAGTCCGGACTTGTATAG
6624	GCTCTAGAGGTAAAGGAGAAGAACTTTTCACTGG

Table 3.2 Co-purified host proteins with p33 from tub2^{ts} yeast

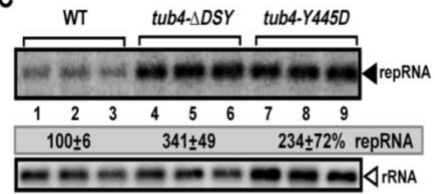
PROTEIN	PERCENTAGE
DED1 HELICASE	78+29
CDC34 E2 ENZYME	161+33
PBP2 RNA BINDING	106+11
PEX19 PEROXISOMAL	136+18
RH2 HELICASE (EIF4AIII)	97+15
RPN11 DEUBIQUITINASE	74+42
TDH2 GAPDH	84+5
TEF1 EEF1A	140+13
VAP27-1 (SCS2-LIKE)	186+27
VPS4 AAA+ ATPASE	137+31
VPS23 ESCRT I	114+10

Co-purification of the given host protein with p33 from wt yeast is taken as 100%

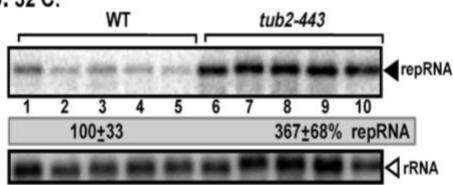
A. 23°C:



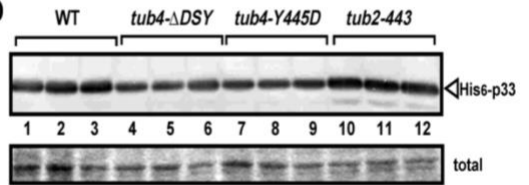
C



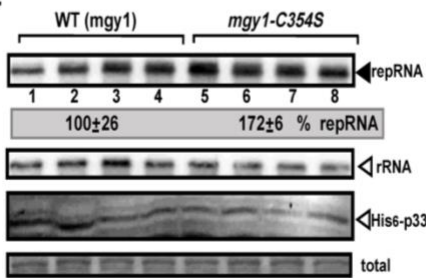
B. 32°C:



D



E



F

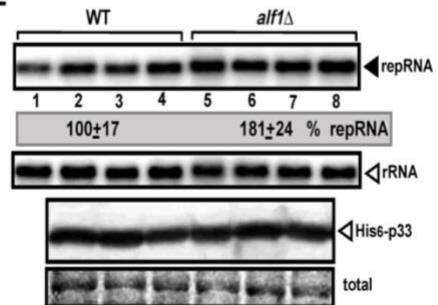
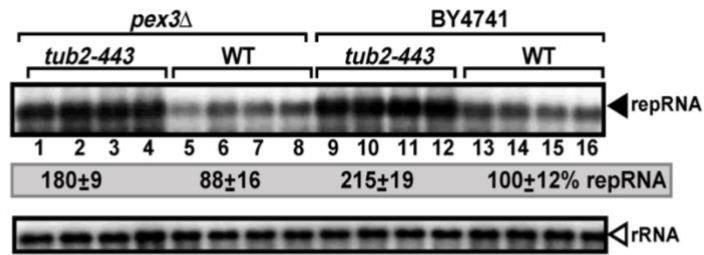


Figure 3.1

Figure 3.1. Temperature-sensitive mutations of β and γ tubulins increase TBSV repRNA accumulation in yeast.

TBSV repRNA replication was induced by expressing His₆-p33 and His₆-p92^{pol} from the copper-inducible *CUP1* promoter and TBSV DI-72(+) repRNA from the constitutive *ADHI* promoter. (A) Northern blot analysis showing the higher accumulation of TBSV repRNA in *tub2^{ts}* mutant compared to wt yeast at 23°C (permissive temperature). (B) Northern blot analysis showing the ~3-fold higher accumulation of TBSV repRNA in *tub2^{ts}* mutant compared to wt yeast at 32°C (semi-permissive temperature). (C) Mutations in *TUB4* γ tubulin gene increased TBSV repRNA accumulation (~2.5-3.5-fold) compared to wt yeast when grown at 32°C. (D) The accumulation of His₆-p33 replication was determined using western blot using anti-His antibody in wt, *tub2^{ts}* and *tub4^{ts}* yeast grown at 32°C. Lower panel shows total protein loading in SDS-PAGE stained with Coomassie blue. (E) A *TUB2* mutant yeast strain with a single cytoplasmic microtubule, supported a higher level of TBSV repRNA accumulation compared to the control strain MGY1. (F) Northern blot analysis of the TBSV repRNA accumulation in an *Alf1p* deletion mutant yeast compared to wt yeast strain. The *alf1* Δ yeast is deficient in microtubule formation and supported a ~2-fold increased level of repRNA. All experiments were repeated three times.

A. TBSV, 23°C:



B. CIRV, 32°C:

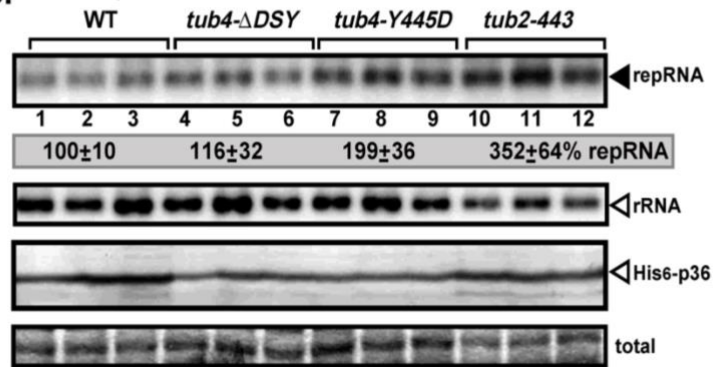


Figure 3.2

Figure 3.2. Microtubules restrict tombusvirus repRNA replication when it takes place at different subcellular locations in yeast.

Northern blot analysis was used to detect DI-72(+) repRNA accumulation, which was normalized based on 18S rRNA. (A) Expression of the mutant *tub2^{ts}* gene in the *pex3Δ* yeast mutant supported a ~2-fold higher accumulation of TBSV repRNA compared to *pex3Δ* expressing the *TUB2* wt gene. Replication in any of the *pex3Δ* mutants take place in the ER due to the absence of peroxisomes. These experiments were performed at 23 °C. (B) CIRV repRNA accumulation in *tub4^{ts}* and *tub2^{ts}* mutant yeast increased ~2-3-fold compared to wt yeast strain when grown at 32 °C. Lower panel: Western blot analysis of the levels of CIRV His₆-p36 replication protein (detected with anti-His antibody) in the mutant and wt cells. Bottom panel: Total protein loading in SDS-PAGE stained with Coomassie blue.

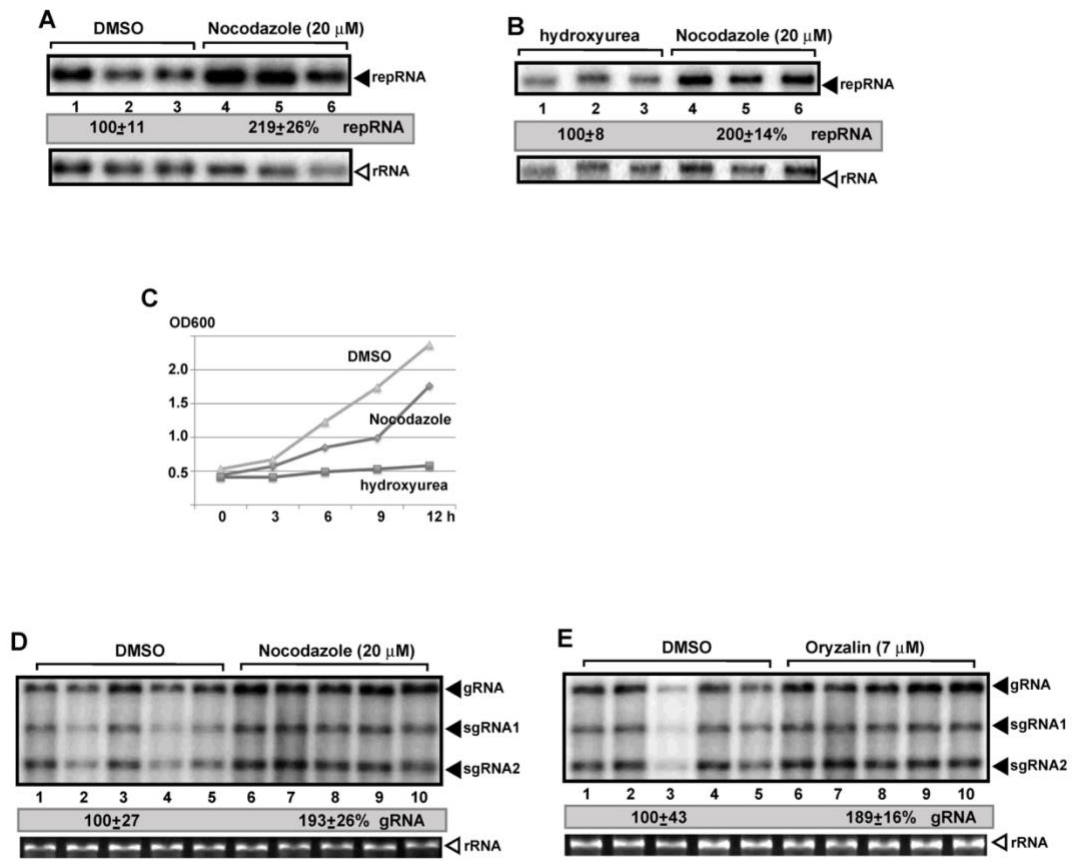


Figure 3.3

Figure 3.3. Pharmacological inhibitors of microtubules enhance TBSV RNA accumulation in yeast and *N. benthamiana* protoplasts.

Accumulation of TBSV repRNA in yeast and protoplast cells treated with pharmacological inhibitors. (A) Treatment of wt yeast cells with nocodazole, a tubulin depolymerizing agent, led to a ~2-fold higher accumulation of TBSV repRNA. DMSO was used as control and did not affect replication. (B) Treatment of wt yeast cells with hydroxyurea, an inhibitor of cell cycle, led to lower accumulation of TBSV repRNA in yeast in comparison with the nocodazole treatment. The accumulation level of TBSV repRNA was normalized based on the rRNA. (C) Comparison of the effect of hydroxyurea and nocodazole on yeast growth at 29°C. The OD₆₀₀ measurements blotted on the graph show the extent of cell-cycle inhibition by these compounds as compared with DMSO over 12 h of continuous growth. Northern blot analysis was used to detect genomic TBSV gRNA accumulation in protoplasts treated with (D) nocodazole or (C) oryzalin to inhibit dynamic microtubule functions. Protoplasts from *N. benthamiana* were electroporated with TBSV gRNA and treated with the shown concentrations of the inhibitors. Comparable concentration of DMSO solvent was used as a control. The ethidium bromide-stained gel at the bottom shows ribosomal RNA as a loading control. Each of the experiments was repeated three times.

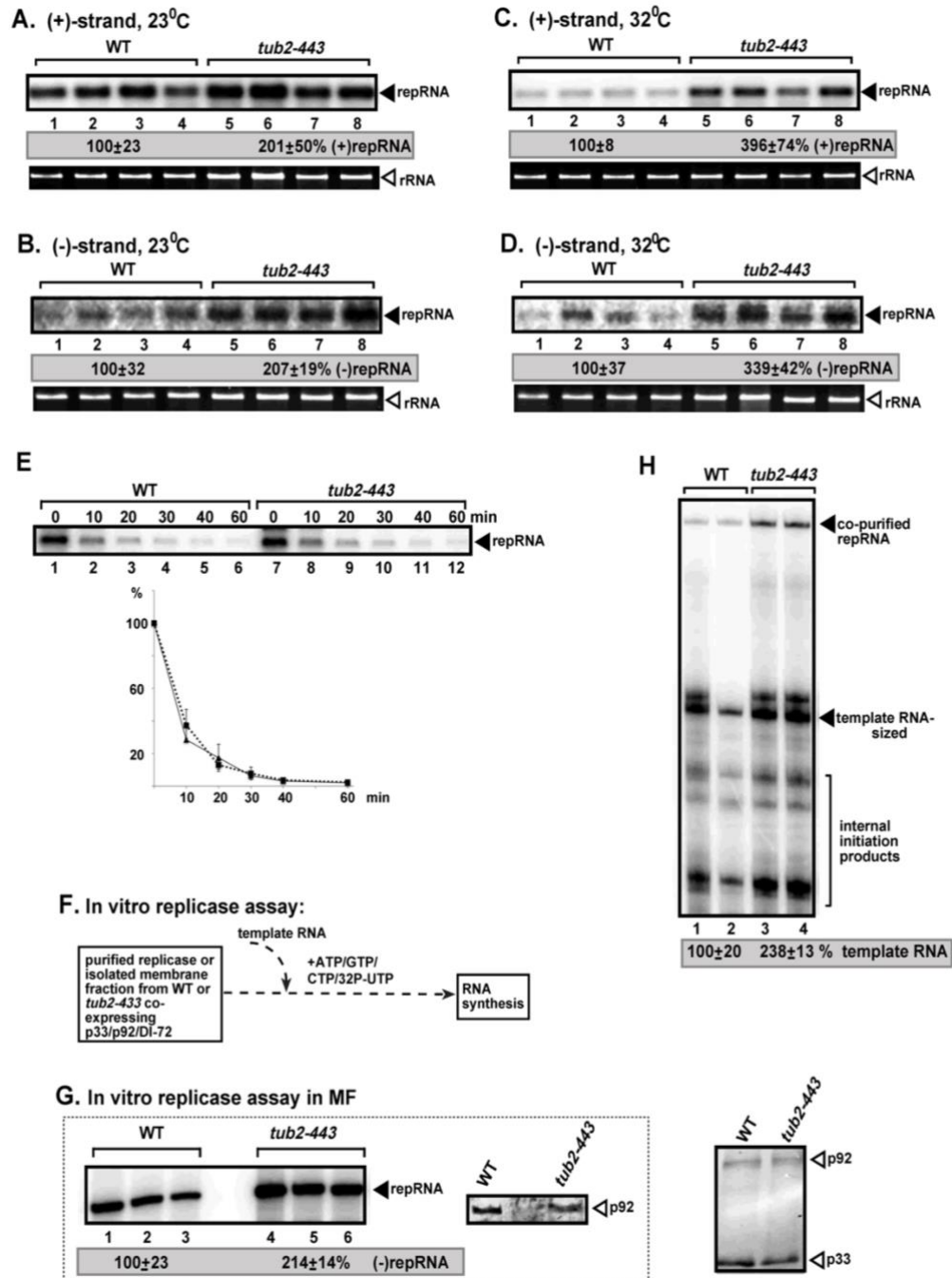


Figure 3.4

Figure 3.4 A beta-tubulin mutation affects viral RNA synthesis in yeast and in vitro.

The accumulation of (+) versus (-)-strand repRNAs in *tub2^{ts}* and wt yeasts was compared by northern blotting using strand-specific probes. (A) At the permissive temperature of 23 °C, (+) strand RNA accumulation is ~2-fold higher in the *tub2^{ts}* mutant, compared to wt cells. (B) The accumulation of (-) strand RNA at 23 °C is also ~2-fold higher in the *tub2^{ts}* mutant, compared to wt cells. When grown at 32 °C semi-permissive temperature, the *tub2^{ts}* mutant yeast showed a ~3-fold higher accumulation of both (+) strand RNA (C) and (-) strand RNA (D) compared to wt cells. (E) Comparison of repRNA stability in *tub2^{ts}* and wt yeasts in the absence of viral replication proteins at semi-permissive temperature (32°C). Triangles represent repRNA levels in *tub2^{ts}* mutant yeast whereas squares show the repRNA levels in wt yeast. Samples were collected every ten minutes for a 1 h period. Each experiment was repeated three times. (F) Scheme of the TBSV *in vitro* replication assay. The membrane-enriched fractions were prepared from *tub2^{ts}* and wt yeasts expressing the tombusvirus p33 and p92 replication proteins at the permissive temperature. Yeasts were also used to obtain Flag affinity-purified tombusvirus replicase preparations. Then, the same amount (1 µg) of DI-72(+) repRNA was added to each reaction, followed by *in vitro* tombusvirus replication assay. (G) Denaturing PAGE analysis shows the production of new ³²P-labeled viral repRNA in the membrane-enriched fractions. The western blot image on the right shows the level of His₆-p33 replication protein in the preparations using anti-His antibody (H) Denaturing PAGE analysis shows the production of complementary ³²P-labeled viral RNA by the affinity-purified tombusvirus replicase preparations. The template-sized RNA product (which was used for quantification) and shorter RNA products produced via internal initiation by the replicase are indicated with arrowheads. Western blot image on the bottom shows the level of Flag-p33 and Flag-p92 replication proteins in the replicase preparations using anti-Flag antibody.

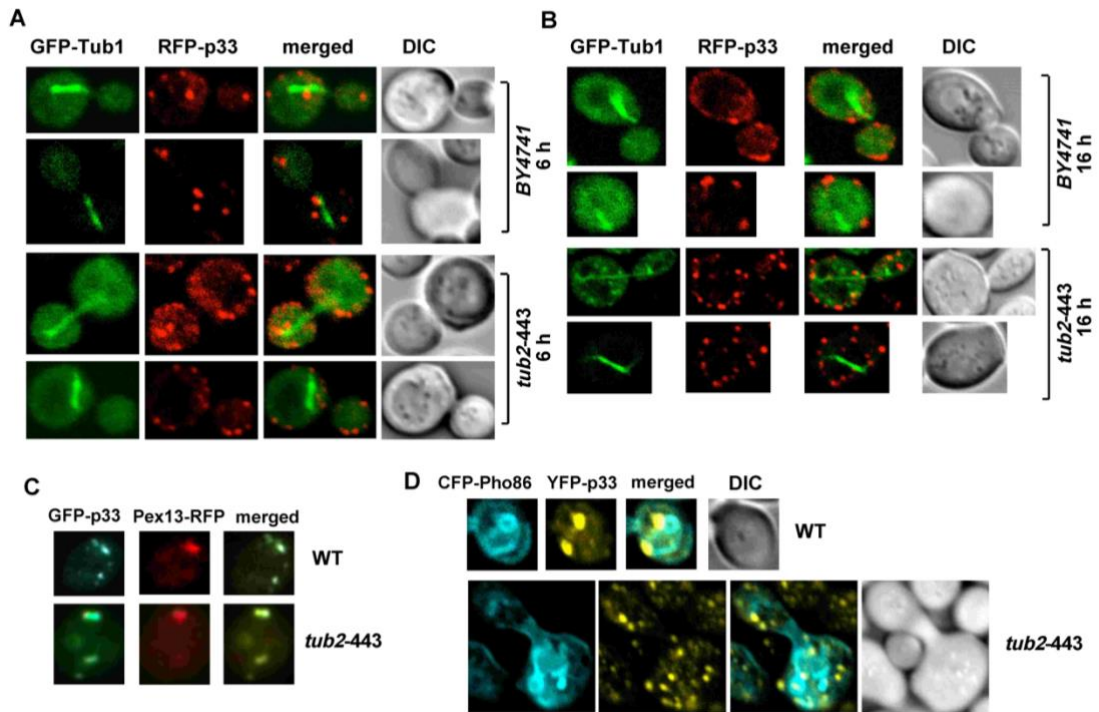


Figure 3.5

Figure 3.5. Microtubules localize at the vicinity of tombusvirus replication sites in yeast.

Confocal laser microscopy images show the partial co-localization of GFP-Tub1 with RFP-p33 expressed from *GAL1* promoter in (A) *tub2^{ts}* or (B) BY4741 wt yeast strains at semi-permissive temperature (32 °C). The merged images show that most of the p33-containing structures (marked with RFP-p33) were not located in proximity to microtubules (marked with GFP-Tub1) in both the *tub2^{ts}* mutant and wt yeast strains. (C) Co-localization of Pex13-RFP with GFP-p33 in *tub2^{ts}* or in wt yeast strains at semi-permissive temperature (32 °C). Note that Pex13 is a peroxisomal marker showing where TBSV forms VRCs and performs RNA replication. (D) Proximal localization of YFP-p33 with CFP-Pho86 in *tub2^{ts}* or in wt yeast strains at semi-permissive temperature (32 °C). Note that Pho86 represents an ER marker that shows where TBSV p33 participates in MCS formation.

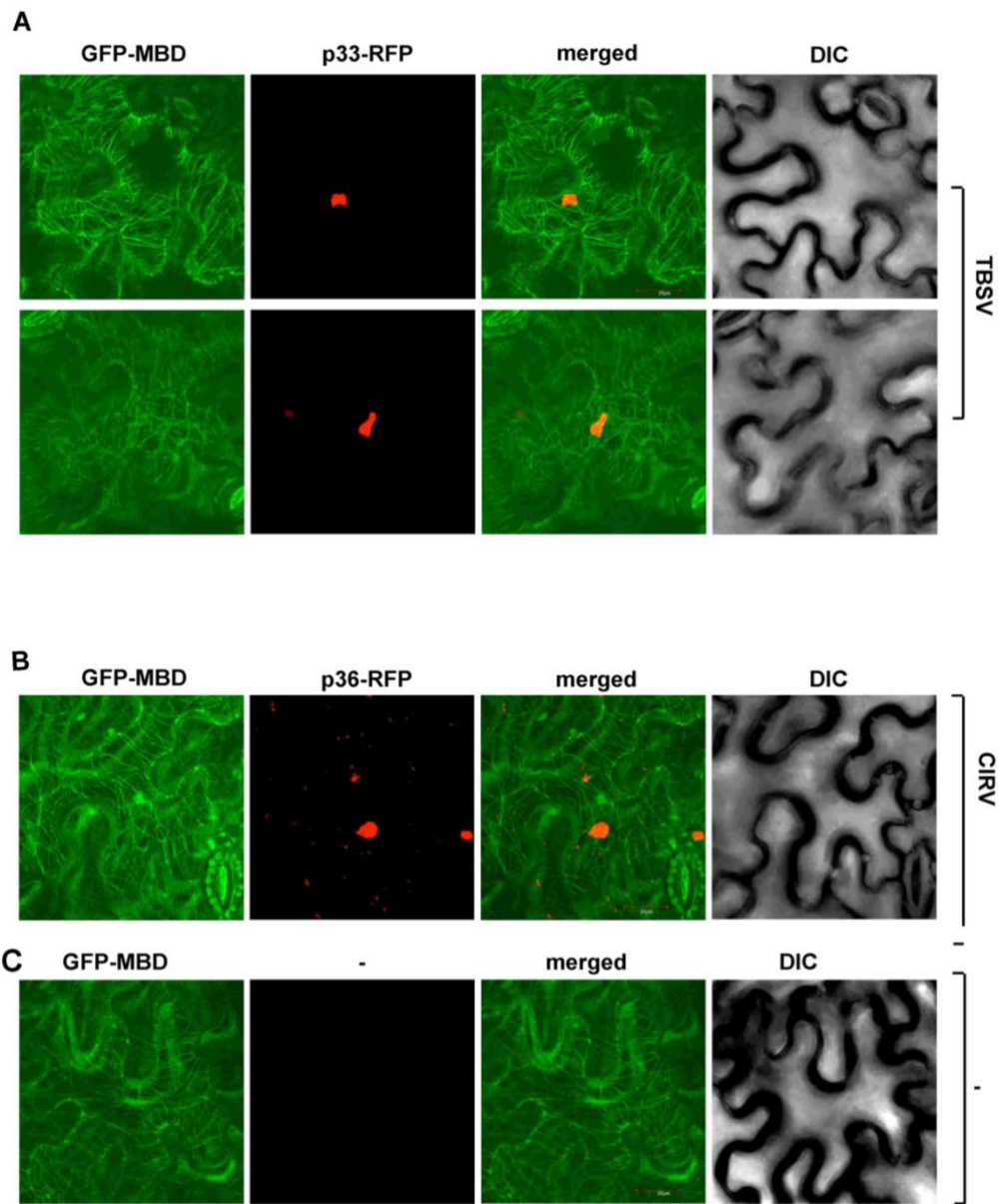


Figure 3.6

Figure 3.6. Microtubules localize at the vicinity of tombusvirus replication sites in plant.

The images represent Z-stack images (overlay of individual images). (A) The GFP-MBD microtubule marker was transiently expressed in *N. benthamiana* leaves along with the fluorescently tagged p33-RFP from TBSV. The large p33-RFP containing areas (i.e., VROs) are crossed by microtubules. (B) CIRV p36-RFP and GFP-MBD microtubule marker were transiently expressed in *N. benthamiana*. The p36-RFP decorated VROs are crossed by microtubules. (C) Control *N. benthamiana* leaves expressing only the GFP-MBD microtubule marker. The bar in the merged images represents 20 μm .

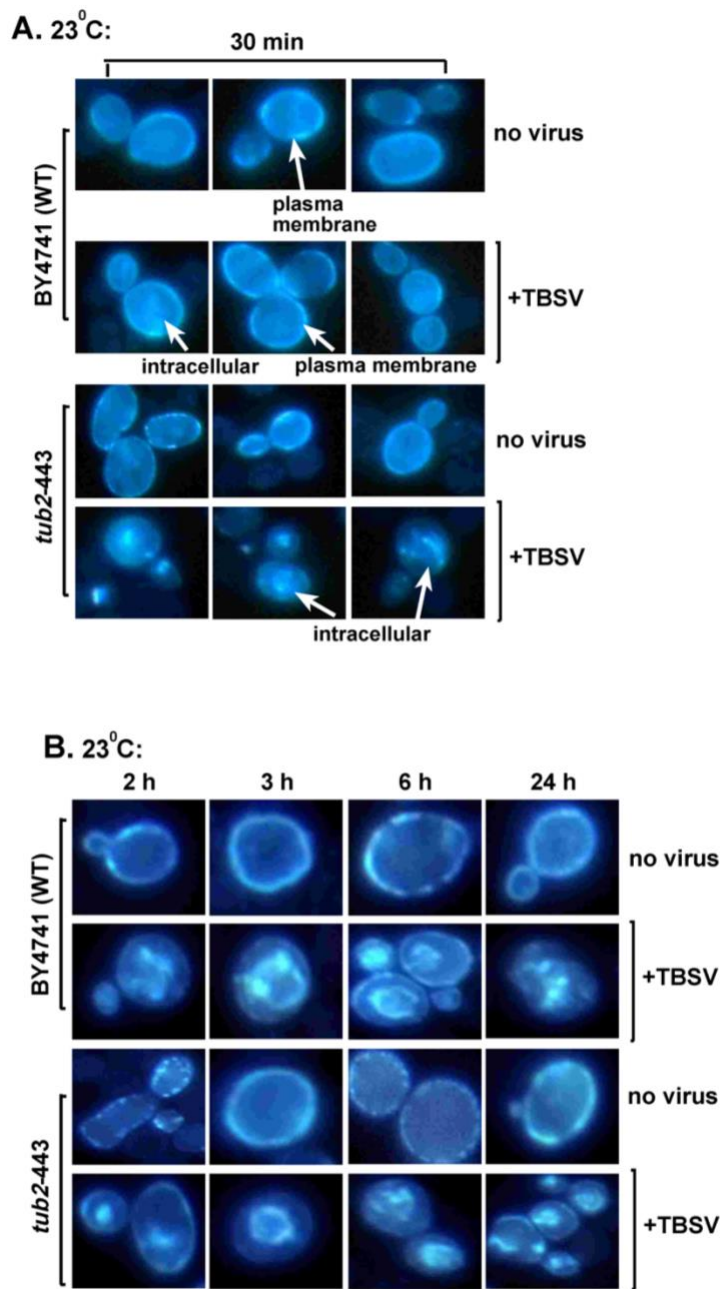


Figure 3.7

Figure 3.7. The $tub2^{ts}$ mutant facilitates the enrichment of sterols at the sites of tombusvirus replication in yeast.

Fluorescent microscopic images of yeast cells stained with filipin dye. Pictures were taken at different time points after launching RNA replication. (A) Re-localization of ergosterols to internal punctate structures in $tub2^{ts}$ yeast after inducing TBSV repRNA replication for 30 min. Note that at this early time point, filipin stains ergosterols present mostly at the plasma membrane in virus-free wt yeast cells. (B) Fluorescent microscopic images show similar enrichment of ergosterols at internal sites in wt and $tub2^{ts}$ yeasts replicating TBSV repRNA for 2 h, 3 h, 6 h and 24 h time points.

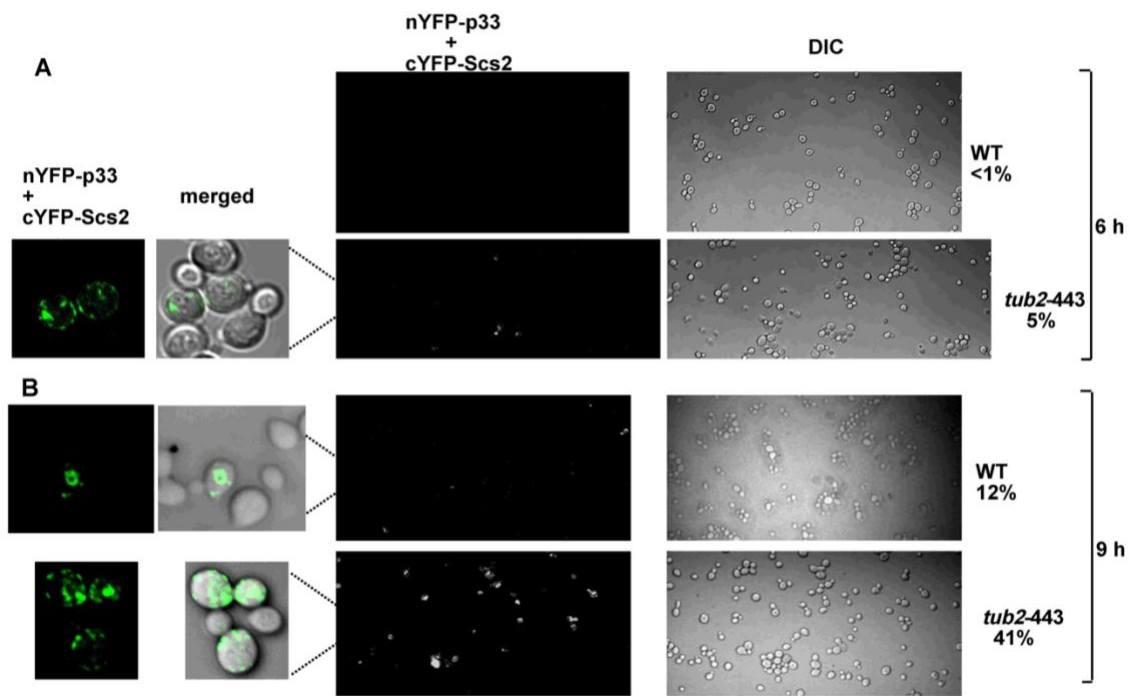


Figure 3.8

Figure 3.8. Rapid interaction between p33 replication protein and Scs2p VAP protein in *tub2^{ts}* yeast.

BiFC images show the binding of cYFP-Scs2 with nYFP-p33 expressed from *GALI* promoter in *tub2^{ts}* or in BY4741 wt yeast strains at semi-permissive temperature (32 °C). The % of yeast cells with positive BiFC signals is calculated based on ~500 cells. (A) BiFC signal is not detected (<1%) in wt yeast cells after 6 h of protein induction. In contrast, signal was detected in ~5% of *tub2^t* mutant yeast cells. Suggesting that the mutation in *tub2^{ts}* yeast allows cYFP-Scs2 and nYFP-p33 to meet more quickly inside the cell (B) After 9 h of protein induction in galactose medium, ~12% of wt yeast cells show BiFC signal. At this time point the percentage of *tub2^t* mutant yeast cells with BiFC signal increased to ~41%. For both panels, magnification images on the left show the distribution of BiFC signals (often seen as punctate structures) in single yeast cells.

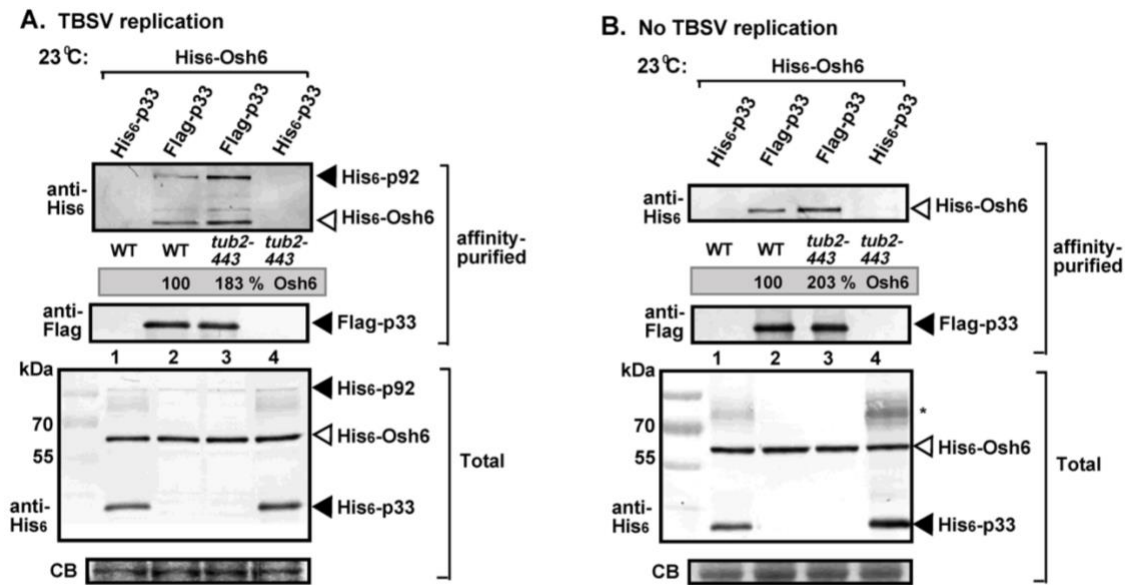


Figure 3.9

Figure 3.9. Enhanced co-purification of cellular ORP protein with the tombusvirus p33 replication protein from tub2^{ts} yeast.

The Flag-tagged p33 was Flag-affinity purified from solubilized membranous fraction of yeast extracts, in the presence (A) or absence (B) of TBSV replication. Top panels: Western blot analysis of the co-purified His₆-tagged Osh6p with anti-His antibody in the Flag-affinity-purified preparations. Middle panels: Western-blot analysis of the same samples as in the top panel but using anti-Flag antibody. Bottom panels: Western blot analysis of His₆-Osh6p or His₆-p33 (as a control) with anti-His antibody in the total protein extract from yeast expressing the shown proteins. CB: Coomassie-stained SDS-PAGE of total protein extract. Each experiment was repeated two times. In (A), yeasts supported TBSV repRNA replication (due to co-expression of p33 and p92 replication proteins), whereas yeast samples in (B) lacked p92 replication protein.

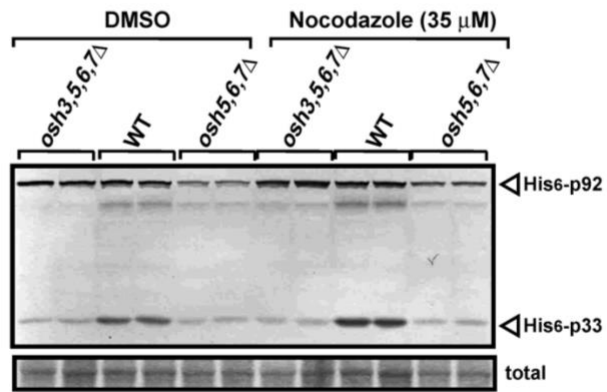
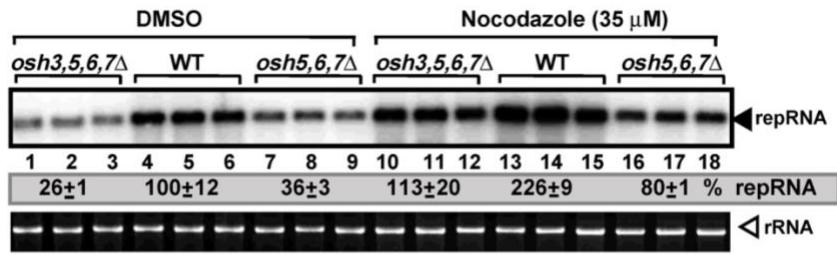


Figure. 3.10

Figure 3.10. The effect of nocodazole on TBSV repRNA replication in the absence of selected ORPs in yeast.

Top: The accumulation of TBSV repRNA was analyzed by northern blot in yeast lacking critical ORPs for TBSV replication. The *osh5,6,7Δ*, *osh3,5,6,7Δ* and wt yeast were treated with nocodazole to inhibit microtubule function. DMSO was used as a control. TBSV replicates poorly in *osh5,6,7Δ*, and *osh3,5,6,7Δ* yeast treated with DMSO when compared to the wt yeast. Nocodazole treatment led to increased replication in wt, *osh5,6,7Δ*, and *osh3,5,6,7Δ* yeast but the mutants lacking important ORPs were still not as efficient as wt yeast. Bottom: The replication proteins His₆-p33 and His₆-p92 levels were analyzed by western blot in the *osh5,6,7Δ*, *osh3,5,6,7Δ* and wt yeast treated with DMSO or nocodazole.

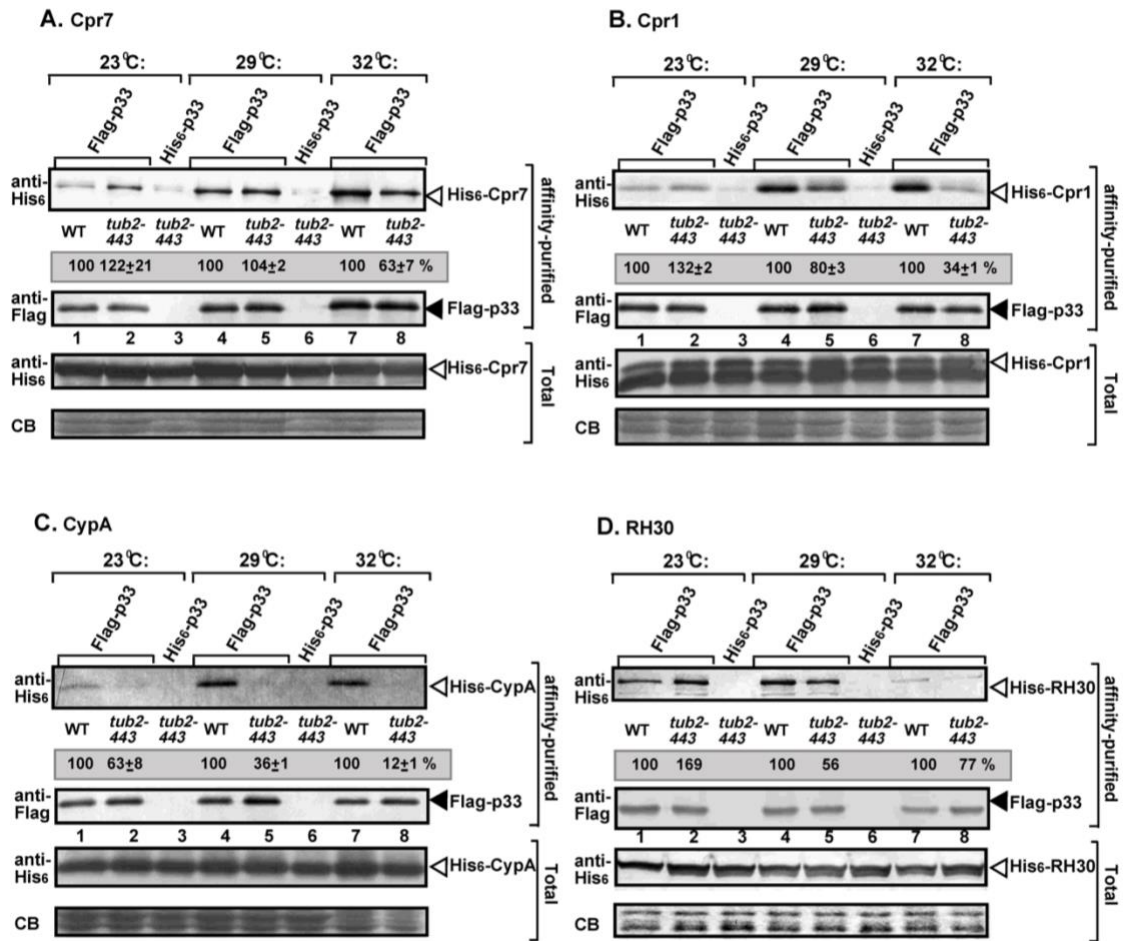


Figure 3.11

Figure 3.11. Reduced co-purification of cellular restriction factors with the tombusvirus p33 replication protein from tub2^{ts} yeast.

The Flag-tagged p33 was Flag-affinity purified from solubilized membranous fraction of yeast extracts. Yeasts were grown at three different temperatures as shown. Western blot analysis of the co-purified His₆-tagged (A) Cpr7, (B) Cpr1, (C) CypA, and (D) RH30 with anti-His antibody in the Flag-affinity-purified p33 preparations. The affinity purified p33 detected with anti-Flag antibody was used to normalize the samples. Bottom panels: Western blot analysis with anti-His antibody of the total protein extracts from yeasts expressing the shown proteins. CB: Coomassie-stained SDS-PAGE of total protein extracts. Standard error is shown. Each experiment was repeated three times.

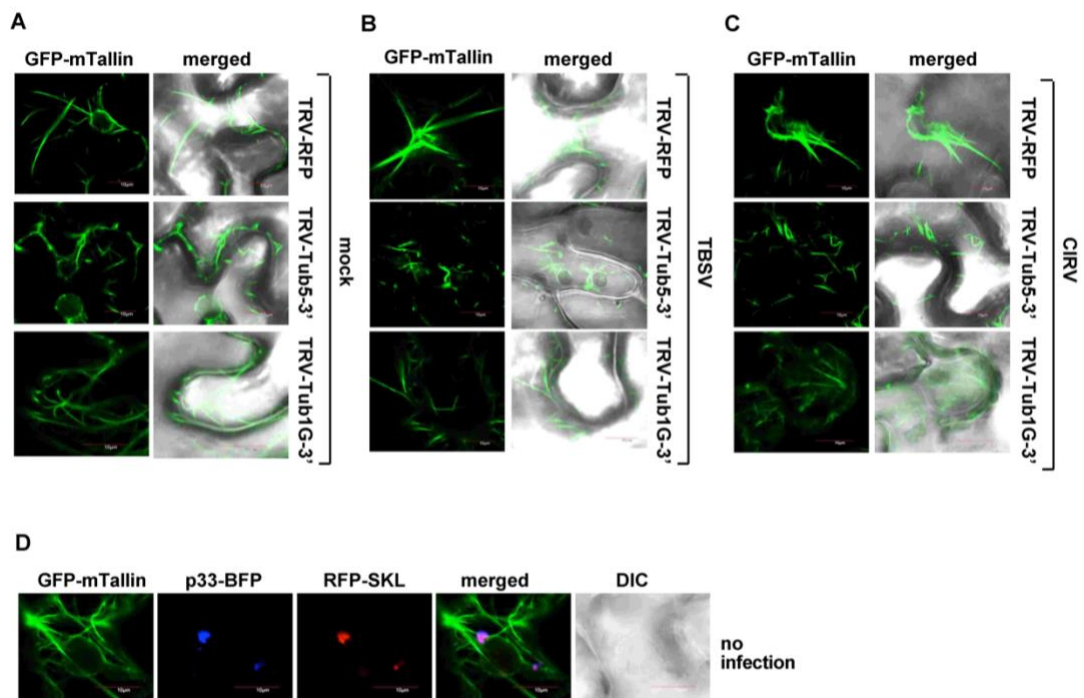


Figure 3.12

Figure 3.12. Knock down of *Tub5* or *TubG1* interferes the formation of actin filaments and cables in plants.

Transgenic *N. benthamiana* plants expressing GFP-mTalin were treated for VIGS to knock down *Tub5* or *TubG1* genes. After 11 d of silencing treatment, leaves were (A) mock inoculated, (B) inoculated with TBSV sap or (D) CIRV sap. Actin filaments are stabilized by TBSV and CIRV infection (B and C, top panels) but this is lost in cells with depleted *Tub5* or *TubG1* (B and C middle and bottom panels). (D) Co-expression of p33-BFP and RFP-SKL in GFP-mTalin mock infected plants shows actin filaments in the vicinity of VROs.

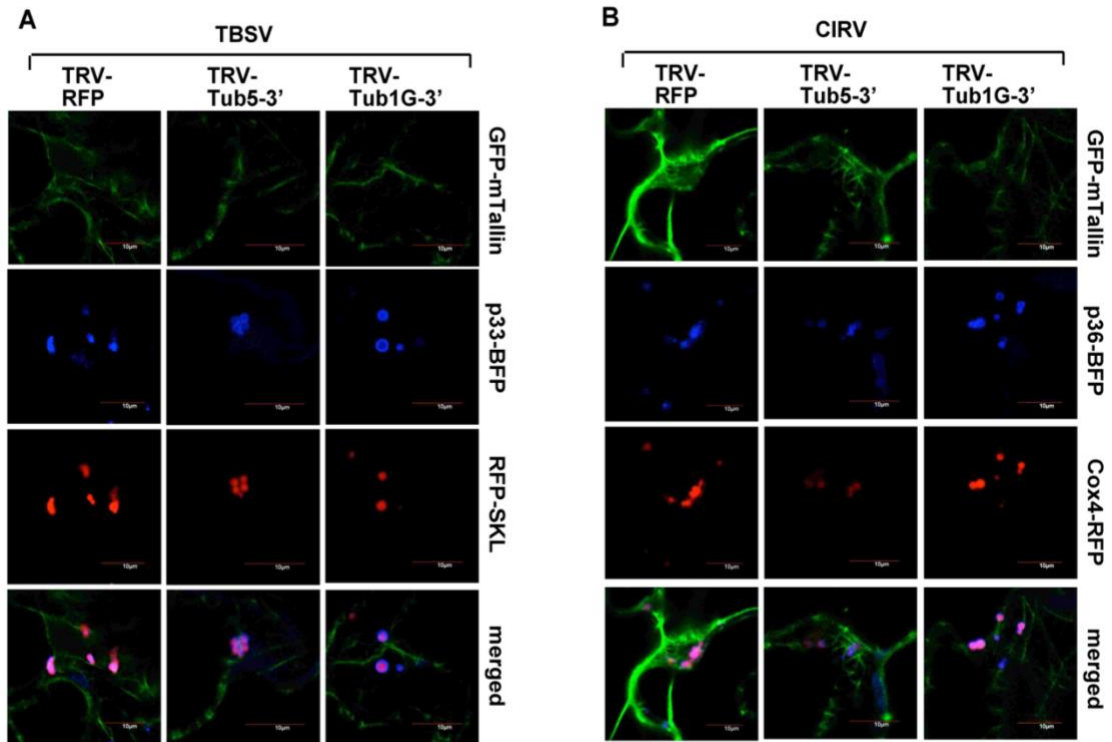


Figure 3.13

Figure 3.13. The microtubule cytoskeleton is important for the biogenesis of tombusvirus VROs.

Transgenic *N. benthamiana* plants expressing GFP-mTalin were treated for VIGS to knock down Tub5 or TubG1 genes. After 11 d of VIGS treatment, BFP-p33 and RFP-SKL (peroxisomal marker) or Cox4-RFP (mitochondrial marker) were co-expressed via agroinfiltration and then inoculated with TBSV or CIRV sap. (A) TBSV infection induced a lesser aggregation of peroxisomes (p33-decorated VROs) in plant cells with depleted Tub5 (middle column) or TubG1 (right column) compared to TBSV infected control plants (left column). (B) Lesser aggregation of mitochondrial VROs is observed in Tub5 and TubG1 silenced plants and infected with CIRV (middle and right columns) compared to control plants (right column). Despite the weak aggregation of peroxisomal or mitochondrial membranes in Tub5 and TubG1 depleted cells, VROs were still associated with actin filaments, which suggests that microtubules and the cytoskeleton in general is important for the biogenesis of virus induced VROs in plants.

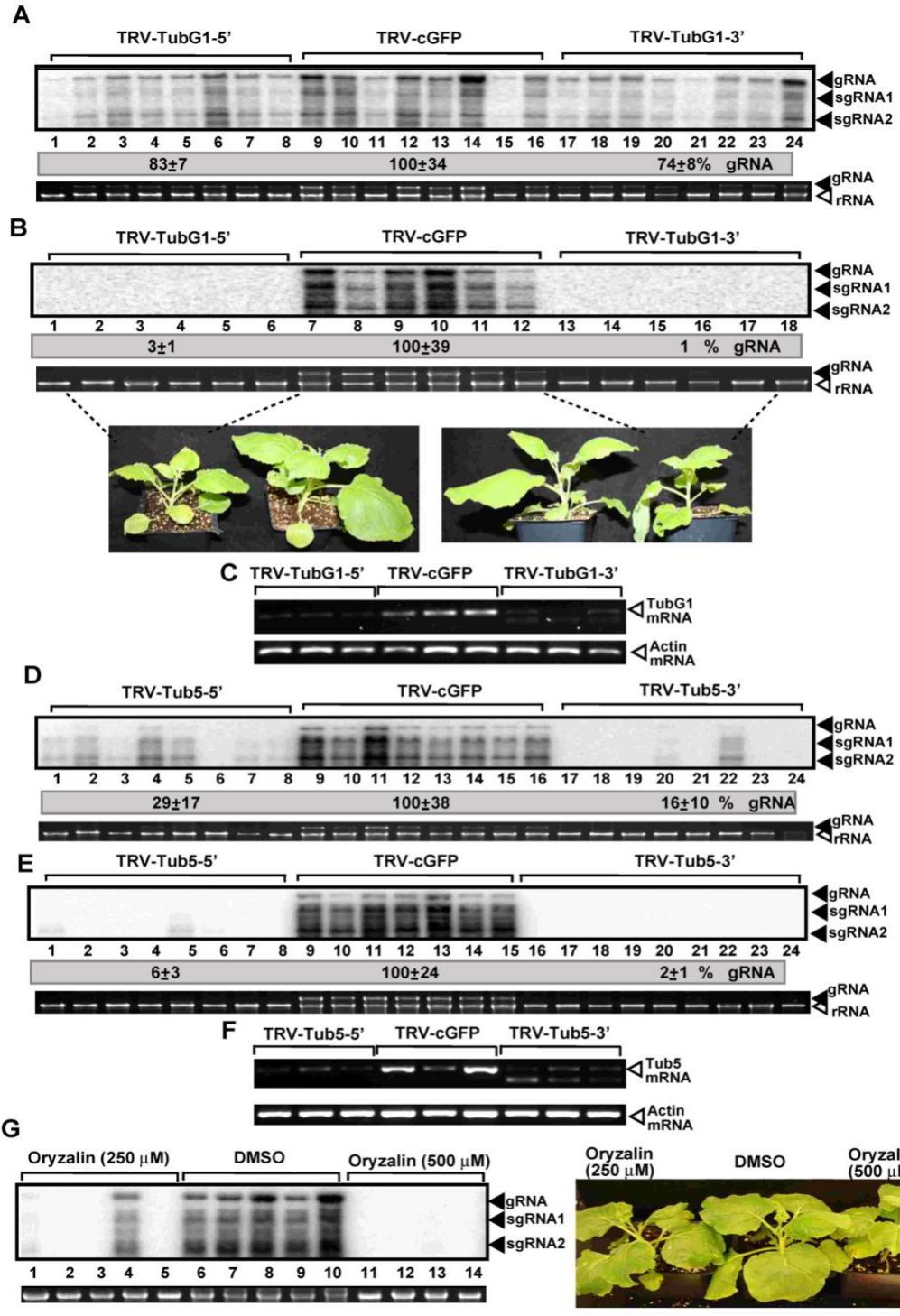


Figure 3.14

Figure 3.14. Silencing of *Tub5* and *TubG1* in *N.benthamiana* plants reduces TBSV RNA accumulation.

(A, B) Top: northern blot analysis of tombusvirus gRNA and sgRNAs accumulation in *TubG1* silenced plants inoculated with TBSV. VIGS was performed via agroinfiltration of tobacco rattle virus (TRV) vector carrying 5' or 3'-terminal *TubG1* sequences or 3'-terminal *GFP* sequences as control. The 3' end specific probe used for northern blot shows reduced accumulation of both gRNA and sgRNAs in silenced plants than in control plants. Bottom: Ethidium bromide-stained gel to visualize rRNA levels in each sample as a loading control. Samples were taken either (A) 2 d post infection from infected leaves or (B) 4 d post infection from systemic leaves. (B, bottom panel) *TubG1* silenced plants are smaller in size compared to control plants. (D, E) Top: northern blot analysis of tombusvirus gRNA and sgRNAs accumulation in *Tub5* silenced plants inoculated with TBSV. VIGS was performed via agroinfiltration of tobacco rattle virus (TRV) vector carrying 5' or 3'-terminal *Tub5* sequences or 3'-terminal *GFP* sequences as control. The 3' end specific probe used for northern blot shows reduced accumulation of both gRNA and sgRNAs in silenced plants than in control plants. Bottom: Ethidium bromide-stained gel to visualize ribosomal RNA levels in each sample as a loading control. Samples were taken either (D) 3 d post infection from infected leaves or (E) 5 d post infection from systemic leaves. (C, F) Silencing confirmation was performed by analyzing *TubG1* and *Tub5* mRNA levels with semi-quantitative RT-PCR in silenced and control plants. (G) Pharmacological disruption of dynamic microtubules with oryzalin results in a major reduction of TBSV RNA accumulation in plants. DMSO was used as treatment control. Right: oryzalin treatment slightly inhibits the growth of leaves compared to control plants.

Chapter 4

EPIGENETIC REPROGRAMMING OF THE HOST BY RECRUITMENT OF THE CENTROMERIC HISTONE 3 BY A CYTOSOLIC RNA VIRUS

4.1 Introduction

Positive-strand (+)RNA viruses use the abundant resources of the host cells to build large viral replication compartments/organelles (VROs) which support their replication in a membranous protective microenvironment [3, 36, 107, 174-176]. Tomato bushy stunt virus (TBSV), a (+)RNA virus, has been intensively studied to decipher virus-host interactions, virus replication and recombination. An emerging theme from TBSV studies is that this cytosolic replicating virus dramatically remodels subcellular membranes, hijacks various transport vesicles and co-opts numerous host proteins to facilitate various steps in the robust viral replication process [5, 89]. Interestingly, however, the originally available resources in the host cells seem to be insufficient to provide optimal conditions for robust TBSV replication. Accordingly, ever-increasing data show that TBSV dramatically rewires metabolic processes, alters the lipid compositions of the targeted endomembranes and organelles, and induces host gene expression to increase host factors, which are co-opted for TBSV replication in the infected cells [5, 89, 117].

TBSV by coding only for two viral replication proteins, termed p33 and p92^{pol}, which are essential for virus replication [81, 111], cannot achieve all the above cellular

changes without the major assistance of co-opted host enzymes and pathways [4, 5, 110]. Therefore, a major frontier in virus-host interaction studies is to advance our understanding of how a (+)RNA virus can rewire cellular pathways and optimize the cellular milieu that then will support robust viral RNA replication. Yet, the picture of virus-host interactions is further complicated by host responses, including an arsenal of restriction factors, which inhibit the viral invasion and replication.

Using a library of temperature-sensitive mutants of yeast (a model host for TBSV), I identified Cse4 centromeric H3 protein variant as a restriction factor for TBSV replication [25]. Based on a protein network analysis, I found that Cse4 is one of the most highly connected nodes among the ~500 host factors identified, which affect TBSV replication or TBSV-host interaction in yeast [24, 27, 82, 83, 113, 177]. This is a surprising discovery, because the DNA-binding nuclear histone proteins are not known to function as antiviral proteins against the cytosolic RNA viruses. Therefore, I decided to dissect the function of Cse4 (called CenH3 in plants and CENP-A in humans) in TBSV replication.

The nucleus of a eukaryotic cell is full of nucleic acid binding proteins, which can potentially be used by the host to fight viral infections. Indeed, many well-characterized nuclear proteins shuttle in and out of the nucleus, making it possible that these cellular proteins could also function in the cytosol [110]. The evolutionarily conserved histone H3 variant, CenH3 is essential for chromosome segregation by marking the centrosome. This protein is so conserved in eukaryotes, such that the yeast Cse4p can complement human CENP-A [178]. CenH3 binds to long noncoding RNAs in the nucleus, which helps CenH3 localize to the centromeric portion of chromosomes [179]. Mislocalization or

overexpression of CenH3 has been found in many cancers and associated with aneuploidy in *Drosophila* [106, 180, 181].

In this chapter, I studied the role of CenH3 in TBSV replication in yeast, plants and *in vitro*. Based on knockdown, mutation or over-expression experiments, it is shown that CenH3/Cse4p acts as a cellular restriction factor against TBSV replication. CenH3/Cse4p was found to be partially re-targeted from the nucleus into the cytosolic VROs. *In vitro* works showed that CenH3/Cse4p binds to the viral RNA and acts as an RNA chaperone. Co-purification and pulldown experiments demonstrated interaction between CenH3/Cse4p and the viral p33 replication protein. However, subsequent analysis revealed that TBSV hijacks CenH3/Cse4p into VROs to sequester this histone 3 variant away from the nucleus, which can affect expression of a set of host genes. These genes include pro-viral host factors. I chose to further test the role of CenH3/Cse4p in regulating the glycolytic and fermentation pathways, which are co-opted by tombusviruses. These pathways are usurped by TBSV to provide plentiful ATP within VROs to fuel the activities of additional co-opted host proteins, such as Hsp70, the ESCRT-associated Vps4 AAA ATPase and DEAD-box helicases needed for robust viral replication [122-124, 153, 182]. Altogether, the data gathered suggests that subversion of CenH3/Cse4p into VROs facilitates epigenetic reprogramming of the cells, which ultimately leads to more efficient ATP generation locally within VROs to support the energy requirement of virus replication.

4.2 Materials and Methods

Yeast strains and expression plasmids. *Saccharomyces cerevisiae* strain BY4741 (*MATa*, *his3 Δ 1*, *leu2 Δ 0*, *met15 Δ 0*, *ura3 Δ 0*) was obtained from Open Biosystems. The temperature-sensitive strain *cse4-1* was a generous gift from C. Boone (University of Toronto) [139]. The following yeast expression plasmids have been previously described: HpGBK-CUP1-Hisp-33/ADH1-DI-72 (*HIS3* selection) [83], LpGAD-CUP1-His-p92 (*LEU* selection) [13]. UpESC-GAL10-DI72/GAL1-His-p33 (*URA3* selection), TpGAD-CUP1-His-92 (*TRP1* selection) [43]. HpGBK-CUP1-His-p33/GAL1-DI-72 (*HIS3* selection), HpGBK-CUP1-Flag-p33/GAL1-DI-72 (*HIS3* selection), LpGAD-CUP1-His-p92 (*LEU2* selection), LpGAD-CUP1-Flag-p92 (*LEU2* selection) [38]. HpESC-GAL1-Hisp36/GAL10-DI-72 (*HIS3* selection) [32]. LpESC-CUP1-Flag-CIRVp95 to be described elsewhere (*LEU2* selection, J. Pogany and P.D. Nagy, unpublished). Overexpression plasmid pGAL-myc-CSE4 was donated by Dr. Sue Biggins (Fred Hutchinson Cancer Research Center) [183]. Plasmid UpESC-His-AtCENH3, used for overexpression of *A. thaliana* CENH3 in yeast, was created by the PCR amplification from total *A. thaliana* cDNA with primers #6376/#6377 followed by insertion into UpESC vector after digestion of both the PCR and the vector with *EcoRI* and *BglII* restriction enzymes.

For expression of the CSE4 truncation mutants in yeast and *E. coli*, reverse primer #6809 and forward primers #6329 (for CSE4), #7080 (for *cse4 Δ N50*), #7081 (for *cse4 Δ N80*), #7083 (for *cse4 Δ N129*) were used for the amplification of the Δ N fragments, whereas forward primer #6329 and reverse primers #7112 (for *cse4 Δ C60*) and #7113 (for *cse4 Δ C100*) were used for the amplification of the Δ C fragments. All PCR products were

digested with *Bam*HI and *Xho*I restriction enzymes and inserted into similarly digested pYES vector (for expression of His-tagged proteins in yeast) generating plasmids UpYES-His-CSE4, UpYES-His-cse4ΔN50, UpYES-His-cse4ΔN80, UpYES-His-cse4ΔN129, UpYES-His-cse4ΔC60 and UpYES-His-cse4ΔC100. The same *Bam*HI/*Xho*I digested truncation fragments were also cloned into pGEX-His-RE and pMALc2X vectors (previously digested with *Bam*HI/*Xho*I) for expression of GST or MBP fusion proteins in *E. coli*. generating plasmids pGEX-CSE4, pGEX-cse4ΔN50, pGEX-cse4ΔN80, pGEX-cse4ΔN129, pGEX-cse4ΔC60, pGEX-cse4ΔC100, pMAL-CSE4, pMAL-cse4ΔN50, pMAL-cse4ΔN80, pMAL-cse4ΔN129, pMAL-cse4ΔC60 and pGEX-cse4ΔC100. Similarly, AtCENH3 PCR product from total *A. thaliana* cDNA with primers #6331/#6609, was inserted into pGEX-his RE plasmid after digestion with *Bam*HI and *Xho*I, generating plasmid pGEX-AtCENH3.

For expression of 6xHis-tagged Histone H3 in yeast, the primers #7116/#7117 were used to amplify Histone H3 sequence from *S. cerevisiae* total cDNA. The product was digested with *Bam*HI and *Xho*I restriction enzymes, followed by cloning into equally digested pYES vector, generating plasmid UpYES-His-Histone H3.

The plasmid HpESC-GAL1-CFP-p33/GAL1-DI72 (*HIS3* selection) [123] was used for confocal laser microscopy as well as plasmid UpYES-GAL1-YFP-CSE4, which was created by PCR amplifying the YFP sequence with primers #1291/#1295 using UpYES-YFP-p92 as template. The PCR product was then cloned into UpYES-His-CSE4 plasmid at the *Bam*HI site.

Plant expression plasmids. The plant expression plasmids pGD-T33-BFP, pGD-RFP-SKL, pGD-Cox4-RFP, pGD-p19 and pGD-C36-BFP have been described before [32, 46]. VIGS plasmids were created as follows: The *Nicotiana tabacum* sequence for *CENH3* was used to do a blast in Benthgenome database (Queensland University of Technology) and obtain the predicted cDNA sequence. To generate the VIGS constructs, 5' or 3' fragments of the NbCENH3 were PCR amplified from total *N. benthamiana* cDNA using primer pairs #6380/6381 and #6382/6383. The fragments were inserted into the plasmid pTRV2 [147] to generate pTRV2-5'CENH3 and pTRV2-3'CENH3. For plasmids pGD-AtCENH3 and pGD-NbCENH3, PCR products were obtained with primers #6378/#6379 from *A. thaliana* or *N. benthamiana* cDNA followed by digestion of the products with *Xho*I and *Sal*II restriction enzymes for insertion into pGD empty vector, generously donated by Dr. Michael Goodin (University of Kentucky) [184]. Plasmid pGD-DI-72(+)-MS2hp has been previously described [88]. Plasmids pGD-p33-ATeamYEMK and pGD-p36-ATeamYEMK have been described [185].

Yeast transformation and cultivation. Yeast strains were co-transformed with different combinations of plasmids using the lithium acetate (LiAc)–single-stranded DNA (ssDNA)–polyethylene glycol (PEG) method [148], and transformants were selected by complementation of auxotrophic markers by plating them on selective SC medium.

Analysis of tombusvirus replication in yeast. For TBSV repRNA accumulation, yeast strains BY4741 and cse4-1 were transformed with HpGBK-CUP1-Hisp-33/ADH1-DI-72

and LpGAD-CUP1-His-p92. Two sets of cultures per strain were grown at 23 °C 12 h overnight in SC-LH⁻ (synthetic complete medium without leucine and histidine) medium containing 2% glucose and 100 μM BCS (bathocuproinedisulfonic acid). Then, cells were centrifuged and washed thoroughly with clean SC-LH⁻ 2% glucose medium, to remove BCS, and pellets were re-suspended in the same medium containing 50 μM CuSO₄ to induce viral protein expression and repRNA replication. Then, a set of cultures was placed at 32 °C and the other set remained at 23 °C and grown for additional 24 h, time after which, total RNA and protein were extracted. For CIRV repRNA accumulation cells were co-transformed with plasmids HpESC-GAL1-Hisp36/GAL10-DI-72 and LpESC-CUP1-Flag-CIRVp95 and grown as above with the exception that pellets were thoroughly washed with SC-LH⁻ medium (2% galactose) and re-suspended in SC-LH⁻ medium containing 2% galactose and 50 μM CuSO₄. Total RNA and protein were extracted after 30 h of viral induction.

For overexpression analysis, BY4741 cells were transformed with plasmids HpGBK-CUP1-Hisp-33/ADH1-DI-72, LpGAD-CUP1-His-p92 and either UpESC empty vector, UpESC-HisAtCENH3, pGAL-myc-CSE4 or. Transformed cell were grown for 24 h in SC-ULH⁻ medium containing 2% galactose and 100 μM BCS. Cells then were centrifuged and washed thoroughly with clean SC-ULH⁻ 2% galactose medium and resuspended in the same medium containing 50 μM CuSO₄ to induce viral replication. Total RNA and protein were isolated after 24 h. The same method was used when expressing the CSE4 truncation mutants but BY471 cells were transformed with HpGBK-CUP1-Hisp-33/ADH1-DI-72, LpGAD-CUP1-His-p92 and either UpYES empty vector,

UpYES-His-CSE4, UpYES-His-cse4 Δ N50, UpYES-His-cse4 Δ N80, UpYES-His-cse4 Δ N129, UpYES-His-cse4 Δ C60, UpYES-His-cse4 Δ C100 or UpYES-His-Histone H3.

Tombusvirus replication assay in N. benthamiana plants. The virus-induced gene silencing (VIGS) in *N. benthamiana* was done as described previously [147, 154]. After 11 d of VIGS treatment (pTRV1 together with pTRV2-5'CENH3, pTRV2-3'CENH3-3' or pTRV2-cGFP) two distal leaves were sap inoculated with TBSV or CIRV virions. Samples were collected 2 d post-infection (dpi) for TBSV infected leaves or 3 dpi from CIRV infected leaves. Viral RNA accumulation was analyzed by northern blot after total RNA extraction. Silencing was confirmed by RT-PCR with primers oligo-d(T) (for RT) and #6380/6381 or #6382/6383, (for PCR) to detect CENH3 mRNA or primers #2859/#2860 to detect tubulin mRNA as amplification control.

To overexpress CENH3, *N. benthamiana* leaves were co-infiltrated with *Agrobacterium* containing pGD-p19 and either pGD empty vector, pGD-NbCENH3 or pGD-AtCENH3. In the experiment with CNV infection, plants were also infiltrated with *Agrobacterium* carrying pGD-CNV^{20KSTOP} 24 h after the first agroinfiltration. In the experiment with TBSV and CIRV infections, plants were inoculated with crude sap inoculum 48 h after agroinfiltration. Samples were collected from CNV infiltrated leaves about 84 h after the second agroinfiltration. For TBSV and CIRV infection, samples were taken from inoculated leaves 48 h and 72 h post-virus inoculation respectively. All samples were used for total RNA extraction and northern blot as described below, to analyze the accumulation levels of these viruses.

RNA analysis. Total RNA isolation and northern blot analysis were performed as described previously [13, 23] with a minor modification. Briefly, for extraction of total RNA, yeast cells were broken by shaking for 1 to 2 min at rt with equal volumes of RNA extraction buffer (50 mM NaOAc [pH 5.2], 10 mM EDTA, and 1% sodium dodecyl sulfate [SDS]) and water-saturated phenol and then incubated for 4 min at 65 °C. After a short incubation on ice and centrifugation at 4 °C for 10 min at 12,000 x g, the aqueous phase (~200 µl) was transferred to phenol-chloroform (~250 µl volume) mixed in 1:1 ratio, followed by vortexing, centrifugation (4 °C for 10 min at 12,000 x g) and ethanol precipitation of the aqueous phase. The obtained RNA samples were separated on a 1.5% agarose gel and transferred to a Hybond-XL membrane (Amersham) before hybridization with a ³²P-labeled DI-72-specific or 18S ribosomal probe [23]. Detection of (+)RNA was made via a ³²P-labeled DI-72-RIII/IV probe prepared with in vitro T7-based transcription using PCR-amplified DNA obtained on pGBK-CUP1-6xHis33/GAL1-DI-72 [38] template, with primers #22 and #1165. Viral RNA accumulation was normalized based on rRNA using the Image Quant software and a Typhoon scanner (General Electric).

Plant RNA isolation is almost the same as above with the difference that leaf discs are cut and frozen in liquid nitrogen, followed by a quick grinding (with a small blue pestle) before adding the RNA extraction buffer and phenol.

Protein analysis by Western Blot and Immunodetection. For protein analysis, yeast strains were grown as for RNA extraction. Pelleted cells were resuspended in 200 µl of 0.1M

NaOH and incubated at rt for 15 min while shaking in an Eppendorf shaker. NaOH was aspirated after a short centrifugation (rt for 1 min at 12,000 x g), and the pellets were re-suspended in 50 μ l of 1X SDS/PAGE buffer with 5% β -mercaptoethanol. After other 15 min of shaking at rt, samples were incubated at 85 °C for 15 min. After a 1 min centrifugation at 12,000 x g the supernatant was used for SDS/PAGE and western blot analysis as previously described [13, 25]. To detect CNV, TBSV and CIRV viral proteins the primary antibody was anti-6xHis (Invitrogen), and the secondary antibody alkaline-phosphatase-conjugated anti-mouse IgG.

Confocal laser scanning microscopy. To observe the subcellular localization of CENH3 in *N. benthamiana* epidermal cells, transgenic *N. benthamiana* (constitutively expressing H2B fused to RFP) leaves were agroinfiltrated with plasmids pGD-T33-BFP or pGD-C36-BFP ($OD_{600} \sim 0.3$), pGD-p19 ($OD_{600} \sim 0.3$) and pGD-GFP-NbCENH3 ($OD_{600} \sim 0.3$). Likewise, wild-type *N. benthamiana* leaves were agroinfiltrated with plasmids pGD-T33-BFP or pGD-C36-BFP ($OD_{600} \sim 0.25$), pGD-p19 ($OD_{600} \sim 0.25$), pGD-GFP-NbCENH3 ($OD_{600} \sim 0.25$) and either pGD-RFP-SKL ($OD_{600} \sim 0.25$) or pGD-Cox4-RFP ($OD_{600} \sim 0.25$). In the experiment with CNV infection, plants were also infiltrated with *Agrobacterium* carrying pGD-CNV^{20KSTOP} ($OD_{600} \sim 0.2$) and the rest of the agrobacteria was adjusted to $OD_{600} \sim 0.2$ each. Plants were additionally inoculated with TBSV or CIRV virions when needed. Live confocal images were obtained with an Olympus FV1000 microscope (Olympus America) 48 hrs. (for CNV and TBSV infection) and 72 hrs. (for CIRV infection) post virus infiltration or inoculation. BFP/Alexa 405, GFP/Alexa 488, and RFP

were excited using 405 nm, 488 nm, or 543 nm lasers, respectively. Images were obtained sequentially and merged using Olympus FLUOVIEW 1.5 software [46].

The subcellular localization of repRNA(+)-MS2hp RNA was observed in plant epidermal cells with C-terminal fusion of MS2 coat protein to GFP, which recognizes MS2 six hairpins inserted into repRNA(+) [9]. Transgenic *N. benthamiana* (constitutively expressing H2B fused to RFP) leaves were agroinfiltrated with agrobacteria carrying pGD-p33 (OD₆₀₀ ~0.2), pGD-p33-BFP (OD₆₀₀ ~0.2), pGD-GFP-MS2CP (OD₆₀₀ ~0.2), pGD-p92 (OD₆₀₀ ~0.2) and pGD-p19 (OD₆₀₀ ~0.15). Infiltrated leaves were then inoculated with DI72(+)-MS2hp or DI72 WT transcripts obtained by T7-based transcription using PCR-amplified DNA on pGD-DI-72(+)-MS2hp or pGBK-CUP1-6xHisp33/GAL1-DI-72. Approximately, 16, 24 and 48 h post transcript inoculation, confocal images were obtained as described above. Transgenic plants agroinfiltrated with pGD-GFP-MS2CP (OD₆₀₀ ~0.2) and pGD-p19 (OD₆₀₀ ~0.15) were used for a no replication control. To test if DI72(+)-MS2hp and DI72 WT transcripts are replication competent in the presence of co-expressed p33 and p92^{pol}, total RNA was isolated from agroinfiltrated plants at 16, 24 and 48 h time points and analyzed by northern blot with a ³²P-labeled DI-72-RIII/IV probe.

For confocal microscopy assays in yeast, BY4741 cells were co-transformed with plasmids UpYES-GAL-YFP-CSE4, LpGAD and HpESC empty vectors or UpYES-GAL-YFP-CSE4, LpGAD-CUP1-His-p92 and HpESC-GAL1-CFP-p33/GAL1-DI72. Transformed cell cultures were grown 12 h overnight in the proper SC-ULH⁻ containing 2% galactose and adding 100 μM BCS only when needed. Next morning cells were centrifuged and washed (with sterile water) and pellets re-suspended in the same medium with 2% galactose and 50 μM CuSO₄ to induce the expression of the fluorescently tagged

proteins. Samples were collected at the time points given in the main figure and analyzed by confocal microscopy as previously described [8].

Recombinant protein purification from E. coli. Recombinant proteins GST-CSE4, GST-AtCENH3, GST-cse4 Δ N50, GST-cse4 Δ N80, GST-cse4 Δ N129, GST, MBP-p33C, MBP-p33, MBP-p92^{pol}, MBP, MBP-CSE4, MBP-cse4 Δ N50, MBP-cse4 Δ N80, MBP-cse4 Δ N129, MBP-cse4 Δ C60 and MBP-cse4 Δ C100 were expressed in *E. coli* and purified as described [153, 186]. Briefly, *E. coli* strain BL21 (DE3) CodonPlus (Stratagene) cells were transformed with the above plasmids to express the recombinant proteins. The cells were then cultured at 37°C for 16h overnight in 2 ml of MB medium with 100 μ g/ml of ampicillin and 34 μ g/ml of chloramphenicol. The culture was then diluted with fresh MB medium with antibiotics to adjust the concentration to OD₆₀₀ ~0.2. After dilution, cultures were incubated at 37°C until reaching OD₆₀₀ ~1. Subsequently, the cultures were incubated at 16°C for 8 hrs. in the presence of isopropyl- β -D-thiogalactopyranoside (IPTG). The cells were then collected by centrifugation at 2,500 x g at 4°C for 5 min, followed by the resuspension with ice-cold column buffer (20mM HEPES [pH7.4], 25 mM NaCl, 1mM EDTA [pH 8.0]) containing 10 mM β -mercaptoethanol and 1 μ g of RNase A for each 4 ml of cell suspension. Sonication was performed on ice to get the cell lysates, followed by centrifugation at 12,000 x g at 4°C for 15 min. The obtained supernatant was incubated with GST bind resin (EMD Millipore) for GST fusion proteins or amylose resin (NEB) for MBP fusion proteins at 4°C for 2 h, respectively. The resin was then washed with ice-cold column buffer four times. The recombinant protein was eluted with column buffer

containing 10 mM glutathione and 1mM DTT in pH 7.5 for GST fusion proteins or 0.36% [W/V] maltose and 1mM DTT for MBP fusion proteins.

Yeast cell free extract (CFE) based in vitro replication assay. This assay was prepared using BY4741 yeast strain as described previously [15, 122]. Yeasts were grown at 23 °C, reaching OD₆₀₀ ~0.2, followed by heat treatment for 1 h at 37 °C. The individual CFE preparations were then adjusted to contain comparable amounts of total proteins. The *in vitro* CFE reactions were prepared in 20 µl total volume containing 1 µl of adjusted CFE, 0.5 µg DI-72 (+)RNA transcripts, 0.5 µg affinity purified MBP-p33, 0.5 µg affinity-purified MBP-p92^{pol}, 30 mM HEPES-KOH, pH 7.4, 150 mM potassium acetate, 5 mM magnesium acetate, 0.13 M sorbitol, 0.4 µl actinomycin-D (5 mg/ml), 2 µl of 150 mM creatine phosphate, 0.2 µl of 10 mg/ml creatine kinase, 0.2 µl of RNase inhibitor, 0.2 µl of 1 M dithiothreitol (DTT), 2 µl of 10 mM ATP, CTP, and GTP and 0.1 mM UTP, 0.1 µl of ³²P-UTP and 0.1, 0.2 or 0.4 µg of affinity purified GST-AtCENH3 or GST as control. Reaction mixtures were incubated for 3 h at 25 °C, followed by phenol/chloroform extraction and isopropanol/ammonium acetate (10:1) precipitation. ³²P-UTP RNA products were analyzed in 5% acrylamide/8 M urea gels [15, 122].

Gel mobility shift assay (EMSA) and RNA competition assay. Labeled RNAs for gel mobility shift experiments were prepared *in vitro* using T7 RNA polymerase. The labeled RNA probes were obtained using ³²P-UTP in the T7 transcription reaction followed by removal of free nucleotides using micro-Bio-Spin columns (Bio-Rad). Template DNA was

removed by DNase I, followed by purification of the RNA transcript with phenol-chloroform extraction and isopropanol precipitation. The pellet was washed with 70% ethanol to remove residual salts. The RNA transcripts were quantified by UV spectrophotometry with a Thermo Scientific™ NanoDrop™. EMSA assays have been described previously [10]. Briefly, the assay was performed with 0.1 pmol of ³²P-labeled RNA probes along with different concentrations (0.1, 0.2 or 0.4 μM) of purified recombinant GST fusion proteins or GST in the presence of RNA binding buffer (10 mM HEPES [pH7.4], 50 mM NaCl, 1 mM DTT, 1 mM EDTA, 5% Glycerol, 2.5 mM MgCl₂), 2 U of RNase inhibitor, as well as 0.1 μg of tRNA in a total of 10 μl reaction volume. After incubation of the reactions at 25°C for 30 min the samples were analyzed by 5% nondenaturing PAGE performed at 200 V in Tris-borate-EDTA buffer for 1 h in a cold room.

Both labeled and unlabeled RNAs competition experiments were prepared *in vitro* using T7 RNA polymerase. Two different amounts (2 and 4 pmol) of unlabeled RNAs (representing one of five regions of TBSV DI-72 RNA), together with 0.2 μM of either GST or GST-AtCENH3 were used for template competition in combination with the ³²P-labeled (+) repRNA or (-) repRNA template (~0.1 pmol). Once again, the binding reaction was performed in the presence of RNA binding buffer (10 mM HEPES [pH7.4], 50 mM NaCl, 1 mM DTT, 1 mM EDTA, 5% Glycerol, 2.5 mM MgCl₂), 2 U of RNase inhibitor, as well as 0.1 μg of tRNA. After incubation of the reactions at 25°C for 30 min the samples were analyzed by 5% nondenaturing PAGE performed at 200 V in Tris-borate-EDTA buffer for 1 h in a cold room.

dsRNA separation assay. Preparation of dsRNA samples was performed as described [186]. Briefly, unlabeled single-stranded DI-72 (+) RNAs were synthesized via T7 polymerase-based *in vitro* transcription. The ³²P-labeled single-stranded DI72(-) was synthesized by T7-based *in vitro* transcription using ³²P-labeled UTP. To prepare partial dsRNA duplexes, 2 pmol of ³²P -labeled DI72(-) were annealed to 6 pmol of unlabeled DI-72(+) in STE buffer (10 mM TRIS [pH 8.0], 1 mM EDTA, and 100 mM NaCl) by slowly cooling down the samples (in a total volume of 20 µl) from 94°C to 25°C in 30 min. Purified GST fusion proteins or GST as a negative control (2 µg) were added separately to the same amount of dsRNA duplex in the RNA binding buffer (10 mM HEPES [pH7.4], 50 mM NaCl, 1 mM DTT, 1 mM EDTA, 5% Glycerol, 2.5 mM MgCl₂) along with 1mM ATP, followed by incubation at 25°C for 25 min. The reaction mixtures were then treated with Proteinase K (2 µg/per reaction) at 37°C for 20 min, followed by loading onto 5% nondenaturing polyacrylamide gel with 200V for 1 h in a cold room. The gels were dried, exposed and analyzed in a phosphoimager.

Detection of host factors mRNA expression levels. For the mRNA detection in yeast, BY4741 and *cse4-1* cells were grown for 12 h at 32 °C. Total RNA was isolated and analyzed by gel electrophoresis in a 1.5% agarose gel to adjust the samples. The same amount of total RNA was used for semi-quantitative RT-PCR reactions. cDNA was first obtained using MMLV reverse transcriptase (Lucigen) and oligo dT. The cDNA was then used to perform the PCR reactions to detect several host factors with the following primers: #5992/#7136 (for CDC19); #7123/#7137 (for ENO2); #6275/#6367 (for PGK1);

#5621/#5604 (for PDC1); #4308/#7140 (for DED1); #2030/#7138 (for SSA1) and #7141/#7142 (for TEF1).

For mRNA detection in plant, a similar approach was performed by using wild-type and CENH3 knockdown *N. benthamiana* leaf samples. VIGS was performed as described above using the pTRV2-3'CENH3-3'construct only. After 12 d of VIGS treatment total RNA was isolated and used for semi-quantitative RT-PCR using the following primers: #6380/#6381 (for CENH3); #7293/#7294 (for ENO2); #7291/#7292 (for PGK1); #7289/#7290 (for PDC1); #7295/#7296 (for RH20/DDX3); #2534/#2535 (for Hsp70-1) and #7297/#7298 (for eE1A).

Real-Time quantitative PCR was also used for the detection of *N. benthamiana* gene expression as follows: VIGS was performed as described above using the pTRV2-3'CENH3-3'construct only. After 11 d of VIGS treatment, plants were inoculated with TBSV virions or rubbed with inoculation buffer (mock infection). Samples were collected 2 d post-inoculation from infected leaves and 4 d post-inoculation from systemic leaves. Total RNA was isolated and used for Real-time PCR. First, primers were designed using Real Time qPCR Tool from Integrated DNA Technologies website (<https://www.idtdna.com/scitools/Applications/RealTimePCR/>). Second, MMLV reverse transcriptase (Lucigen) and Oligo DT were used to obtain cDNA. Finally, the Real-Time PCR reactions were prepared using Applied Biosystem Power Up™ SYBR® green master mix (Thermo Fisher Scientific) in a 96 well plate and the Eppendorf's Mastercycler® ep realplex instrument and primers #8217/#8218 (for GAPC1); #8219/#8220 (for PGK1); #8221/#8222 (for CENH3); #8174/#8175 (for PDC1); #8176/#8177 (for PK1) and #8178/#8179 (for Tubulin β 2) as the housekeeping gene control. PCR conditions were

selected following the Power Up™ SYBR® green master mix user manual recommendations.

Visualization and measurement of ATP levels in plants. Intracellular ATP levels were visualized using the ATeam-based biosensor [187] by using a confocal microscope and measured by FRET analysis. To detect the ATP levels within the tombusvirus replication compartment in CENH3 silenced or control *N. benthamiana* plants (see above), leaves were co-agroinfiltrated with plasmids pGD-p33-ATeam^{YEMK}, pGD-p92, pGD-DI-72 and pGD-p19 (for CNV) or plasmids pGD-p36-ATeam^{YEMK}, pGD-p95, pGD-DI-72 and pGD-p19 (for CIRV). Samples were analyzed in a confocal microscope 2 d post-agroinfiltration. Confocal FRET images were obtained with an Olympus FV1000 microscope (Olympus America). Cells were excited by a 405-nm laser diode, and CFP and Venus were detected at 480–500 nm and 515–615 nm wavelength ranges, respectively. Each YFP/CFP ratio was calculated by dividing pixel-by-pixel a Venus image with a CFP image using Olympus FLUOVIEW software and ImageJ software.

In the case of CENH3 overexpression conditions, wild-type *N. benthamiana* leaves were co-infiltrated with the above plasmid combinations for CNV and CIRV with the addition of pGD-NbCENH3 plasmid as well. Confocal FRET images were obtained as above, 2.5 d post-agroinfiltration.

Visualization and measurement of ATP levels in yeast. To analyze the ATP level in the TBSV replication compartment in yeast, BY4741 and *cse4-1* cells were transformed with

plasmids LpGAD-ADH-ATeam^{YEMK}-p92^{pol}, UpYC-GAL1-DI-72 and HpESC-GAL1-p33/GAL10-pex13-RFP. Transformed yeast cells were pre-grown in SC-ULH- medium supplemented with 2% raffinose at 23 °C for 12 h overnight and then washed with sterile water and resuspended in SC-ULH- with 2% glucose for 1 hour at 32 °C. FRET images were obtained and analyzed as described above.

Protein co-purification assays in yeast cells. For the co-purification of CSE4 with Flag-p33 from cellular membranes, BY4741 yeast cells were co-transformed with plasmids HpGBK-CUP1-Flag-p33 (or HpGBK-CUP1-His-p33 as control), LpGAD-CUP1-Flag-p92 (or LpGAD-CUP1-His-p92 as a control), and UpGal-myc-CSE4. Cell growth and Flag-p33 purification from detergent-solubilized cellular membranes using anti-Flag M2 agarose was done as described previously [43]. Purified Flag-p33 was analyzed by western blot using anti-Flag antibody followed by anti-mouse antibody conjugated to alkaline phosphatase. Co-purified Myc-tagged proteins were analyzed with anti-Myc antibody followed by anti-mouse antibody conjugated to alkaline phosphatase. A similar approach was used for the co-purification of p33 with Flag-AtCENH3. Cells were transformed with plasmids HpGBK-CUP1-His-p33, LpGAD-CUP1-His-p92 and UpESC-GAL1-Flag-AtCENH3 (or UpESC-GAL1-His-AtCENH3 as a control). Cell growth and Flag-p33 purification using anti-Flag M2 agarose was done as described previously [43] but Flag-AtCENH3 was purified from the soluble fraction instead of the cellular membranes.

CSE4 Pull-down assay. This assay was performed as described previously [149]. Briefly, *E. coli* expressing GST-tagged p33C or GST were resuspended in ice-cold column buffer (10 mM Tris-HCl [pH 7.4], 1 mM EDTA, 25 mM NaCl, 10 mM β -mercaptoethanol) and lysed by sonication. The cleared lysate was passed through a column containing glutathione resin to capture the GST-tagged viral proteins or GST (negative control). The columns were washed three times with cold column buffer prior to the addition of recombinant MBP fusion proteins purified from *E. coli* (see above). The same amount of MBP fusion proteins were loaded onto columns with captured GST-p33C or GST, followed by incubation at 4 °C for 2 h. After washing the columns 5 times with chilled column buffer, the bound proteins were eluted with 50 ml SDS-PAGE sample buffer from the columns and analyzed by Western blotting using an anti-MBP antibody.

4.3 Results

The nuclear CenH3 histone variant restricts tombusvirus replication in yeast and plants. To explore the possible role of Cse4p (CenH3) in tombusvirus replication, I used the temperature-sensitive haploid yeast strain with a mutated single copy of *cse4-1* [25, 188]. Partial inhibition of Cse4p by growing the yeast *cse4-1* strain at the semi-permissive 32 °C resulted in a ~4-fold increased level of TBSV repRNA replication when compared with the BY4741 yeast strain carrying the WT copy of *CSE4* (Figure 4.1A, compare lanes 13-16 to 9-12). TBSV replication was also higher in the *cse4-1* strain than in the WT strain even at the permissive temperature (23 °C, Figure 4.1A). This might indicate that the canonical function of Cse4p in chromosome segregation is not effective against TBSV

replication. Western blot analysis revealed that the tombusvirus p33 replication protein was expressed close to WT level in the *cse4-1* strain (Figure 4.1A). I also tested the closely related virus CIRV, which replicates on the boundary membranes of mitochondria in contrast with the peroxisome associated TBSV. CIRV replication also increased by ~4-fold in *cse4-1* strain at the semi-permissive 32 °C (Figure 4.1B) compared to wt cells. These findings suggest that Cse4p is a restriction factor for tombusvirus replication occurring in different subcellular environments.

I used another approach to test the restriction function of CenH3 by expressing the WT *Arabidopsis* CenH3 in yeast replicating TBSV. I observed ~3-fold inhibition of TBSV repRNA accumulation in comparison with the control yeast (Figure 4.1C). Similarly, overexpression of the yeast Cse4p also inhibited TBSV repRNA replication in yeast (Figure 4.1C). These experiments confirmed that under these conditions, CenH3/Cse4 acts as a restriction factor during TBSV replication.

To further explore if the plant CenH3 acts as a restriction factor of tombusvirus replication, I used a virus-induced gene silencing (VIGS) approach to deplete CenH3 level in *Nicotiana benthamiana* (Figure 4.1D, bottom panels) [154]. Replication of TBSV genomic (g)RNA was increased by ~3-to-5-fold in the CenH3 knockdown plants when compared to the non-silenced control plants two days after inoculation (Figure 4.1D, lanes 7-18 versus 1-6). Knockdown of CenH3 (TRV-5'CENH3, Figure 4.1D) rendered the plants smaller than the control (TRV-cGFP) plants, yet the knockdown plants supported higher levels of TBSV replication, suggesting that low CenH3 expression makes the plants more suited to support TBSV replication. Comparable experiments with CIRV showed that the

CenH3 knockdown plants were indeed highly supportive of tombusvirus replication (Figure 4.1E).

To further test the restriction function of CenH3 against tombusvirus replication in plants, I transiently expressed either NbCenH3 or AtCenH3 in *N. benthamiana* followed by inoculation of the same leaves with two peroxisome-associated tombusviruses (i.e. TBSV and the closely-related cucumber necrosis virus, CNV) and the mitochondrial membrane-associated CIRV. Northern blot analysis revealed ~8-to-10-fold reduction in TBSV, CNV and CIRV gRNA accumulation in the inoculated leaves of *N. benthamiana* plants transiently expressing NbCENH3 and AtCENH3 compared to the control plants (Figure 4.1F-H). Therefore, all the above data support a strong tombusvirus restriction function of the plant CenH3 histone variant.

Recruitment of the nuclear CenH3 histone variant into the tombusvirus replication organelles in plants. To test if the restriction function of CenH3 is performed in the nucleus or in the cytosol, where tombusviruses assemble the large viral replication organelles (VROs), I co-expressed TBSV p33-BFP replication protein and the GFP-tagged *A. thaliana* CenH3, the ortholog of the yeast Cse4, in transgenic *N. benthamiana* leaves expressing the RFP-H2B (Histone 2B) nuclear marker protein (Figure 4.2A). Confocal laser microscopy analysis revealed the co-localization of p33-BFP and GFP-CenH3 in *N. benthamiana* cells replicating CNV (Figure 4.2A). Interestingly, a portion of GFP-CenH3 was still localized in the nucleus marked by the RFP-H2B marker protein in plant cells infected with CNV (Figure 4.2A). In contrast, GFP-CenH3 was exclusively localized to the nucleus in mock-inoculated plant leaves under these transient expression conditions

(Figure 4.2A, top image). Importantly, the re-localized GFP-CenH3 in the cytosol was present in the TBSV VROs marked by both p33-BFP and RFP-SKL peroxisome lumen marker protein (Figure 4.2B). The expression of p33-BFP alone (in the absence of TBSV infection) facilitated the partial re-localization of GFP-CenH3 into VRO-like structures (Figure 4.2B), albeit this process was not as robust as in the case of TBSV or CNV infections. I also performed comparable experiments with the mitochondrial CIRV in either transgenic RFP-H2B or WT *N. benthamiana* plants. The results showed partial re-localization of GFP-CenH3 into CIRV-induced VRO structures marked by p36-BFP and RFP-Cox4 mitochondrial marker protein (Figure 4.2C). The expression of p36-BFP alone (in the absence of CIRV infection) did not induce the re-localization of GFP-CenH3 into VRO-like structures (Figure 4.2C). Based on these results, I suggest that tombusvirus infections of *N. benthamiana* plants induce the partial re-localization of the nuclear GFP-CenH3 into the cytosolic VROs.

Subcellular localization experiments were also performed in WT yeast cells expressing YFP-Cse4 and co-expressing CFP-p33 together with p92pol and the repRNA to induce VRO formation [9]. Timepoint experiments revealed the partial co-localization of YFP-Cse4 with CFP-p33 12 h after induction of protein expression (Figure 4.3). The co-localization of YFP-Cse4 and CFP-p33 was even more pronounced at the 16 h and 24 h time points (Figure 4.3). This is in contrast with the nuclear localization of YFP-Cse4 in WT yeast in the absence of viral components (Figure 4.3). The data suggest that Cse4p is relocalized from the nucleus into the cytosolic VROs marked by p33 replication protein in yeast. Thus, CenH3 and Cse4p are re-targeted by TBSV in both plant and yeast cells.

The CenH3 histone variant is an RNA chaperone that inhibit tombusvirus replication *in vitro*. To test if the yeast Cse4 affects TBSV replication *in vitro*, I reconstituted the tombusvirus replicase by using (+)repRNA transcripts and purified recombinant TBSV p33 and p92pol replication proteins in cell-free extracts (CFE) prepared from WT yeast (Figure 4.4A) [15, 122]. The affinity-purified recombinant yeast Cse4p was added in different amounts to the CFE-based replication assay at the beginning of the assay. At the end of the assay, I performed nondenaturing PAGE analysis of the *in vitro* replicase products. The replication assay revealed up to ~2-fold reduction in dsRNA replication intermediate and ~3-fold reduction in (+)ssRNA products in CFE with the highest amount of Cse4p in comparison with the RNA replication supported by WT CFE in the presence of GST control (Figure 4.4A, lanes 4-6 versus 1-3). The finding that both the new (-)RNA (present in dsRNA replication intermediate) and the new (+)RNA products were decreased when CFE contained the highest Cse4p level suggests that Cse4p likely inhibits the TBSV replicase assembly steps, which occurs prior to (-)RNA and (+)RNA synthesis *in vitro*.

To identify the activity of CenH3 important for its viral restriction function, I tested if purified recombinant Cse4p or AtCenH3 could bind to the viral repRNA. Gel mobility shift assays with radiolabeled RNA probes showed that both Cse4p and AtCenH3 bound efficiently to the TBSV (+)RNA template *in vitro* (Figure 4.4B-C). Template competition assays revealed that three of the four regions of the repRNA with known cis-acting functions during TBSV replication [10, 14, 189] competed efficiently with (+)repRNA or (-)repRNA templates *in vitro* (Figure 4.4D-E). Because the secondary structures of these various regions are critical to support various steps in TBSV replication [190], I tested if CenH3 can modify double-stranded viral RNA structures. I found that Cse4p unwound

partial dsRNA regions in the viral repRNA template in the absence of ATP (Figure 4.4G), whereas Cse4p was not efficient in separating complete dsRNA structure *in vitro* (Figure 4.4F). The ability of Cse4p to bind to the viral RNA and unwind a partial dsRNA template suggests that Cse4p functions as an RNA chaperone in TBSV replication *in vitro*.

To determine which domain of CenH3 is important to bind to the viral RNA and its chaperone function, a series of truncation mutants of Cse4p were generated, including the N-terminal domain involved in protein interactions and post-translation modifications (protein stability) and the C-terminal Histone-fold domain (HFD) containing the centromere targeting domain (CATD) [191]. Expression of two N-terminal deletion mutants (i. e., $\Delta N50$ and $\Delta N80$) in yeast inhibited TBSV repRNA accumulation at similar extents to the full-length Cse4p (Figure 4.5A). Expression of $\Delta N129$ led to low protein accumulation, suggesting the N-terminal region of Cse4p is needed for protein stability (Figure 4.5A). In contrast, expression of the Cse4p mutants lacking the highly conserved HFD domain (I, e., $\Delta C60$ and $\Delta C100$) in yeast did not inhibit TBSV repRNA accumulation (Figure 4.5A). The *in vitro* RNA binding experiments suggested that the N-terminal region in Cse4p is not required, whereas the C-terminal HFD domain is critical for Cse4p to bind to the TBSV repRNA (Figure 4.5C-D). RNA strand-separation experiments revealed that the mutants, similar to the full-length Cse4p, did not unwind a fully dsRNA structure (Figure 4.5E), whereas mutant $\Delta C100$ was defective in separation of the partial ds/ssRNA structure, unlike the full-length and the N-terminal mutants (Figure 4.5F). Based on these experiments, I propose that the highly conserved HFD domain of Cse4p is involved in viral RNA binding and this domain also acts as an RNA chaperone on viral RNA templates.

To test if CenH3 can also interact with other viral components, I performed co-purification experiments from yeast co-expressing Flag-tagged AtCenH3 and His6-tagged p33 replication protein. After detergent-solubilization of the membrane-fraction of yeast, the Flag-CenH3 was immobilized to the Flag-column. Western blot analysis of the eluted proteins from the column revealed the co-purified His6-p33 (Figure 4.6A, lane 1). In a reverse co-purification experiment, Flag-p33 was purified from the detergent-solubilized membrane-fraction of yeast. The purified preparation also contained the Myc-tagged full-length Cse4p (Figure 4.6B, lane 2). Additional co-purification experiments revealed that the N-terminal fragment of Cse4p was not co-purified, whereas the C-terminal HFD domain of Cse4p was present in similarly purified Flag-p33 preparations (Figure 4.6B, lanes 3 and 4). These co-purification experiments demonstrated the interaction involving p33 replication protein and CenH3/Cse4p in the yeast membrane fraction.

To confirm direct interactions between TBSV p33 and Cse4p proteins in the absence of the viral RNA, I used a pull-down assay with the TBSV GST-tagged p33 and MBP-tagged Cse4p proteins from *E. coli* (Figure 4.6C). For the pull-down assay, I used truncated TBSV p33 protein missing its membrane-binding region to aid its solubility in *E. coli* (termed p33C, Figure 4.6C). The GST-based pull-down experiments suggested that the interaction between the p33 replication protein and Cse4p host protein occurs within the highly conserved HFD domain of Cse4p.

Epigenetic reprogramming of the host gene expression by TBSV depends on CenH3 in yeast and plants. Previous work with *cse4-1* yeast suggested that Cse4p has noncanonical functions in yeast outside of the centromeric area of the chromosome [192-

194]. Cse4p acts as a negative regulator of selected number of host genes via replacing histone H3 molecules on the DNA. Interestingly, genes whose expression is negatively affected by Cse4p include several pro-viral host factors needed for robust TBSV replication. These host genes include glycolytic and fermentation enzymes, which are selectively hijacked by TBSV into VROs to provide plentiful ATP locally to promote efficient TBSV replication [177, 185, 195]. Indeed, it has been confirmed that mRNA expression for pyruvate kinase (PK, termed Cdc19 in yeast), Eno2 (Enolase 2), Pgc1 (phosphoglycerate kinase) and Pdc1 (pyruvate decarboxylase) glycolytic and fermentation enzymes and the pro-viral Ded1 DEAD-box helicase was increased in *cse4-1* yeast at the semi-permissive temperature (Figure 4.7A). VIGS-based knockdown of CenH3 level also led to enhanced expression of Eno2, Pgc1 and Pdc1 glycolytic/fermentation enzymes and the pro-viral RH20 (ortholog of the yeast Ded1) DEAD-box helicase (Figure 4.7B). Moreover, it was found that CenH3 knockdown in combination with TBSV infection of *N. benthamiana* led to the highest expression levels of PK1, Pgc1, GAPC1 and Pdc1 (Figure 4.7C). TBSV infection also enhanced the expression level of PK1, Pgc1, GAPC1 (glyceraldehyde-3-phosphate dehydrogenase) and Pdc1 by ~4-to-8-fold (Figure 4.7D). CenH3 expression was increased by ~3-fold at 2 dpi, followed by close to normal level of CenH3 expression at 4 dpi (Figure 4.7D). These surprising findings on the shared function of TBSV infection and CenH3-based regulation of expression of glycolytic/fermentation enzymes led to a new working model that TBSV hijacks CenH3/Cse4 from the nucleus into the VROs to interfere with the normal cellular negative gene-regulatory function of this conserved histone variant. This might lead to epigenetic reprogramming of gene

expression of a select group of genes whose expression is affected by the noncanonical function of CenH3/Cse4.

Regulation of expression of selected glycolytic and fermentation enzymes via CenH3 affects local ATP generation within TBSV VROs in yeast and plants.

To test the above model, I decided to measure ATP generation within VROs, which depends on the availability of co-opted glycolytic and fermentation enzymes [39]. The ATP level within VROs was measured using a FRET-based biosensor [187], which has been used previously [185, 195]. Briefly, I expressed p33-ATeam fusion protein in *N. benthamiana* leaves. The ATeam domain of the fusion protein can measure ATP level due to a conformational change in the enhanced ϵ subunit of the bacterial F₀F₁-ATP synthase upon ATP binding [185, 195]. This is based on increased FRET signal in confocal laser microscopy when the ϵ subunit binds to ATP, resulting in a conformational change, which results in drawing the CFP and YFP fluorescent tags in close vicinity. On the other hand, the ATP-free form of the ϵ subunit is present in an extended conformation, which places CFP and YFP fluorescent tags in a distal position. This leads to low FRET signal [187]. It was documented previously [185, 195] that the p33-ATeam localizes to VROs representing aggregated peroxisomes. I found that the ATP level within VROs was ~40% higher in CenH3-silenced plants than in the control non-silenced *N. benthamiana* plants (Figure 4.8A).

Similarly, increased levels of ATP production was detected within the CIRV-induced VROs using p36-ATeam fusion protein in CenH3-silenced *N. benthamiana* plants

(Figure 4.8B). In contrast, transient over-expression of CenH3 in *N. benthamiana* leaves reduced the ATP levels within CNV or CIRV-induced VROs by ~2- and ~4- fold, respectively (Figure 4.8C-D). Overall, these results support the model that CenH3 is a critical host factor affecting local ATP generation within the tombusvirus VROs in plant cells.

The regulatory role of the orthologous Cse4p was also confirmed in yeast cells by using ATeam-p92pol biosensor. It was found previously [185, 195] that the ATeam-tagged p92pol is a fully functional RdRp, which localizes to VROs representing aggregated peroxisomes in yeast cells. Since these experiments are best performed in the presence of glucose in yeast medium [185], *cse4-1* temperature sensitive mutant was used at semi-permissive 32 °C as well as the wt BY4741 strain. Increased production of ATP was detected within VROs in *cse4-1* strain than in the control yeast strain under the same growth conditions (Figure 4.9). The emerging picture from the above experiments is that subversion of CenH3/Cse4p into VROs facilitates the more efficient ATP generation locally to support the energy requirement of virus replication.

The tombusviral RNA enters the nucleus in plants cells. CenH3/Cse4p is mostly located in the nucleus, therefore its retargeting to the cytosol and into the VROs during tombusvirus replication may require a nuclear phase for a viral component. Since the viral replication proteins are bound to membranes [9, 13], I tested the possibility that the viral RNA might be able to enter the nucleus to interact with nuclear proteins, such as CenH3/Cse4p. To test this model, I used a TBSV repRNA (termed repRNA-hp), which carried six copies of the coat protein recognition sequence from bacteriophage MS2 [9, 88]. The MS2 coat protein

(CP) was fused with GFP fluorescent protein to aid detection via confocal microscopy. In the control experiment, based on transient expression of p33 and p92pol and the rub-inoculated repRNA lacking the MS2-derived hairpin sequences in the transgenic H2B *N. benthamiana*, confocal microscopy showed different distributions of p33-BFP (peroxisome), GFP-MS2-CP (cytosol) and RFP-H2B (nucleus) (Figure 4.10A-C). In contrast, I observed the partial re-localization of GFP-MS2-CP into both the cytosolic VROs decorated by p33-BFP and the nucleus marked by RFP-H2B at the 16 h time point in several plant cells co-expressing p33 and p92pol, when the repRNA-hp transcripts were introduced via rub-inoculation onto leaves (Figure 4.10A). Note that repRNA-hp is replication competent in the presence of co-expressed p33 and p92^{pol} (Figure 4.11). The dual cytosolic (in VROs) and nuclear distribution pattern of GFP-MS2-CP remained at later time points (24 and 48 h, respectively, Figure 4.10B-C). Interestingly, I found that replication of repRNA-hp transcripts was not absolutely required for the RNA to enter the nucleus. This observation is based on partial nuclear localization of GFP-MS2-CP in transgenic H2B *N. benthamiana*, rub-inoculated with repRNA-hp, but in the absence of p33 and p92pol expression (Figure 4.10D). Rub-inoculation of the WT repRNA did not result in nuclear localization of GFP-MS2-CP (Figure 4.10D, bottom panel), excluding that GFP-MS2-CP can enter the nucleus without recognition of repRNA-hp. Altogether, these results support the idea that a portion of the viral (+)RNA enters the nucleus, likely to co-opt nuclear factors such as CenH3/Cse4p (see Discussion).

4.4 Discussion

Tombusviruses, similar to other (+)RNA viruses, exploit the host cells by co-opting the cellular translation machinery, subverting host proteins, intracellular membranes, metabolites and energy to build virus-induced extensive VROs in infected cells. It seems, however, that the molecular resources available in susceptible cells to support robust TBSV replication are suboptimal at the start of viral replication. Therefore, TBSV drives intensive remodeling and subversion of many cellular processes [37, 124, 196]. The virus-induced changes also include the dramatic alteration of gene expression in the nucleus. How the cytosolic TBSV accomplishes this feat is incompletely understood. The identification of the key role of the centromeric H3 variant in regulation of TBSV replication opens up a new page in TBSV-host interactions as discussed below.

Is the nuclear CenH3/Cse4 histone variant a conventional viral restriction factor for the cytosolic tombusviruses? Our gene and protein interaction network studies based on a dozen genome and proteome-wide screens, which previously identified host components affecting TBSV replication and recombination or interactions with host components, revealed that Cse4 H3 histone variant is one of the highest connected nodes in the network (Figures 2.1, 2.2 and 2.4). Because Cse4 (CenH3 in plants and CENP-A in human) is a nuclear protein with function within the centromere, it is a puzzle how CenH3/Cse4 could be an important host factor for the cytosolic TBSV. However, yeast studies with a temperature-sensitive mutant of Cse4, over-expression, and knockdown of the orthologous CenH3 in plants, all confirmed a strong restriction factor role for CenH3/Cse4 in

tombusvirus replication. This conclusion with the peroxisome-associated TBSV is further supported by results obtained with the mitochondrion-associated CIRV in yeast and plants.

How can a nuclear, DNA-binding histone variant be a restriction factor for a cytosolic RNA virus? Subcellular localization studies confirmed that CenH3/Cse4 is partially re-localized to the cytosol, namely into the large VROs, during TBSV or CIRV replication. Moreover, CenH3/Cse4 bound the viral RNA *in vitro* via its HFD domain. I also showed RNA chaperone activity for Cse4 *in vitro*, which activity might contribute to the inhibitory function of Cse4 via unwinding critical cis-acting elements in the viral RNA. I also documented interaction of CenH3/Cse4 with the p33 replication protein, which completely overlaps with the N-terminal region of the p92 RdRp. All these results are in agreement with a proposed antiviral activity of the CenH3/Cse4. Accordingly, I have shown in this chapter that the purified recombinant Cse4p is indeed inhibitory to TBSV replication in an *in vitro* replicase reconstitution assay.

Is CenH3/Cse4 recruited to VROs to selectively reprogram host gene transcription during tombusvirus replication? Our initial results in yeast, plants and *in vitro* were not consistent with the idea that the centromeric role of CenH3/Cse4 is exploited by the host to fight off tombusvirus infection. Moreover, tombusviruses replicate in mature plant leaf and root cells, which are not going through cell division and chromosomal segregation. An interesting noncanonical function of Cse4 is to replace histones bound to the chromosome in many, though not well-defined places [192]. In this role, Cse4 acts as a negative regulator

of gene expression of several hundred genes [192-194]. Because these genes also include critical host factors, such as glycolytic and fermentation enzymes, with pro-tombusvirus functions, I propose that tombusviruses subvert CenH3/Cse4 into VROs to prevent the gene regulatory function of CenH3/Cse4 in the nucleus. I predict that the TBSV-driven subversion of CenH3/Cse4 and partial sequestration to VROs would have two major consequences for tombusvirus replication: (i) this would lead to epigenetic reprogramming of host gene transcription in the nucleus. Accordingly, I show that similar to knocking down/inhibiting CenH3/Cse4 activities, TBSV infection also increased the expression of selected host genes, namely glycolytic and fermentation enzymes and others. Altogether, these activities led to the increased generation of ATP locally within VROs, which is essential for robust TBSV replication as shown previously [185] [39]. On the other hand, over-expression of CenH3/Cse4 might interfere with the TBSV-driven efficient sequestration of this host factor from the nucleus. Indeed, over-expression of CenH3/Cse4 inhibited local ATP generation within VROs and strongly inhibited TBSV replication. (ii) the second consequence of subverting CenH3/Cse4 to the VROs from the nucleus is that this process is “costly” to TBSV, because the virus must dedicate viral components, namely a portion of the viral RNA population or possibly p33 molecules in the VROs, to subvert CenH3/Cse4 from the nucleus. A lower level of CenH3/Cse4 in the cell via mutation or depletion might help TBSV commit less of its components to sequester CenH3/Cse4 away from the nucleus. Accordingly, the above conditions led to highly enhanced TBSV and CIRV replication in yeast and plant cells. In contrast, over-expression of CenH3/Cse4 would force TBSV to commit even more viral components for sequestration (i.e., taking the viral RNA away from replication function), thus leading to reduced viral replication. I

propose that this sequestration process of CenH3/Cse4 via TBSV components renders CenH3/Cse4 functioning as a restriction factor under given circumstances. However, the emerging big picture seems to be that the sequestration of CenH3/Cse4 is orchestrated by TBSV to reprogram the host cell transcription. This in turn helps TBSV to recruit pro-viral host factors from the more abundant protein pool, which is the consequence of reduced CenH3/Cse4-driven regulation of select gene expression. This was shown through the example of glycolytic and fermentation enzymes, which are exploited more efficiently by tombusviruses to produce abundant ATP locally within the VROs in infected cells.

Hijacking and regulating CenH3 function might be conducted by other viruses as well. For example, Hepatitis B virus x protein (HBx) induces hepatocellular carcinoma (HCC) by inducing the over-expression of CENP-A (CenH3) protein [197]. The hepatitis C virus (HCV)-related chronic liver disease also correlates with increased level of CENP-A expression [198]. Interestingly, the NS1 protein of the influenza A H3N2 subtype contains a histone H3-like sequence (mimicking H3 structure), which is used to hijack host proteins [199]. In summary, CenH3/Cse4 histone variant is a central interaction node, which plays a major role in tombusvirus replication in plants and in yeast model host.

Table 4.1 List of primers used in Chapter 4

Primer #	Sequence
22	GTAATACGACTCACTATAGGGCTGCATTTCTGCAATGTTCC
1165	AGCGAGTAAGACAGACTCTTCA
1291	CGGCGGATCCGTGAGCAAGGGCGAGGAGCTGTTCA
1295	CGGCGGATCCCTTGTACAGCTCGTCCATGCCGA
2030	CGCGGGATCCATGTCAAAGCTGTCGGTATTG
2534	GTAATACGACTCACTATAGGGAGCCACCAACAAGA
2535	TGTATGGAACCAGTTGAAAAGTGTTTGAGGG
2859	TAATACGACTCACTATAGGAACCAAATCATTTCATGTTGCTCTC
2860	TAGTGTATGTGATATCCCACCAA
4308	CCAGACTAGTATGGCTGAACTGAGCGAACAAG
5604	GTAATACGACTCACTATAGGACCGTTACCCAAGGTGTGG
5621	CGCCGGATCCATGTCTGAAATTACTTTGGGTAAATA
5992	CGCCGGATCCATGTCTAGATTAGAAAGATTGA
6275	CGGGATCCCGATGTCTTTATCTTCAAAGTTG
6329	CGCCGGATCCATGTCAAGTAAACAACAATGGGTTAG
6331	CGCCGGATCCATGGCGAGAACCAAGCATCG
6367	TAATACGACTCACTATAGGGCTTACCCAACAATGATTGCA
6376	CGCCGAATTCATGCATCATCATCATCATCATGCGAGAACCAAG CATC
6377	CGCCAGATCTTCACCATGGTCTGCCTTTTC
6378	CGCCCTCGAGATGCATCATCATCATCATCATGCGAGAACCAAG CATC
6379	CGCCGTCGACTCACCATGGTCTGCCTTTTC
6380	CAACGGATCCATGGCGAGAACCAACACCT
6381	CAACCTCGAGACAAGTCTGATGAAAGGAGCAGC

Table 4.1 (continued)

6382	CAACGGATCCTTTGCACCAGAGGTAACCTCGC
6383	CAACCTCGAGTCACCAAGGTCGTGCTTTTC
6609	CGCCCTCGAGTCACCATGGTCTGCCTTTTC
6809	CGCCCTCGAGCTAAATAAACTGTCCCCTGATTCTTC
8174	GTGCTGAAATCGTGGAATCTG
8175	TCCATTCCCAATAGTCACACG
8176	AAGTGTGATCCTCTGTGCAG
8177	CAGATCCACAATTACTCCAGGG
8178	CTGGGAAGTTATCTGTGACGAG
8179	AACAGCCCTAGGAACATAACG
8217	ACGAGAAGGAATACAAGCCAG
8218	CAGTAAGGGAGTGGACAGTAG
8219	GGTATCTCTATTGCTTCCCCTG
8220	AATATCCAATCCCATCCAGCC
8221	TTGCCTTACCAGTTGTCTCG
8222	TCCCCTGTAAAGACCTGAATTG
7080	CGCCGGATCCCTGTTTCCAAGAAGAGAGGAAAG
7081	CGCCGGATCCCTAGAAATCGAGACAGAAAATGAAG
7083	CGCCGGATCCAAGAAATATACTCCTAGTGAATTAGCTCTG
7112	CGCCCTCGAGAACTCGTCTGTAACCTCTTTCACTAG
7113	CGCCCTCGAGTTCGACGCGCTTTAAGCTC
7116	CGCCGGATCCATGGCCAGAACAAAGCAAAC
7117	CGCCCTCGAGCTATGATCTTTCACCTCTTAATCTTCTAG
7123	CGCCGGATCCATGGCTGTCTCTAAAGTTTACG
7136	TAATACGACTCACTATAGGGCAACATCGTTGGTGGTGGTAC
7137	TAATACGACTCACTATAGGGAGGACTTAGACAAGTCAGCCAA ATG

Table 4.1 (continued)

7138	TAATACGACTCACTATAGGGAGGTTTCACCCTTAAATTCAACT TG
7140	TAATACGACTCACTATAGGGCATCGATCCATCTACCACCA
7141	AGGATGGTCAAACCAGAGAACAC
7142	TAATACGACTCACTATAGGGATGGAGCGTTGGTGGTAGC
7295	GTGATCTCATTGGAATAGCAGAAACA
7296	TAATACGACTCACTATAGGGAGCAGCAACATCTGTAGCTGTC
7297	TTGAGACCACCAAGTACTACTGC
7298	TAATACGACTCACTATAGGGTGGAAGCAACAAACCCAC

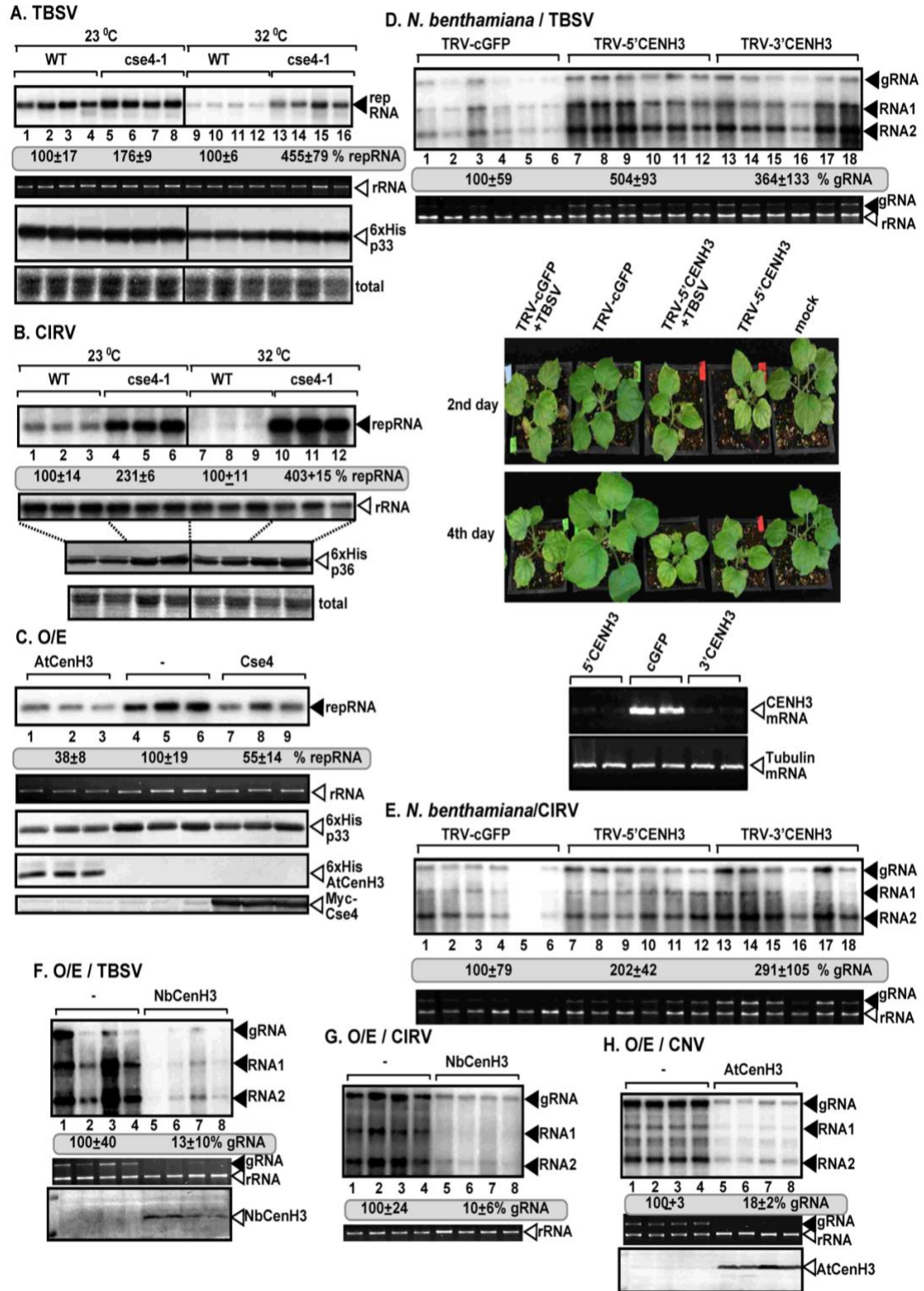
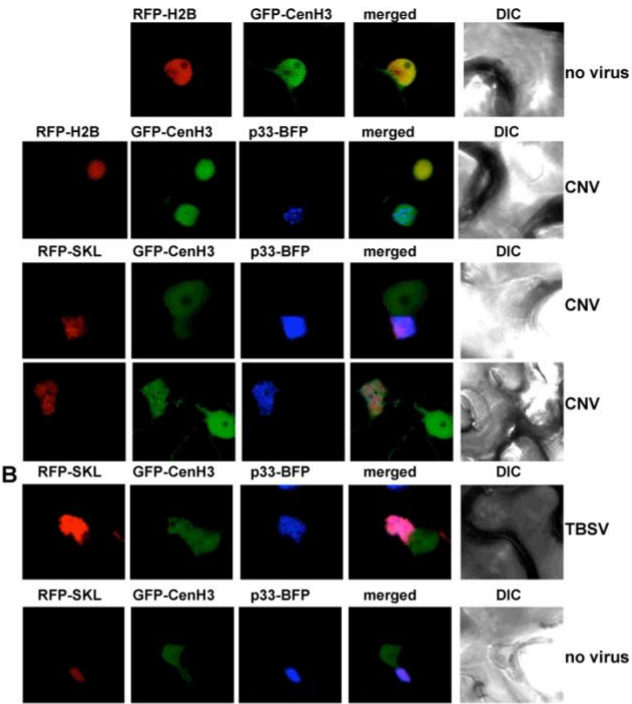


Figure 4.1

Figure 4.1 The essential centromeric histone variant CenH3 is a restriction factor of tombusvirus replication in yeast and plants.

(A and B) Top: northern blot analyses show increased TBSV (A) or CIRV (B) repRNA accumulation in wt and *cse4-1* yeast grown at permissive and semi-permissive temperatures. Middle: The accumulation level of repRNA was normalized based on 18S rRNA levels. Bottom: The levels of His₆-p33 or His₆-p36 were measured by western blotting with anti-His antibody. (C) CenH3 overexpression in yeast cells. Top: The 3' end specific probe used for northern blot shows a reduction in the accumulation of repRNA in cells expressing *A. thaliana* CenH3 (lanes 1-3) or *S. cerevisiae* CenH3 (lanes 7-9) compared to the empty vector control (lanes 4-6). Middle: Northern blot with 18S ribosomal RNA specific probe was used as a loading control. Bottom: Western blot analyses of the level of His₆-p33, His₆-p92^{pol}, His₆-AtCenH3 with anti-His antibody and Myc-ScCse4 with anti-Myc antibody. (D) Top: Northern blot analysis of tombusvirus gRNA and sgRNAs accumulation in NbCenH3 silenced plants inoculated with TBSV. VIGS was performed via agroinfiltration of tobacco rattle virus (TRV) vector carrying 5' or 3'-terminal NbCenH3 sequences or 3'-terminal GFP sequences as control. The 3' end specific probe used for northern blot shows increased accumulation of both gRNA and sgRNAs in NbcCenH3 silenced plants compared to control plants. Middle: Ethidium bromide-stained gel to visualize rRNA levels in each sample as a loading control. Bottom: CenH3 silencing restricts the growth of plants. Pictures were taken 2- or 4-days post virus inoculation. NbCenH3 mRNA levels were analyzed by semi-quantitative RT-PCR in the silenced and control plants. Tubulin mRNA was used as a control. (E) Accumulation of CIRV gRNA and sgRNA in CenH3 silenced *N. benthamiana* plants was measured by northern blot analysis. See further details in panel D. (F-H) Northern blot analysis of tombusvirus gRNA and sgRNAs accumulation in plants expressing CenH3 and inoculated with TBSV (F), CIRV (G) or CNV (H). Top: Accumulation of both gRNA and sgRNAs is greatly reduced in plants expressing NbCenH3 compared to control plants. Samples were taken 48 h (F), 72 h (G) or 84 h (H) after virus inoculation or agroinfiltration. Middle: Ethidium bromide-stained gels showing 18S ribosomal RNA as a loading control. (F and H, bottom) His₆-NbCenH3 and His₆-AtCenH3 levels were measured by western blot. Each experiment was performed at least three times

A. *N. benthamiana* / CNV



C. *N. benthamiana* / CIRV

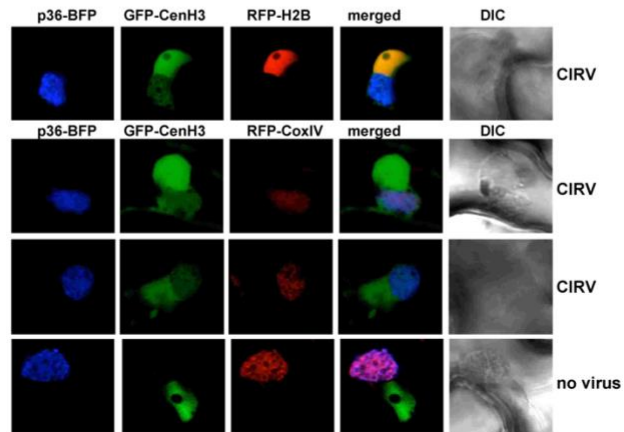


Figure 4.2

Figure 4.2 Re-distribution of nuclear CenH3 to the sites of viral replication in plants.

Confocal laser microscopy images show the localization of GFP-CenH3 in *N. benthamiana* cells. (A) First panel: In the absence of virus replication, GFP-CenH3 localizes solely in the nucleus, as shown by its co-localization with the fluorescently tagged histone RFP-H2B. Second panel: Co-localization of p33-BFP and GFP-CenH3 in cells replicating CNV. Third and fourth panels: The re-distributed GFP-CenH3 is present in the VROs, marked by p33-BFP and RFP-SKL peroxisomal marker protein. Note that a portion of GFP-CenH3 remains at the nucleus after virus replication induced re-localization. (B) GFP-CenH3 partially re-localizes into the VRO structures, in the absence of TBSV replication when only p33-BFP is expressed. (C) First panel: Co-localization of p36-BFP and GFP-CenH3 in cells replicating CIRV. Second and third panels: GFP-CenH3 is re-distributed into the CIRV-induced VROs at the mitochondrial membranes, marked with both p36-BFP and RFP-CoxIV. Fourth panel: GFP-CenH3 does not re-localize into the VRO structures, in the absence of CIRV replication when only p36-BFP is expressed.

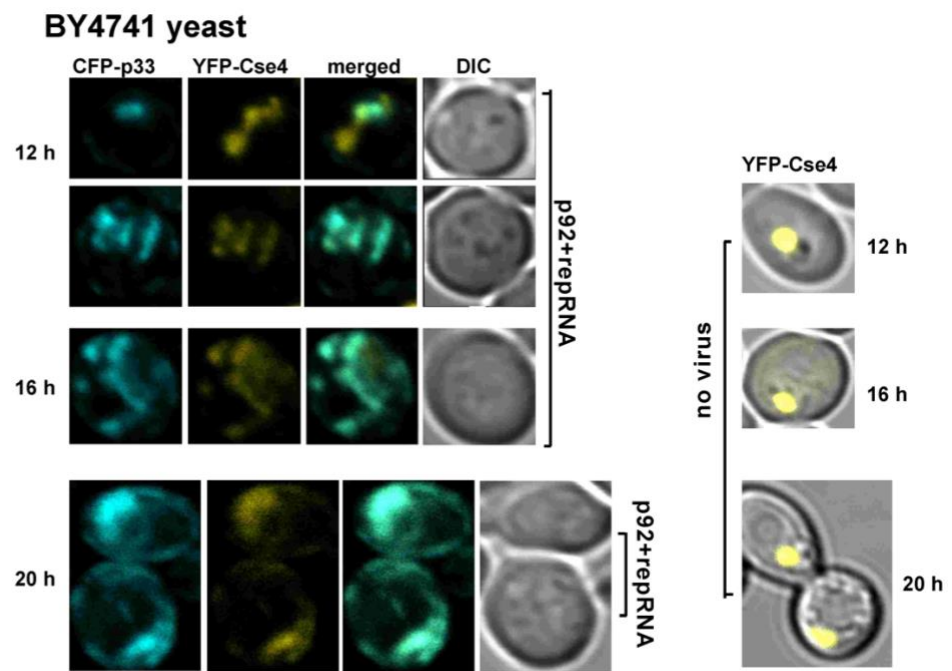


Figure 4.3

Figure 4.3 Re-distribution of nuclear CenH3 to the sites of viral replication in yeast.

Confocal laser microscopy analyses in wt yeast cells co-expressing YFP-Cse4 together with CFP-p33, p92^{pol} and the repRNA show partial co-localization of YFP-Cse4 with CFP-p33 at 12 h, 16 h and 24 h after induction of protein expression. Images on the right show the nuclear distribution of YFP-Cse4 in the absence of viral components in wt yeast cells at the same timepoints.

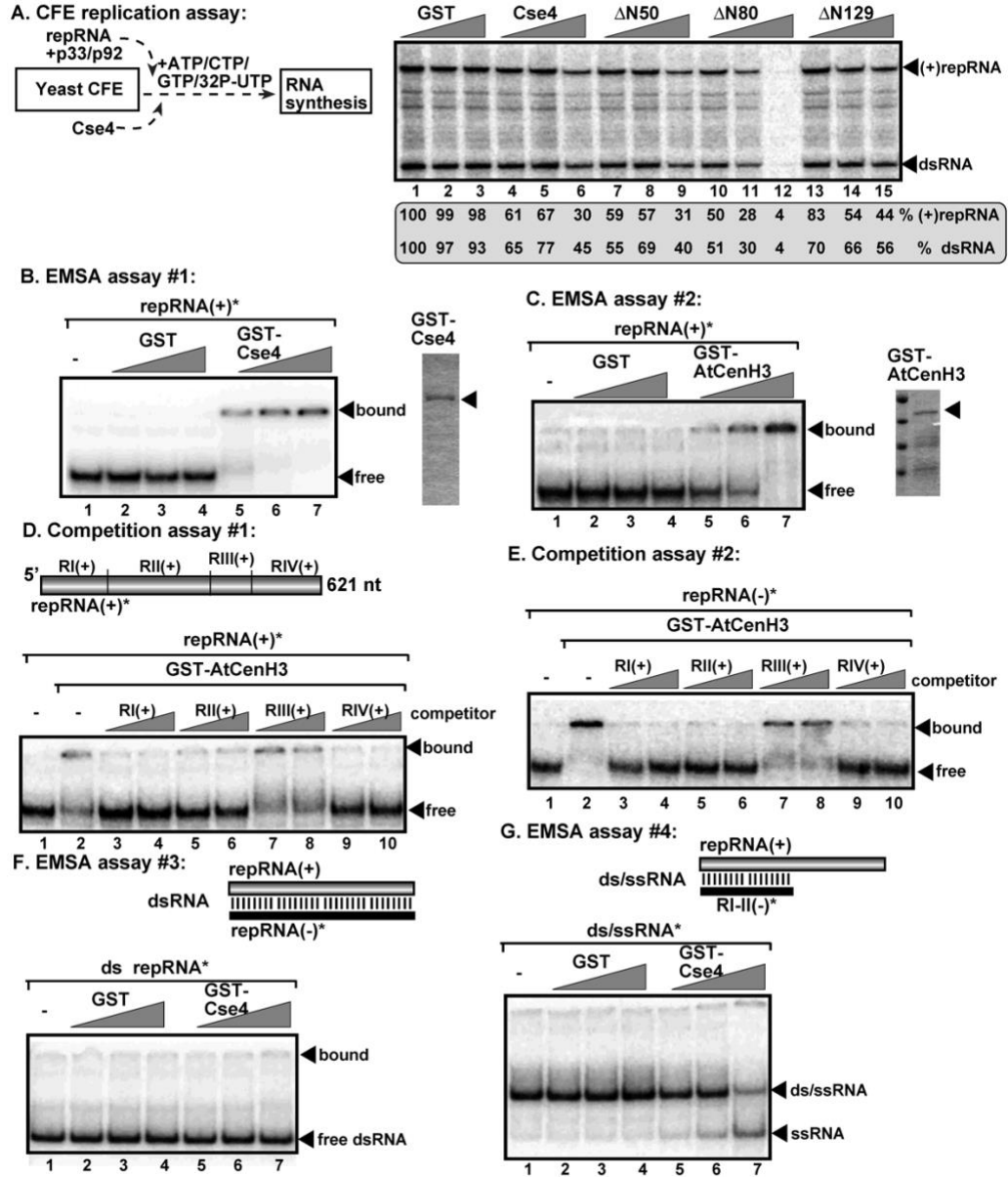


Figure 4.4

Figure 4.4 *CenH3* has an RNA chaperone activity and inhibits tombusvirus replication *in vitro*.

(A) Left panel: Scheme of the CFE replication assay prepared from wt yeast strain. Purified recombinant p33 and p92^{pol} TBSV replication proteins and *in vitro* transcribed TBSV DI-72 (+)repRNA were added to the CFE as well as affinity purified recombinant *S. cerevisiae* WT Cse4 (CenH3 homolog) or Cse4 N-terminal deletion mutants. Right panel: Denaturing PAGE analysis of the ³²P-labeled TBSV repRNA products obtained in the CFE-based replication assay shows inhibition of TBSV replication by recombinant Cse4 or Cse4 mutants *in vitro*. Affinity purified recombinant GST was used as a control. (B, C) RNA gel mobility shift analysis shows that GST-Cse4 and GST-AtCenH3 bind to ³²P-labeled (+)repRNA *in vitro*. Purified GST-Cse4, GST-AtCenH3 or GST were added in increasing concentrations (0.1, 0.2 or 0.4 μM) to the assays. The ³²P-labeled ssRNA-protein complexes were visualized on nondenaturing 5% polyacrylamide gels. (D, E) RNA competition experiments. The assays contained 0.2 μM of purified GST or GST-AtCenH3 along with the ³²P-labeled (+)repRNA or (-)repRNA templates (~0.1 pmol), and unlabeled competitor RNAs (2 and 4 pmol) representing one of the four regions of TBSV DI-72 RNA from both RNA strands (see panel D, top). The GST-AtCenH3-³²P-labeled ssRNA complex was visualized on nondenaturing 5% acrylamide gels. (F, G) Strand separation assays. Top: Schematic representation of the RNA/RNA duplexes used in the assays. The templates consists of DI-72 (+)repRNA and a ³²P-labeled complementary (-)RNA creating a complete (F) or partial (G) RNA/RNA duplex. Bottom: Increasing amounts (0.1, 0.2 or 0.4 μM) of purified recombinant GST-Cse4 or GST (as a control), were added to the reactions. The ³²P-labeled RNA products after the *in vitro* strand separation assay were analyzed on nondenaturing 5% polyacrylamide gels. All experiments were repeated at least three times.

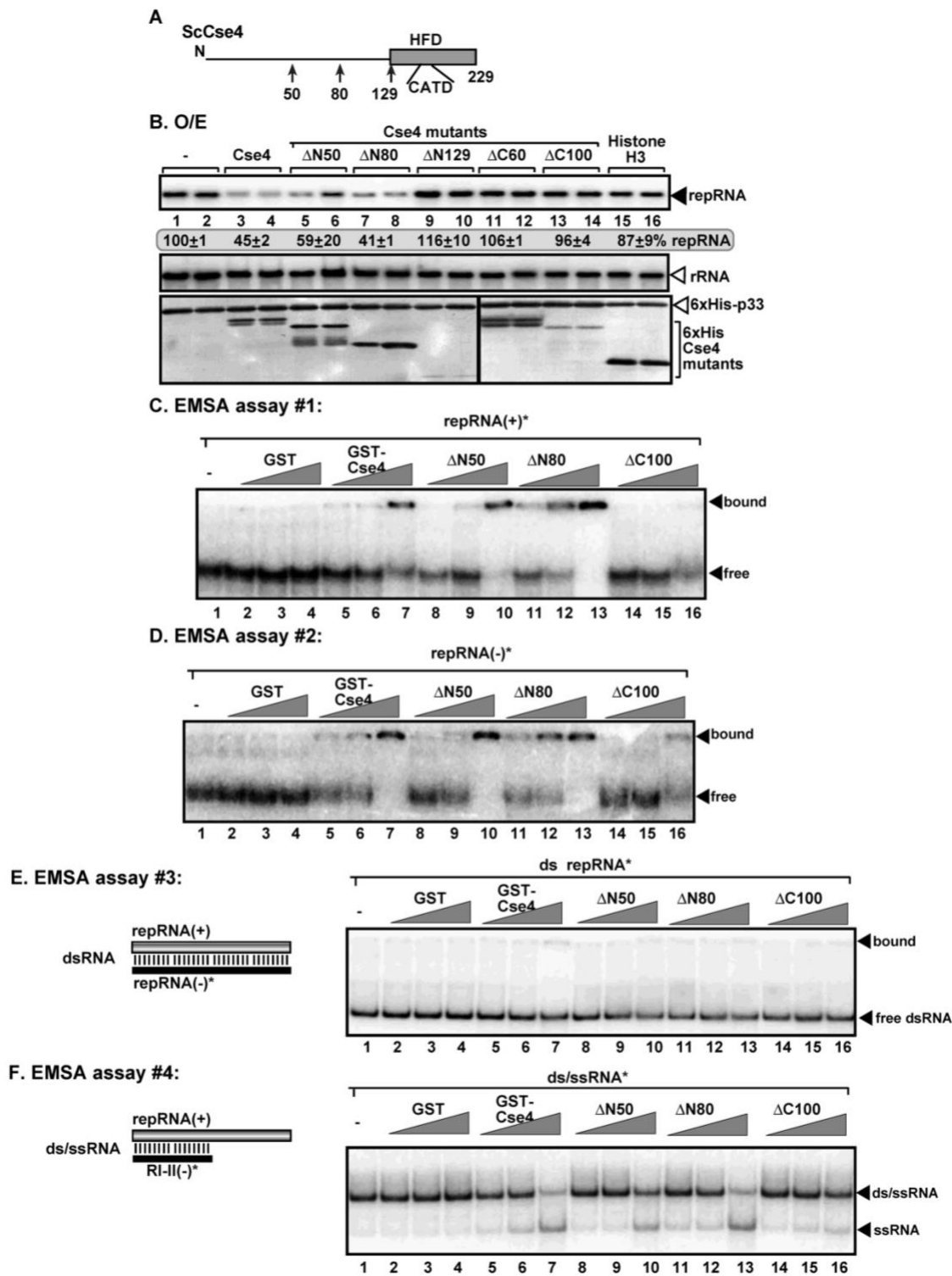
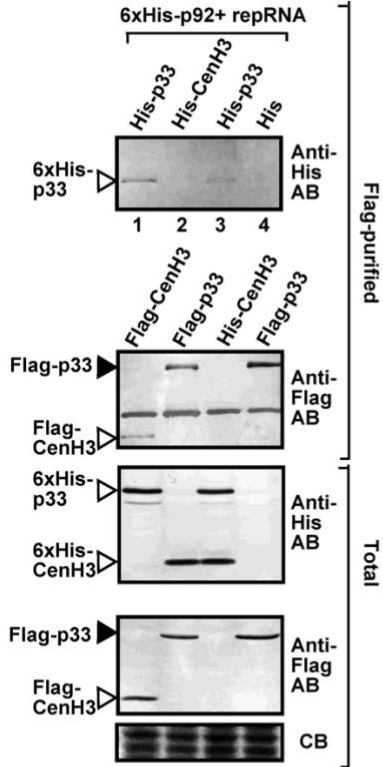


Figure 4.5

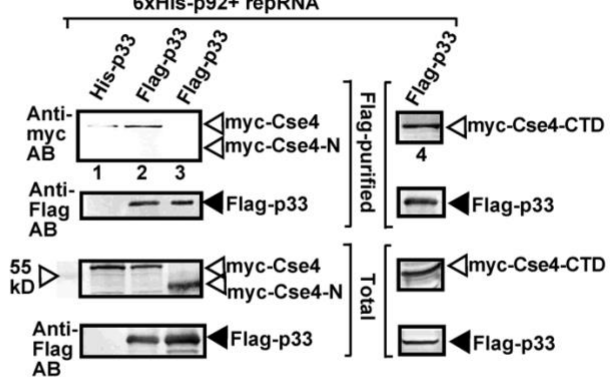
Figure 4.5 The highly conserved HFD of Cse4p is involved in viral RNA binding and RNA chaperone activity.

(A) Schematic diagram showing the endpoints of the Cse4 deletion mutants used in this study. The proteins were named by the number of the last amino acid deleted. (B) Top: northern blot analyses show a significant reduction in the accumulation of repRNA in cells expressing full length Cse4 (lanes 3-4) and the N-terminal deletion mutants Δ N50 (lanes 5-6) and Δ N80 (lanes 7-8) compared to the control samples (lanes 1-2). Expression of Δ N129, Δ C60, Δ C100 and Histone H3 did not affect TBSV repRNA accumulation (lanes 9-16). Middle: Northern blot with 18S ribosomal RNA specific probe was used as a loading control. Bottom: Western blot analyses of the level of His₆-p33 and His₆-Cse4 mutants with anti-His antibody. Note that levels of Δ N129 are very low, suggesting that the N-terminal region of Cse4 has a role in protein stability. (C, D) RNA gel mobility shift analysis shows that GST-Cse4, GST- Δ N50 and GST- Δ N80 efficiently bind to ³²P-labeled (+)repRNA (C) or (-)repRNA (D) *in vitro*, whereas GST- Δ C100 show defective binding capability to both repRNAs. Purified GST-Cse4, GST- Δ N50, GST- Δ N80, GST- Δ C100 and GST were added in increasing concentrations (0.1, 0.2 or 0.4 μ M) to the assays. The ³²P-labeled ssRNA-protein complexes were visualized on nondenaturing 5% polyacrylamide gels. (E, F) Strand separation assays. Left: Schematic representation of the RNA/RNA duplexes used in the assays. See details in Figure 4.4F-4.4G. Right: Increasing amounts (0.1, 0.2 or 0.4 μ M) of purified recombinant GST-Cse4, GST- Δ N50, GST- Δ N80, GST- Δ C100 and GST (as a control), were added to the reactions. The ³²P-labeled RNA products after the *in vitro* strand separation assay were analyzed on nondenaturing 5% polyacrylamide gels. Full length Cse4 and all mutants were unable to unwind a fully dsRNA (E) but WT Cse4 and N-terminal deletion mutants unwound the partial dsRNA (F). Each experiment was repeated at least three times.

A. Co-purification from yeast



B. Co-purification from yeast



C. Pull-down

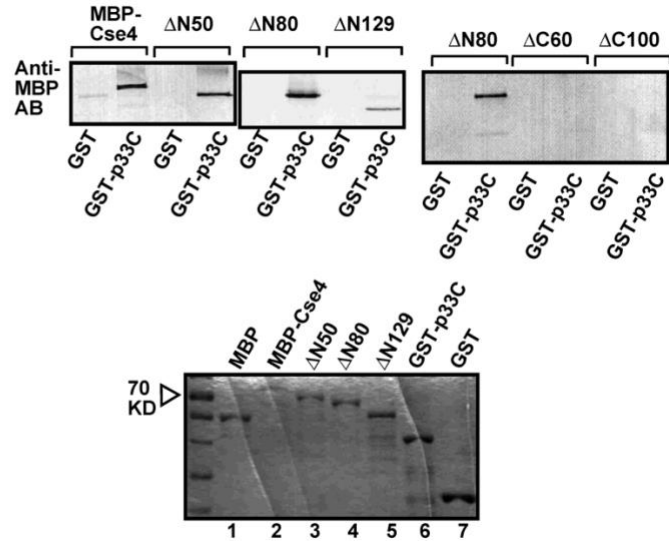


Figure 4.6

Figure 4.6 *CenH3* interacts with TBSV p33 replication protein.

(A) Co-purification of viral p33 replication protein with plant CenH3. First panel: western blot analysis of co-purified, His₆-p33 with Flag affinity purified *A. thaliana* CenH3 from membrane fraction of WT yeast. p33 was detected with anti-His antibody. The negative control was His-tagged AtCenH3 which was not co-purified from yeast extracts when using a Flag-affinity column (lane 2). Second panel: Western blot of purified Flag-AtCenH3 and Flag-p33 detected with anti-Flag antibody. Bottom panels: Western blot of His or Flag-tagged proteins in total yeast extracts. (B) Co-purification of yeast Cse4p with the viral replicase complex. First panels: western blot analysis of co-purified Myc-tagged Cse4 (lane 2) and Cse4 C-terminal domain (Cse4-CTD, lane 4) with Flag-affinity purified p33 from WT yeast membrane fraction. Cse4 and Cse4-CTD were detected with anti-Myc antibody. The negative control was His₆ tagged p33 (lane 1). Second panels: Western blots of purified Flag-p33 detected with anti-Flag antibody. Bottom panels: Western blot of Myc-Cse4, Myc-Cse4-CTD, Myc-Cse4 N terminal domain (Myc-Cse4-N) and Flag-tagged p33 in the total yeast extracts. Note that after affinity-purification, Myc-Cse4-N was not co-purified with p33 (lane 3). (C) Pull-down assay including TBSV GST-p33 replication protein and the MBP-tagged Cse4 or Cse4 deletion mutants. The C-terminal region of TBSV p33 replication protein was used instead of the full-length protein, which includes the non-soluble N-terminal region with the trans-membrane domain. Top: Western blot analysis of the captured GST-p33C with MBP purified WT Cse4 or Δ N50, Δ N80, Δ N129 Cse4 deletion mutants. GST was used as a control. Note that similar to Myc-Cse4-N, the C-terminal deletion mutants Δ C60 and Δ C100 were not pulled-down with GST-p33C suggesting that the HFD is also important for the interaction between p33 and Cse4p. Bottom: Coomassie-blue stained SDS-PAGE of the purified recombinant proteins. All experiments were performed three times.

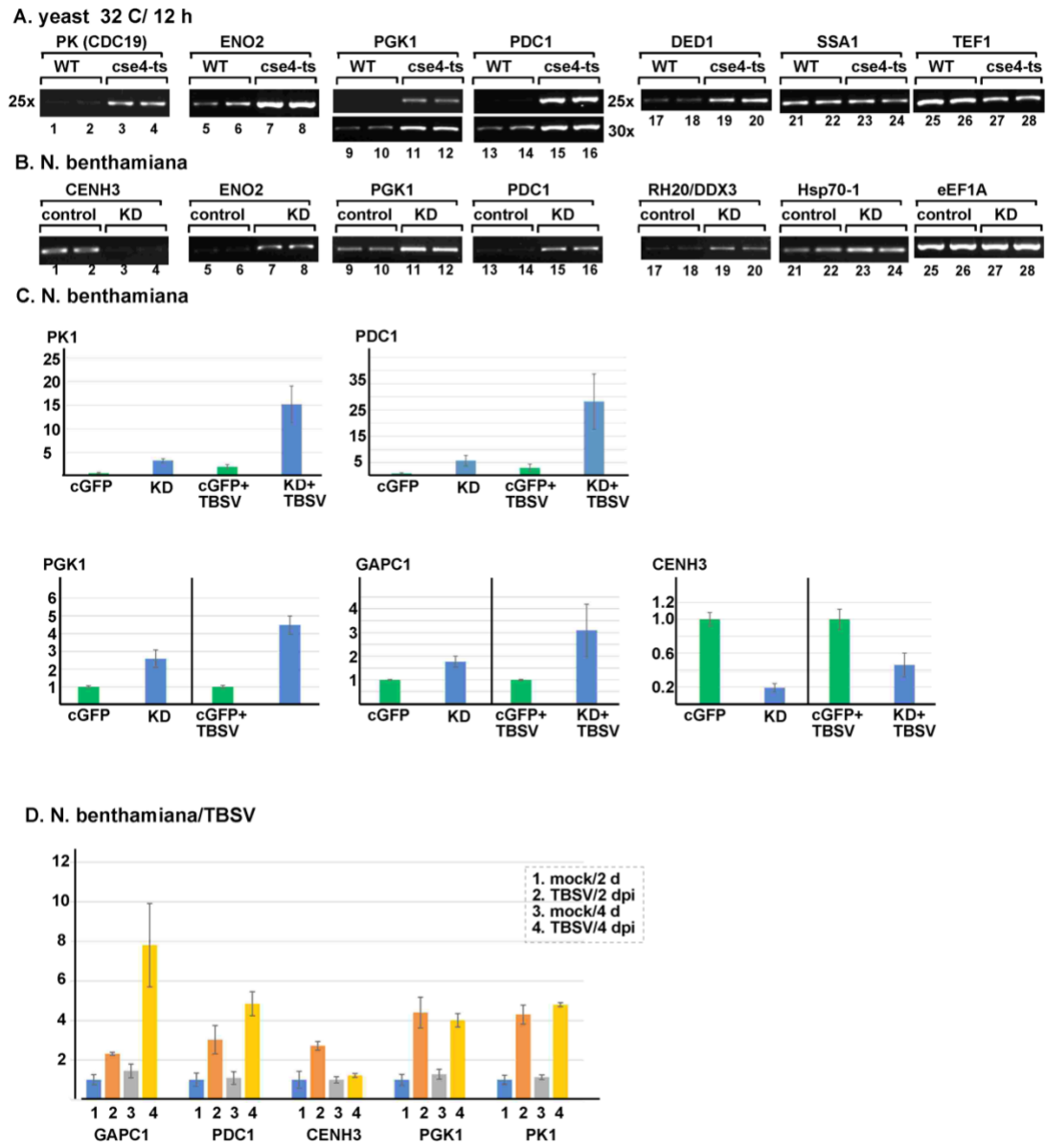


Figure 4.7

Figure 4.7 TBSV reprograms host gene expression via CenH3 in yeasts and plants.

(A) Upregulation of pro-viral host factors expression in *cse4-1* mutant yeast. The mRNA levels were estimated by semi-quantitative RT-PCR in total RNA samples obtained from wt or *cse4-1* yeast cells grown at 32 °C for 12 h. (B) Upregulation of pro-viral host factors expression in CenH3 silenced plants. The mRNA levels were estimated by semi-quantitative RT-PCR in total RNA samples obtained from either CenH3 knockdown or control plants, 12 d after VIGS treatment. (C) *N. benthamiana* glycolytic/fermentation enzymes mRNA levels were estimated by Real-Time PCR in total RNA samples obtained from CenH3 knockdown or control plants in the absence or presence of TBSV replication. (D) Real-Time PCR was also used to estimate *N. benthamiana* glycolytic/fermentation enzymes mRNA levels in total RNA samples obtained from either mock or TBSV inoculated plants, 2 d (for inoculated leaves) or 4 d (for systemic leaves) post inoculation. Each experiment was repeated three times or more.

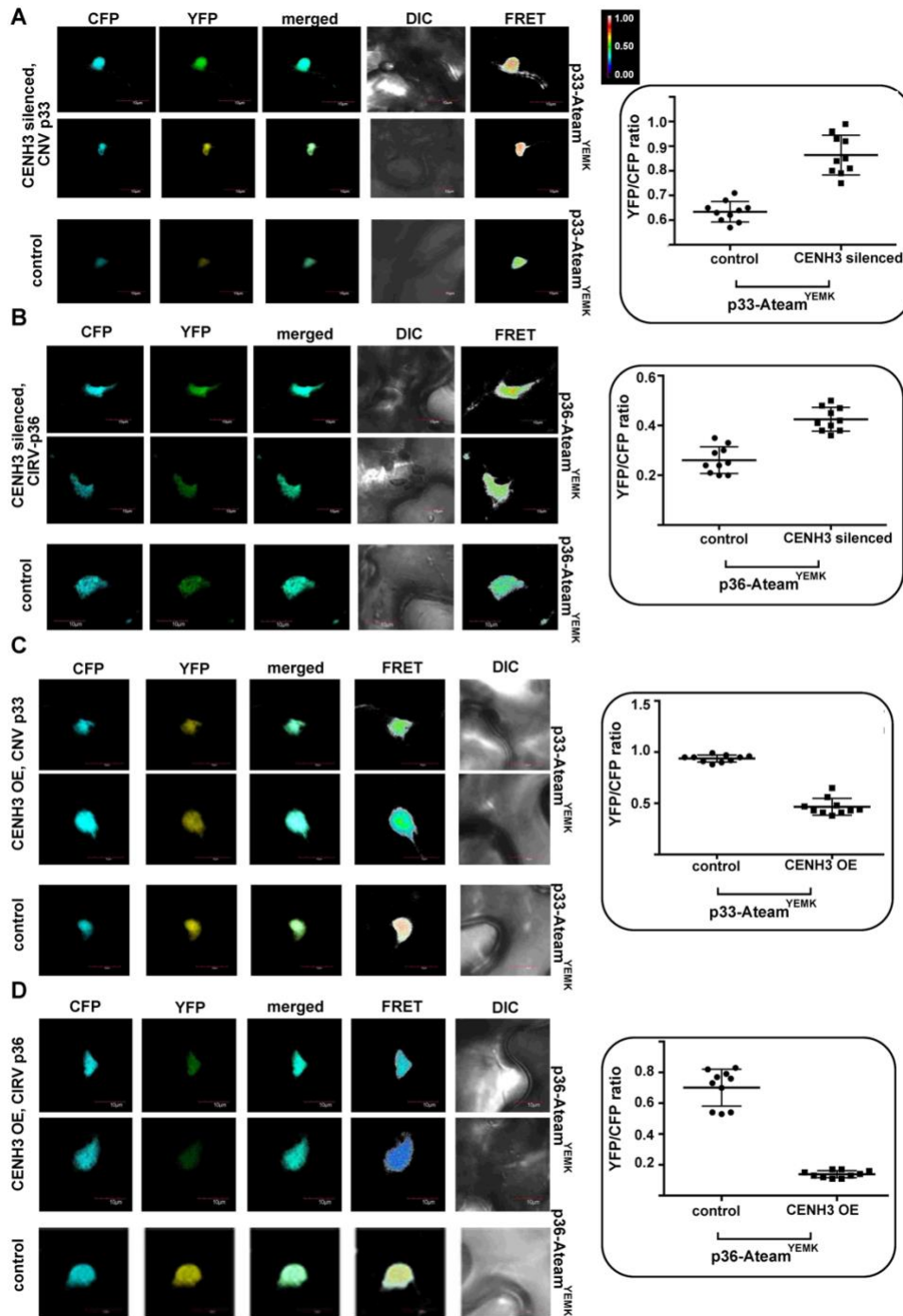


Figure 4.8

Figure 4.8 Reprogramming of glycolytic and fermentation enzymes expression by TBSV via CenH3 affects ATP accumulation within VROs in plants.

The ATP levels inside the VROs was measured using a FRET-based biosensor. In this system ATP concentration is linearly correlated with the YFP:CFP ratio. Intense FRET signals (with high ratios between 0.5 to 1.0) are white and red, whereas weak FRET signals (ratios 0.1 and below) are dark and light blue. (A) VIGS-based knockdown of NbCenH3 was done as in Figure 1D. Eleven days later, co-expression of p33-A_{Team}^{YEMK}, p92^{pol}, DI-72 and p19 was done in upper leaves by agroinfiltration. Quantitative FRET values (obtained with ImageJ) for a number of samples are shown on the graph to the right. Top panels show CenH3 silenced plants, whereas the lower panel shows representative images obtained from non-silenced control plants. (B) Comparable experiments with NbCenH3 knockdown plants using the mitochondrial p36-A_{Team}^{YEMK} and p95^{pol}. See further details in (A). (C, D) ATP generation levels were measured in plants where CenH3 was transiently overexpressed. Top panels: CenH3 overexpression plants infiltrated with p33-A_{Team}^{YEMK} (C) or p36-A_{Team}^{YEMK} (D) plus the rest of the viral components. The FRET signal is shown on the right graph. Bottom panels: Representative images obtained from control plants.

Yeast, p92-ATP-biosensor

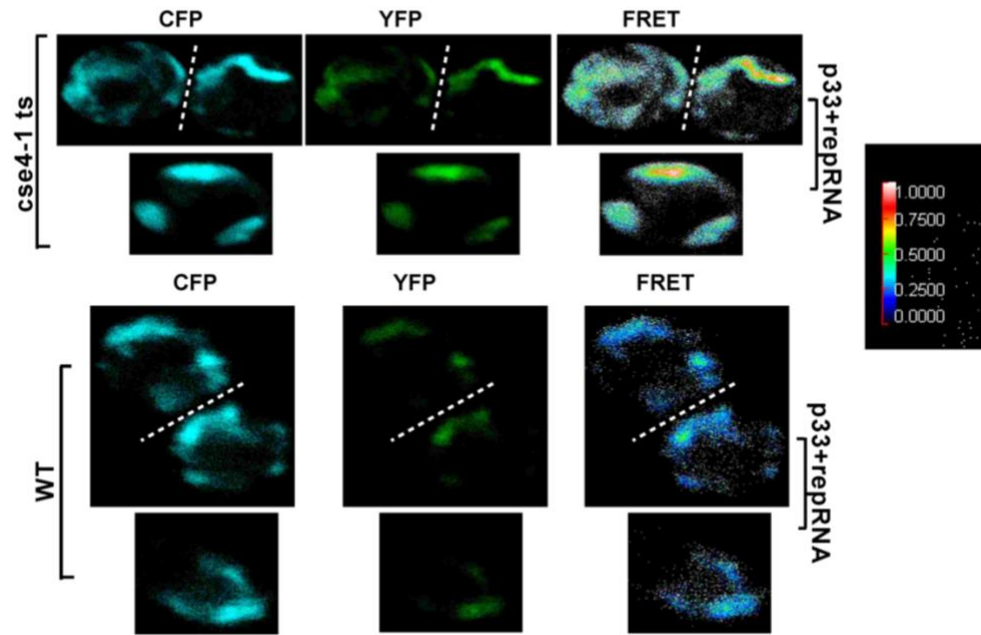


Figure 4.9

Figure 4.9 Reprogramming of glycolytic and fermentation enzymes expression by TBSV via CenH3 affects ATP accumulation within VROs in yeast.

Comparison of the ATP level within the tombusvirus replication compartment in wt and *cse4-1* yeasts grown at 23 °C using ATeam^{YEMK}-p92^{pol}. See further details in Figure 4.8. Increased generation of ATP was observed in *cse4-1* temperature sensitive strain compared to control wt yeast growth under the same conditions. White dashed lines mark the neck of budding yeast cells.

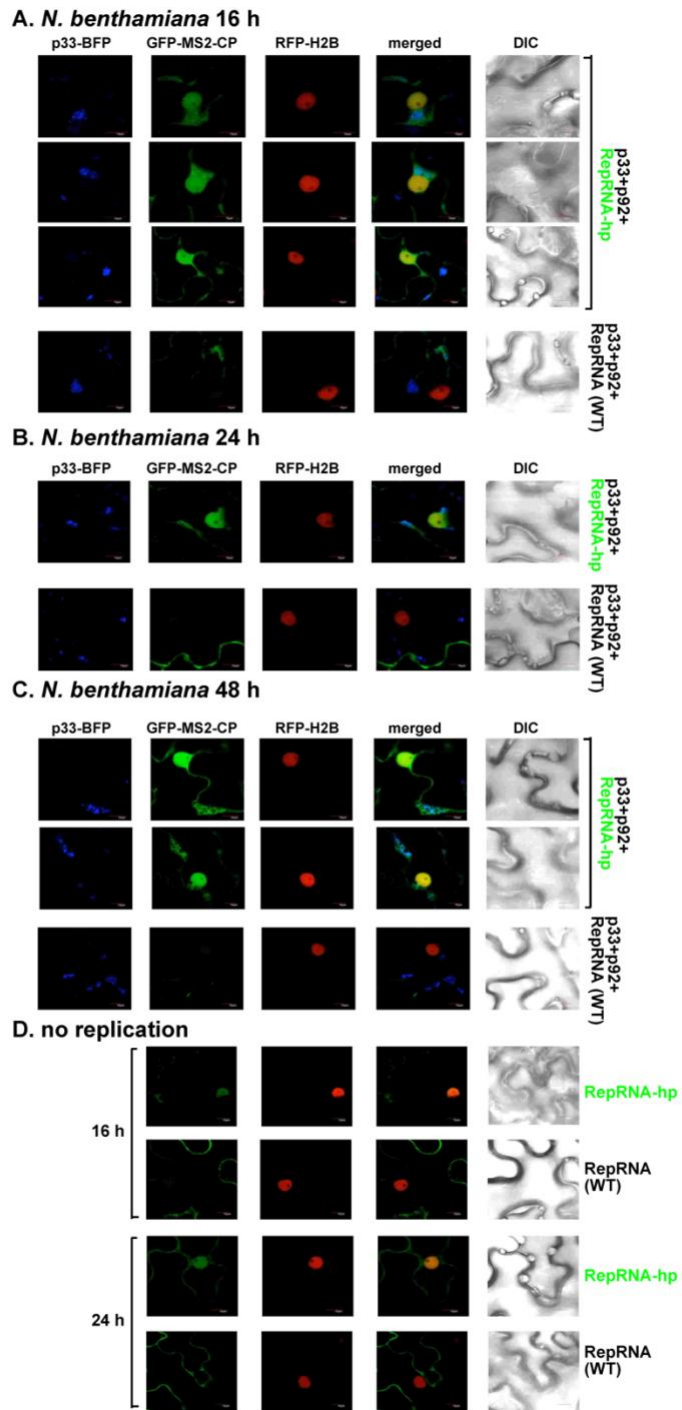


Figure 4.10

Figure 4.10 A portion of the viral (+)RNA distributes into the nucleus of plant cells.

Transgenic *N. benthamiana* (constitutively expressing H2B fused to RFP) leaves were co-infiltrated with p33, p33-BFP, GFP-MS2-CP, p92^{pol} and p19. After 24 h, infiltrated plants were rub-inoculated with repRNA-hp, (which carried six copies of the MS2 phage RNA hairpin recognized by GFP-MS2-CP) or regular repRNA. (A, top panels) Confocal microscopy analyses show that GFP-MS2-CP re-localizes into both the cytosolic VROs (marked by p33-BFP) and the nucleus (marked with RFP-HB2) 16 h after inoculation of the repRNA-hp transcripts. The cytosolic and nuclear distribution of GFP-MS2-CP remained at the 24 h (B, top panel) and 48 h (C, top panels) timepoints. (A-C, bottom panels) Localization of p33-BFP, GFP-MS2-CP and RFP-H2B in repRNA rub-inoculated plants was at the peroxisome, cytosol and nucleus respectively and no GFP-MS2-CP re-localization was observed. (D) Replication of repRNA-hp transcripts is not required for the RNA to re-localize into the nucleus. GFP-MS2-CP partially localizes in the nucleus of repRNA-hp rub-inoculated plants in the absence of p33 and p92^{pol}, 16 h and 24 h after inoculation. Inoculation of repRNA WT did not alter GFP-MS2-CP cytosolic localization.

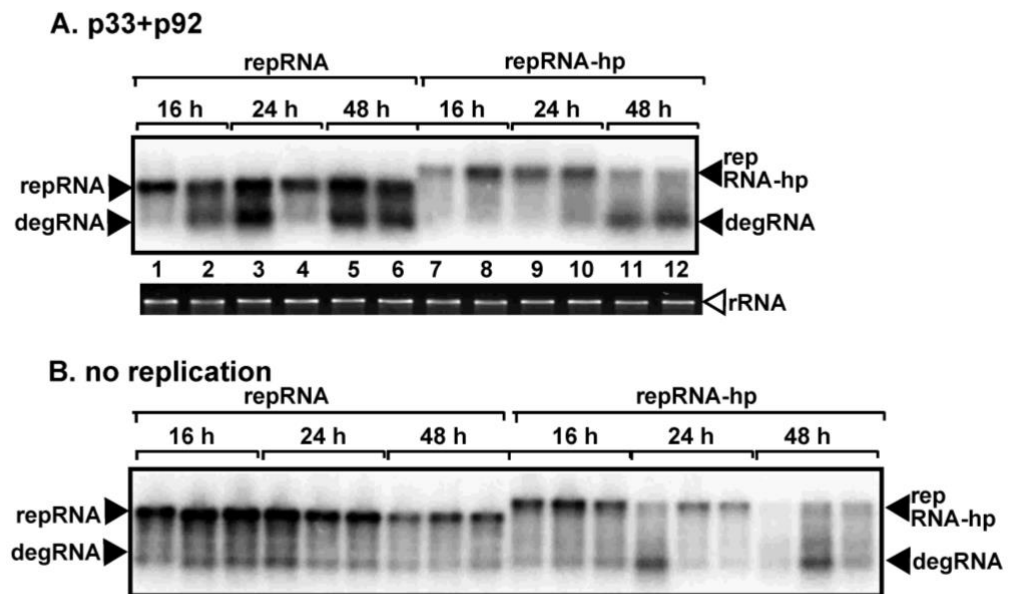


Figure 4.11

Figure 4.11 RepRNA-hp is replication competent in the presence of p33 and p92^{pol}.

Nicotiana benthamiana epidermal cells were treated as in Figure 4.10. Samples were collected at 16 h, 24 h and 48 h after transcript inoculation and total RNA was isolated. (A) Northern blot analysis with a ³²P-labeled DI-72-RIII/IV probe show that similar to the repRNA, repRNA-hp is replicated in the presence of co-expressed viral replication proteins p33 and p92^{pol}. In contrast, in the absence of the viral replication machinery (B), both the repRNA and the repRNA-hp accumulation start to decrease over time as shown by northern blot analysis of the samples collected at 24 h and 48 h after transcript inoculation. Experiments were repeated at least three times.

Chapter 5

CONCLUSIONS AND PERSPECTIVES

5.1 Conclusions

Network analysis of viral host factor interactions provides systems-level insights of the viral replication process. A large number of studies using yeast as a surrogate for tombusviruses have explored how, in order to achieve robust replication and evade antiviral responses, these small (+)RNA viruses remodel several cellular processes and membrane structures by hijacking key host-coded proteins and lipids and altering signaling pathways. The result of these studies has been a long list of host factors affecting tombusvirus replication with different functions. In Chapter 2, taking advantage of the extensively characterized *S. cerevisiae* interactome, interaction networks were assembled with previously identified host proteins in search of information about how these proteins work during tombusvirus replication. With the first network analysis, which included 73 CIRFs and some other pro-viral host factors, I found that virus replication is limited by a wide variety of gene functions, particularly RNA metabolism, processing and maturation, and protein folding and modification/ubiquitination (Figure 2.1). Unexpected groups of proteins suppressing TBSV replication have functions related to chromatin remodeling, transcription and nuclear transport (Figure 2.1-2.2). The yeast proteins with the highest connectivity in the network map included the well-characterized Xrn1p 5'–3'

exoribonuclease, and the not-yet characterized (as anti-TBSV proteins) Act1p actin protein and Cse4p centromere protein.

In the second network analysis, it was observed that the replication steps requiring more host factors are VRO and VRC biogenesis as well as lipid metabolism and MCS formation. Within the VRO and VRC biogenesis group, the ESCRT proteins (Table 2.2) are the more abundant, with seven identified. For the lipid metabolism and MCS group, the most represented genes are the ones involved in sterol transfer and phospholipid synthesis. The overall hubs for the physical and genetic interactions networks were Act1, Rsp5, Rpn11 and Sec22 proteins. By removing the genetic interactions from the network, some of the host proteins were missing possibly because their interactome is not yet complete. There was also a shift of network hubs with Rpn11 metalloprotease becoming the main hub in this network along with Ssa1 and Cse4. Of specific interest was that despite the network differences (different sets of host factors, types of interactions), Act1, Rpn11 and Cse4 kept reappearing as hubs.

The findings made with the network's assembly became evidence of the importance of this type of analysis and encouraged the detailed characterization of Act1, Rpn11 and Cse4 which have contributed to an increased understanding of tombusvirus replication.

The microtubule cytoskeleton has a role in the recruitment of host factors into the VROs.

Diverse studies have led to the identification of the important roles of cell cytoskeleton during the viral infection process. Whereas most analyses have focused on viral trafficking inside or between cells, only a few explore other kinds of roles for the cytoskeleton in viral

infection such as transcription, gene regulation or replication. Temperature-sensitive (ts) mutants of β -tubulin and γ -tubulin proteins and pharmacological inhibitors have shown that stability of microtubules as a consequence of the decrease in polymerization turnover rate enhances TBSV replication (Chapter 3). Elevated *in vitro* activity of the tombusvirus replicase isolated from tubulin mutant yeast was found, suggesting that assembly and/or efficiency of the replicase is more robust in the *tub2^{ts}* mutant.

Although interaction between TBSV replication proteins and the components of microtubules do not seem to occur directly, evidence showed that microtubules affect the enrichment of sterols at replication sites. For example, Vap27-1 protein was co-opted more efficiently from *tub2^{ts}* yeast in comparison with wt, as observed with co-purification and BiFC experiments. Similarly, an ORP protein was more efficiently co-purified with p33 in the mutant yeast. Vap27-1 and ORP proteins have a role in the formation of MCS which are important for the channeling of lipids to the viral replication sites, whereas microtubules are involved in the localization of Vap27-1 at the MCS. In addition to this, microtubules affected the hijacking of pro-viral host factors involved in VRC assembly such as Pex19, eEF1A, Vps4 and Cdc34. Based on these findings, I propose that microtubules and the cytoskeleton overall is important for the biogenesis of tombusvirus-induced viral replication organelles.

The essential centromeric histone H3 is a novel regulatory and antiviral factor for tombusviruses. Plants limit virus replication via cell-intrinsic restriction factors (CIRFs). Several of these antiviral factors have been identified for tombusviruses in the surrogate host *S. cerevisiae* using high-throughput screens with genomic libraries. Based on Chapter

2 protein network analyses, among the recognized CIRFs, CenH3/Cse4 is a highly connected node within the ~500 host factors previously identified to affect TBSV replication or TBSV-host interactions in yeast. Experiments with a yeast temperature-sensitive mutant and silencing or overexpression of the plant homolog CenH3 in *N. benthamiana* suggested a significant effect of this protein on viral replication. Whereas over-expression of CenH3 greatly interferes with tombusvirus replication, mutation or knockdown of CenH3 enhances TBSV replication in yeast and plants. Despite the fact that histones are crucial components of nucleosomes, new viral RNA binding activity was found between the plant or yeast CENH3 and the viral RNA. CENH3 is also partially re-distributed to the sites of replication upon virus infection.

Although, these data support a restriction role of CenH3 in tombusvirus replication, it was demonstrated that by partially sequestering CenH3 into VROs, TBSV can reprogram selective gene expression of the host, leading to a more abundant protein pool. This in turn helps TBSV to recruit pro-viral host factors from the protein pool. This was shown for the glycolytic and fermentation enzymes which are exploited more efficiently by tombusviruses to produce abundant ATP locally within the VROs in infected cells.

Altogether, the data shown in Chapter 4, suggest that subversion of CenH3/Cse4p from the nucleus into cytosolic VROs facilitates epigenetic reprogramming of the cells, which ultimately leads to more efficient ATP generation locally within VROs by the co-opted glycolytic enzymes to support the energy requirement of virus replication.

5.2 Perspectives

Analysis of the interactions between identified host-coded proteins affecting viral replication should be performed routinely. Annotations of proteins in databases are incomplete or not well curated. Furthermore, the variety of methods used for the identification of protein-protein associations are noisy in nature and can contain many false positives and false negatives (i.e., missing interactions). It is important then, that network analyses with protein-protein interactions of characterized host factors become a frequently used approach to study the viral replication process. Some relevant points to keep in mind are: (i) the inferences we make after a network analysis should be used to elaborate hypotheses and to generate experimental plans involving further validation experiments; and (ii) biological networks are dynamic and undergo significant re-wiring according to different conditions and the specific cell type being considered, making some network construction approaches insufficient to identify interactions that are condition specific.

As PPI network construction and analysis for viral host factors become easier to perform, either because gene function annotations become widely available or because the process is automated with the development of new software tools and programs, researchers would need to consider new conditions and parameters to try. For example, as observed with the construction of networks in Figures 2.3 and 2.4 (Chapter 2), including both genetic and physical interactions generates different types of results compared to the network created from physical interactions only. The integration of multiple datasets (i.e. gene expression, protein interaction and functional annotation) together with the

comparisons between different databases should also be taken into consideration when used for network inference and interpreting the data.

Small (+)RNA viruses target several hundred host proteins during infection but their relationship with host cells focuses on more than just protein-protein interactions. The virus-host interactome clearly does not consist of protein alone as it also involves lipids, nucleic acids, carbohydrates and small molecules (e.g., hormones, metabolites). Ideally, interaction network analyses should include these types of molecules too, but unfortunately databases vary widely in the coverage of these types of molecular interactions. Integration of this and other types of data, in a standardized fashion, still needs to be developed. So, in the meantime, virologists should try to make the most of the available tools and data.

Friends or foes? Understanding the role of microtubules in tombusvirus replication. Being part of a robust system such in the cell, the microtubule cytoskeleton plays many roles for cellular homeostasis. This complicates the elucidation of its effect in the specific steps of viral infection. Preliminarily, I thought about two possibilities with the first one being related to antiviral responses within the cells. It is straightforward to think that many of the antiviral factors such as the well-known interferons in mammalian cells [200], the small interfering RNAs deeply characterized in plants [201] or cytosolic ribonucleases (e.g., the 5'-3' RNase Xnr1p), a major RNA stability factor), use microtubule “highways” to move from their normal subcellular localization to the sites of viral replication. Furthermore, viruses need to co-opt many types of host factors for their own benefit, many of which are also moved through microtubule fibers. In this manner, a competition for control of the cell is established between viruses and host cells. An

increased number of stable microtubules (characteristic of the *tub2^{ts}* yeast mutant cells) might facilitate the recruitment of resources for the virus, favoring its replication.

The second alternative involves the internal changes that occur when microtubules are mutated or chemically disrupted and does not exclude the alternative above. It is known that viruses replicate by altering several cellular pathways or remodeling membrane compartments, but what happens when the cellular environment is already altered, due to environmental changes or genetic mutations of the host? We can imagine that in the case of γ and β -tubulin ts mutants and nocodazole treated yeasts and *N. benthamiana* leaves, the cellular conditions are different compared to wt cells. Indeed, I observed that the tombusvirus replicase showed altered properties when purified from the mutant cells, suggesting changes in the assembly process. This is consistent with the fact that microtubules are crucial for many processes and their disruption may in turn alter other aspects such as cell cycle, organelle biogenesis or vesicular transport, creating a new microenvironment suitable for viral replication. The current suggested model for the role of microtubules was described in Chapter 3.

Friends or foes? I can say that microtubules can be coincidentally both. All depends on their structure and dynamicity at the time when viruses enter the cells. Though more experiments are needed to unravel the exact role of microtubules during tombusvirus replication (besides movement of host factors), such as biochemical or genetic interactions, organelle positional or structural alterations and possible suppressed antiviral responses, I showed that the function of the replicase complex is affected by the function of microtubules.

Do microtubules affect TBSV replication through crosstalk with the actin network? It has become apparent that although microtubules and actin filaments form two distinct networks, they also engage in substantial crosstalk and work in a coordinated manner. This communication is mediated by accessory proteins which interact with both networks, creating the organized cytoskeleton [166]. Besides, intracellular traffic stops when actin filaments meet microtubules. These crossing sites become places for unloading or exchanging cargos between the trafficking routes in plant cells [167]. It has been found that cofilin (actin depolymerization factor) interacts with TBSV p33 replication protein, facilitating the recruitment of viral and cellular components for VRC assembly and formation of VROs [68]. Therefore, it is possible that plants use the coordinated functions of microtubules and the actin cytoskeleton to restrict tombusvirus replication. In contrast, the active manipulation of the cytoskeleton by TBSV counteracts CIRF functions and enables the co-option of pro-viral host components to build protective VROs in infected cells. In summary, the dynamic cytoskeleton of actin filaments and microtubules is a central determinant of TBSV-host interactions.

The functional characterization of host factors during viral replication provides deeper understanding of the host cell biology. CenH3 function is well conserved among eukaryotes and over the years its centromeric canonical function has been studied extensively. Nonetheless, studies presented in Chapter 4 suggest that virus infection can uncover noncanonical functions for this factor, that have not been previously identified or at least not characterized on the basis of their antiviral properties. The emerging theme from Chapter 4 studies is that sequestration of CenH3/Cse4 from the nucleus into the

cytosolic VROs by tombusviruses requires an important balancing act. Robust TBSV replication depends on the virus's ability to reprogram host gene transcription, in which CenH3/Cse4 plays a mostly unexplored role. It is fascinating how the study of viral replication in plant cells allows for the discovery of novel and different roles that a protein can have inside a host cell. This has not only been beneficial to deepen our understanding of plant virus infection processes but has expanded our potential to develop new ways of engineering disease resistance and has opened new avenues to study cellular plant biology and disease states.

Dependence of cellular resources and the cellular alterations induced by animal viruses have many similarities with what is observed for plant virus infection. There is some fundamental and universal nature of virus replication that can be illustrated by the fact that certain plant viruses replicate in other hosts, such as insects or yeast. Thus, the characterization of plant virus replication is intertwined with that of animal viruses, and important discoveries in one area greatly impact the other.

Microtubules and the centromeric histone H3 are negative regulatory cell-intrinsic restriction factors. Subversion of CenH3/Cse4 is a “double-edged sword”: advantageous for TBSV under some conditions, but disadvantageous under over-expression conditions when CenH3/Cse4 acts as a strong restriction factor. Therefore, CenH3 activities might affect host susceptibility and also tombusvirus host ranges. The data obtained in Chapter 4 point at a new frontier in cytosolic RNA virus-host interaction, which involves the nucleus and epigenetic reprogramming of the host cells to facilitate virus replication. Likewise, the dynamicity of the microtubule network is beneficial for the virus when it is disrupted but

detrimental under normal conditions. Altogether, the studies with the microtubule cytoskeleton and CenH3 revealed an emerging picture for positive stranded (+)RNA tombusviruses, suggesting that their ability to exploit cellular membrane structures and rewiring complex pathways requires the activities of particular kinds of CIRFs. These types of factors, which I called negative regulatory CIRFs, have an intrinsic antiviral function but are exploited by the virus to achieve robust replication at the expense of certain viral resources.

Recommendations for future research directions. The research discussed in Chapter 3 suggest that the effect of microtubules to restrict tombusvirus replication is coordinated with the functions and dynamics of the actin network. It will be important that further studies investigate how microtubules and actin filaments communicate with each other during tombusvirus replication. For example, one direct way of actin–microtubule crosstalk is provided by proteins that crosslink microtubules to actin bundles [166]. Then, an interesting topic for future work is the potential involvement of these crosslinking proteins in the organization of both cytoskeleton components when cells are being challenged by tombusviruses.

Another interesting question for future research that can be derived from Chapter 4 is the functionality of the tombusvirus RNA inside the nucleus. The intensive remodeling of the cell by tombusviruses suggest that targeting of the viral RNA into the nucleus has multiple purposes that can range from disruption of gene expression, co-option of nuclear components and alterations of the nuclear architecture. Further work is certainly required to explore the mechanism of viral RNA import into the nucleus and the roles it plays once it is inside this important cellular organelle.

REFERENCES

1. Russo M, Burgyan J, Martelli GP. Molecular biology of tombusviridae. *Adv Virus Res.* 1994;44:381-428. Epub 1994/01/01. doi: 10.1016/s0065-3527(08)60334-6. PubMed PMID: 7817878.
2. White KA, Nagy PD. Advances in the molecular biology of tombusviruses: gene expression, genome replication, and recombination. *Prog Nucleic Acid Res Mol Biol.* 2004;78:187-226. Epub 2004/06/24. doi: 10.1016/S0079-6603(04)78005-8. PubMed PMID: 15210331.
3. Nagy PD, Pogany J. The dependence of viral RNA replication on co-opted host factors. *Nat Rev Microbiol.* 2011;10(2):137-49. Epub 2011/12/21. doi: 10.1038/nrmicro2692. PubMed PMID: 22183253; PubMed Central PMCID: PMC7097227.
4. Nagy PD, Barajas D, Pogany J. Host factors with regulatory roles in tombusvirus replication. *Curr Opin Virol.* 2012;2(6):691-8. Epub 2012/11/06. doi: 10.1016/j.coviro.2012.10.004. PubMed PMID: 23122856.
5. Nagy PD. Tombusvirus-Host Interactions: Co-Opted Evolutionarily Conserved Host Factors Take Center Court. *Annu Rev Virol.* 2016;3(1):491-515. Epub 2016/09/01. doi: 10.1146/annurev-virology-110615-042312. PubMed PMID: 27578441.
6. Oster SK, Wu B, White KA. Uncoupled expression of p33 and p92 permits amplification of tomato bushy stunt virus RNAs. *J Virol.* 1998;72(7):5845-51. Epub 1998/06/17. doi: 10.1128/JVI.72.7.5845-5851.1998. PubMed PMID: 9621045; PubMed Central PMCID: PMC110387.
7. Scholthof KB, Scholthof HB, Jackson AO. The tomato bushy stunt virus replicase proteins are coordinately expressed and membrane associated. *Virology.* 1995;208(1):365-9. Epub 1995/04/01. doi: 10.1006/viro.1995.1162. PubMed PMID: 11831721.
8. Jonezyk M, Pathak KB, Sharma M, Nagy PD. Exploiting alternative subcellular location for replication: tombusvirus replication switches to the endoplasmic reticulum in the absence of peroxisomes. *Virology.* 2007;362(2):320-30. Epub 2007/02/13. doi: 10.1016/j.virol.2007.01.004. PubMed PMID: 17292435.
9. Panavas T, Hawkins CM, Panaviene Z, Nagy PD. The role of the p33:p33/p92 interaction domain in RNA replication and intracellular localization of p33 and p92 proteins of Cucumber necrosis tombusvirus. *Virology.* 2005;338(1):81-95. Epub 2005/06/07. doi: 10.1016/j.virol.2005.04.025. PubMed PMID: 15936051.
10. Pogany J, White KA, Nagy PD. Specific binding of tombusvirus replication protein p33 to an internal replication element in the viral RNA is essential for replication. *J Virol.* 2005;79(8):4859-69. Epub 2005/03/30. doi: 10.1128/JVI.79.8.4859-4869.2005. PubMed PMID: 15795271; PubMed Central PMCID: PMC1069559.
11. Stork J, Kovalev N, Sasvari Z, Nagy PD. RNA chaperone activity of the tombusviral p33 replication protein facilitates initiation of RNA synthesis by the viral RdRp in vitro. *Virology.* 2011;409(2):338-47. Epub 2010/11/13. doi:

- 10.1016/j.virol.2010.10.015. PubMed PMID: 21071052; PubMed Central PMCID: PMCPMC7173327.
12. Panaviene Z, Panavas T, Nagy PD. Role of an internal and two 3'-terminal RNA elements in assembly of tombusvirus replicase. *J Virol.* 2005;79(16):10608-18. Epub 2005/07/30. doi: 10.1128/JVI.79.16.10608-10618.2005. PubMed PMID: 16051853; PubMed Central PMCID: PMCPMC1182651.
 13. Panaviene Z, Panavas T, Serva S, Nagy PD. Purification of the cucumber necrosis virus replicase from yeast cells: role of coexpressed viral RNA in stimulation of replicase activity. *J Virol.* 2004;78(15):8254-63. Epub 2004/07/16. doi: 10.1128/JVI.78.15.8254-8263.2004. PubMed PMID: 15254197; PubMed Central PMCID: PMCPMC446104.
 14. Pathak KB, Pogany J, Xu K, White KA, Nagy PD. Defining the roles of cis-acting RNA elements in tombusvirus replicase assembly in vitro. *J Virol.* 2012;86(1):156-71. Epub 2011/10/21. doi: 10.1128/JVI.00404-11. PubMed PMID: 22013057; PubMed Central PMCID: PMCPMC3255868.
 15. Pogany J, Nagy PD. Authentic replication and recombination of Tomato bushy stunt virus RNA in a cell-free extract from yeast. *J Virol.* 2008;82(12):5967-80. Epub 2008/04/18. doi: 10.1128/JVI.02737-07. PubMed PMID: 18417594; PubMed Central PMCID: PMCPMC2395147.
 16. Miller WA, Koev G. Synthesis of subgenomic RNAs by positive-strand RNA viruses. *Virology.* 2000;273(1):1-8. Epub 2000/07/13. doi: 10.1006/viro.2000.0421. PubMed PMID: 10891401.
 17. Scholthof HB, Scholthof KB, Kikkert M, Jackson AO. Tomato bushy stunt virus spread is regulated by two nested genes that function in cell-to-cell movement and host-dependent systemic invasion. *Virology.* 1995;213(2):425-38. Epub 1995/11/10. doi: 10.1006/viro.1995.0015. PubMed PMID: 7491767.
 18. Qu F, Morris TJ. Efficient infection of *Nicotiana benthamiana* by Tomato bushy stunt virus is facilitated by the coat protein and maintained by p19 through suppression of gene silencing. *Mol Plant Microbe Interact.* 2002;15(3):193-202. Epub 2002/04/16. doi: 10.1094/MPMI.2002.15.3.193. PubMed PMID: 11952121.
 19. Voinnet O, Pinto YM, Baulcombe DC. Suppression of gene silencing: a general strategy used by diverse DNA and RNA viruses of plants. *Proc Natl Acad Sci U S A.* 1999;96(24):14147-52. Epub 1999/11/26. doi: 10.1073/pnas.96.24.14147. PubMed PMID: 10570213; PubMed Central PMCID: PMCPMC24205.
 20. Qiu W, Park JW, Scholthof HB. Tombusvirus P19-mediated suppression of virus-induced gene silencing is controlled by genetic and dosage features that influence pathogenicity. *Mol Plant Microbe Interact.* 2002;15(3):269-80. Epub 2002/04/16. doi: 10.1094/MPMI.2002.15.3.269. PubMed PMID: 11952130.
 21. Hillman BI, Hearne P, Rochon D, Morris TJ. Organization of tomato bushy stunt virus genome: characterization of the coat protein gene and the 3' terminus. *Virology.* 1989;169(1):42-50. Epub 1989/03/01. doi: 10.1016/0042-6822(89)90039-1. PubMed PMID: 2922927.
 22. Nagy PD, Pogany J. Partial purification and characterization of Cucumber necrosis virus and Tomato bushy stunt virus RNA-dependent RNA polymerases: similarities and differences in template usage between tombusvirus and carmovirus RNA-

- dependent RNA polymerases. *Virology*. 2000;276(2):279-88. Epub 2000/10/21. doi: 10.1006/viro.2000.0577. PubMed PMID: 11040120.
23. Panavas T, Nagy PD. Yeast as a model host to study replication and recombination of defective interfering RNA of Tomato bushy stunt virus. *Virology*. 2003;314(1):315-25. Epub 2003/10/01. doi: 10.1016/s0042-6822(03)00436-7. PubMed PMID: 14517084.
 24. Shah Nawaz-ul-Rehman M, Martinez-Ochoa N, Pascal H, Sasvari Z, Herbst C, Xu K, et al. Proteome-wide overexpression of host proteins for identification of factors affecting tombusvirus RNA replication: an inhibitory role of protein kinase C. *J Virol*. 2012;86(17):9384-95. Epub 2012/06/22. doi: 10.1128/JVI.00019-12. PubMed PMID: 22718827; PubMed Central PMCID: PMC3416130.
 25. Nawaz-ul-Rehman MS, Reddisiva Prasanth K, Baker J, Nagy PD. Yeast screens for host factors in positive-strand RNA virus replication based on a library of temperature-sensitive mutants. *Methods*. 2013;59(2):207-16. Epub 2012/11/14. doi: 10.1016/j.ymeth.2012.11.001. PubMed PMID: 23147170.
 26. Kushner DB, Lindenbach BD, Grdzlishvili VZ, Noueiry AO, Paul SM, Ahlquist P. Systematic, genome-wide identification of host genes affecting replication of a positive-strand RNA virus. *Proc Natl Acad Sci U S A*. 2003;100(26):15764-9. Epub 2003/12/13. doi: 10.1073/pnas.2536857100. PubMed PMID: 14671320; PubMed Central PMCID: PMC307642.
 27. Panavas T, Serviene E, Brasher J, Nagy PD. Yeast genome-wide screen reveals dissimilar sets of host genes affecting replication of RNA viruses. *Proc Natl Acad Sci U S A*. 2005;102(20):7326-31. Epub 2005/05/11. doi: 10.1073/pnas.0502604102. PubMed PMID: 15883361; PubMed Central PMCID: PMC1129141.
 28. Serviene E, Shapka N, Cheng CP, Panavas T, Phuangrat B, Baker J, et al. Genome-wide screen identifies host genes affecting viral RNA recombination. *Proc Natl Acad Sci U S A*. 2005;102(30):10545-50. Epub 2005/07/20. doi: 10.1073/pnas.0504844102. PubMed PMID: 16027361; PubMed Central PMCID: PMC1180806.
 29. Jiang Y, Serviene E, Gal J, Panavas T, Nagy PD. Identification of essential host factors affecting tombusvirus RNA replication based on the yeast Tet promoters Hughes Collection. *J Virol*. 2006;80(15):7394-404. Epub 2006/07/15. doi: 10.1128/JVI.02686-05. PubMed PMID: 16840320; PubMed Central PMCID: PMC1563710.
 30. Serviene E, Jiang Y, Cheng CP, Baker J, Nagy PD. Screening of the yeast yTHC collection identifies essential host factors affecting tombusvirus RNA recombination. *J Virol*. 2006;80(3):1231-41. Epub 2006/01/18. doi: 10.1128/JVI.80.3.1231-1241.2006. PubMed PMID: 16415000; PubMed Central PMCID: PMC1346934.
 31. Cheng CP, Nagy PD. Mechanism of RNA recombination in carmo- and tombusviruses: evidence for template switching by the RNA-dependent RNA polymerase in vitro. *J Virol*. 2003;77(22):12033-47. Epub 2003/10/29. doi: 10.1128/jvi.77.22.12033-12047.2003. PubMed PMID: 14581540; PubMed Central PMCID: PMC1346934.

32. Xu K, Huang TS, Nagy PD. Authentic in vitro replication of two tombusviruses in isolated mitochondrial and endoplasmic reticulum membranes. *J Virol.* 2012;86(23):12779-94. Epub 2012/09/14. doi: 10.1128/JVI.00973-12. PubMed PMID: 22973028; PubMed Central PMCID: PMCPMC3497632.
33. Medina-Puche L, Lozano-Duran R. Tailoring the cell: a glimpse of how plant viruses manipulate their hosts. *Curr Opin Plant Biol.* 2019;52:164-73. Epub 2019/11/16. doi: 10.1016/j.pbi.2019.09.007. PubMed PMID: 31731105.
34. Laliberte JF, Sanfacon H. Cellular remodeling during plant virus infection. *Annu Rev Phytopathol.* 2010;48:69-91. Epub 2010/03/27. doi: 10.1146/annurev-phyto-073009-114239. PubMed PMID: 20337516.
35. Romero-Brey I, Bartenschlager R. Membranous replication factories induced by plus-strand RNA viruses. *Viruses.* 2014;6(7):2826-57. Epub 2014/07/24. doi: 10.3390/v6072826. PubMed PMID: 25054883; PubMed Central PMCID: PMCPMC4113795.
36. Wang A. Dissecting the molecular network of virus-plant interactions: the complex roles of host factors. *Annu Rev Phytopathol.* 2015;53:45-66. Epub 2015/05/06. doi: 10.1146/annurev-phyto-080614-120001. PubMed PMID: 25938276.
37. Fernandez de Castro I, Fernandez JJ, Barajas D, Nagy PD, Risco C. Three-dimensional imaging of the intracellular assembly of a functional viral RNA replicase complex. *J Cell Sci.* 2017;130(1):260-8. Epub 2016/03/31. doi: 10.1242/jcs.181586. PubMed PMID: 27026525.
38. Barajas D, Jiang Y, Nagy PD. A unique role for the host ESCRT proteins in replication of Tomato bushy stunt virus. *PLoS Pathog.* 2009;5(12):e1000705. Epub 2009/12/31. doi: 10.1371/journal.ppat.1000705. PubMed PMID: 20041173; PubMed Central PMCID: PMCPMC2791863.
39. Nagy PD, Lin W. Taking over Cellular Energy-Metabolism for TBSV Replication: The High ATP Requirement of an RNA Virus within the Viral Replication Organelle. *Viruses.* 2020;12(1). Epub 2020/01/18. doi: 10.3390/v12010056. PubMed PMID: 31947719; PubMed Central PMCID: PMCPMC7019945.
40. Zhang Z, He G, Filipowicz NA, Randall G, Belov GA, Kopek BG, et al. Host Lipids in Positive-Strand RNA Virus Genome Replication. *Front Microbiol.* 2019;10:286. Epub 2019/03/14. doi: 10.3389/fmicb.2019.00286. PubMed PMID: 30863375; PubMed Central PMCID: PMCPMC6399474.
41. Jin X, Cao X, Wang X, Jiang J, Wan J, Laliberte JF, et al. Three-Dimensional Architecture and Biogenesis of Membrane Structures Associated with Plant Virus Replication. *Front Plant Sci.* 2018;9:57. Epub 2018/02/15. doi: 10.3389/fpls.2018.00057. PubMed PMID: 29441085; PubMed Central PMCID: PMCPMC5797596.
42. Levy A, Tilsner J. Creating Contacts Between Replication and Movement at Plasmodesmata - A Role for Membrane Contact Sites in Plant Virus Infections? *Front Plant Sci.* 2020;11:862. Epub 2020/07/29. doi: 10.3389/fpls.2020.00862. PubMed PMID: 32719692; PubMed Central PMCID: PMCPMC7350983.
43. Barajas D, Xu K, de Castro Martin IF, Sasvari Z, Brandizzi F, Risco C, et al. Co-opted oxysterol-binding ORP and VAP proteins channel sterols to RNA virus replication sites via membrane contact sites. *PLoS Pathog.* 2014;10(10):e1004388.

- Epub 2014/10/21. doi: 10.1371/journal.ppat.1004388. PubMed PMID: 25329172; PubMed Central PMCID: PMC4199759.
44. Feng Z, Xu K, Kovalev N, Nagy PD. Recruitment of Vps34 PI3K and enrichment of PI3P phosphoinositide in the viral replication compartment is crucial for replication of a positive-strand RNA virus. *PLoS Pathog.* 2019;15(1):e1007530. Epub 2019/01/10. doi: 10.1371/journal.ppat.1007530. PubMed PMID: 30625229; PubMed Central PMCID: PMC6342326.
 45. Kovalev N, Inaba JI, Li Z, Nagy PD. The role of co-opted ESCRT proteins and lipid factors in protection of tombusviral double-stranded RNA replication intermediate against reconstituted RNAi in yeast. *PLoS Pathog.* 2017;13(7):e1006520. Epub 2017/08/02. doi: 10.1371/journal.ppat.1006520. PubMed PMID: 28759634; PubMed Central PMCID: PMC5552349.
 46. Xu K, Nagy PD. Enrichment of Phosphatidylethanolamine in Viral Replication Compartments via Co-opting the Endosomal Rab5 Small GTPase by a Positive-Strand RNA Virus. *PLoS Biol.* 2016;14(10):e2000128. Epub 2016/10/21. doi: 10.1371/journal.pbio.2000128. PubMed PMID: 27760128; PubMed Central PMCID: PMC5070881.
 47. Nagy PD, Strating JR, van Kuppeveld FJ. Building Viral Replication Organelles: Close Encounters of the Membrane Types. *PLoS Pathog.* 2016;12(10):e1005912. Epub 2016/10/28. doi: 10.1371/journal.ppat.1005912. PubMed PMID: 27788266; PubMed Central PMCID: PMC5082816.
 48. Paul D, Bartenschlager R. Architecture and biogenesis of plus-strand RNA virus replication factories. *World J Virol.* 2013;2(2):32-48. Epub 2013/11/01. doi: 10.5501/wjv.v2.i2.32. PubMed PMID: 24175228; PubMed Central PMCID: PMC3785047.
 49. Fletcher DA, Mullins RD. Cell mechanics and the cytoskeleton. *Nature.* 2010;463(7280):485-92. Epub 2010/01/30. doi: 10.1038/nature08908. PubMed PMID: 20110992; PubMed Central PMCID: PMC2851742.
 50. Howard J, Hyman AA. Dynamics and mechanics of the microtubule plus end. *Nature.* 2003;422(6933):753-8. Epub 2003/04/18. doi: 10.1038/nature01600. PubMed PMID: 12700769.
 51. Chhabra ES, Higgs HN. The many faces of actin: matching assembly factors with cellular structures. *Nat Cell Biol.* 2007;9(10):1110-21. Epub 2007/10/03. doi: 10.1038/ncb1007-1110. PubMed PMID: 17909522.
 52. Radtke K, Dohner K, Sodeik B. Viral interactions with the cytoskeleton: a hitchhiker's guide to the cell. *Cell Microbiol.* 2006;8(3):387-400. Epub 2006/02/14. doi: 10.1111/j.1462-5822.2005.00679.x. PubMed PMID: 16469052.
 53. Taylor MP, Koyuncu OO, Enquist LW. Subversion of the actin cytoskeleton during viral infection. *Nat Rev Microbiol.* 2011;9(6):427-39. Epub 2011/04/28. doi: 10.1038/nrmicro2574. PubMed PMID: 21522191; PubMed Central PMCID: PMC3229036.
 54. Naghavi MH, Walsh D. Microtubule Regulation and Function during Virus Infection. *J Virol.* 2017;91(16). Epub 2017/06/16. doi: 10.1128/JVI.00538-17. PubMed PMID: 28615197; PubMed Central PMCID: PMC5533906.
 55. Pelkmans L, Puntener D, Helenius A. Local actin polymerization and dynamin recruitment in SV40-induced internalization of caveolae. *Science.*

- 2002;296(5567):535-9. Epub 2002/04/20. doi: 10.1126/science.1069784. PubMed PMID: 11964480.
56. Lehmann MJ, Sherer NM, Marks CB, Pypaert M, Mothes W. Actin- and myosin-driven movement of viruses along filopodia precedes their entry into cells. *J Cell Biol.* 2005;170(2):317-25. Epub 2005/07/20. doi: 10.1083/jcb.200503059. PubMed PMID: 16027225; PubMed Central PMCID: PMCPMC2171413.
 57. Nakano MY, Boucke K, Suomalainen M, Stidwill RP, Greber UF. The first step of adenovirus type 2 disassembly occurs at the cell surface, independently of endocytosis and escape to the cytosol. *J Virol.* 2000;74(15):7085-95. Epub 2000/07/11. doi: 10.1128/jvi.74.15.7085-7095.2000. PubMed PMID: 10888649; PubMed Central PMCID: PMCPMC112227.
 58. Komano J, Miyauchi K, Matsuda Z, Yamamoto N. Inhibiting the Arp2/3 complex limits infection of both intracellular mature vaccinia virus and primate lentiviruses. *Mol Biol Cell.* 2004;15(12):5197-207. Epub 2004/09/24. doi: 10.1091/mbc.e04-04-0279. PubMed PMID: 15385624; PubMed Central PMCID: PMCPMC532003.
 59. Lai CK, Jeng KS, Machida K, Lai MM. Association of hepatitis C virus replication complexes with microtubules and actin filaments is dependent on the interaction of NS3 and NS5A. *J Virol.* 2008;82(17):8838-48. Epub 2008/06/20. doi: 10.1128/JVI.00398-08. PubMed PMID: 18562541; PubMed Central PMCID: PMCPMC2519648.
 60. Lakadamyali M, Rust MJ, Babcock HP, Zhuang X. Visualizing infection of individual influenza viruses. *Proc Natl Acad Sci U S A.* 2003;100(16):9280-5. Epub 2003/07/29. doi: 10.1073/pnas.0832269100. PubMed PMID: 12883000; PubMed Central PMCID: PMCPMC170909.
 61. Lyman MG, Enquist LW. Herpesvirus interactions with the host cytoskeleton. *J Virol.* 2009;83(5):2058-66. Epub 2008/10/10. doi: 10.1128/JVI.01718-08. PubMed PMID: 18842724; PubMed Central PMCID: PMCPMC2643721.
 62. Yonezawa A, Cavrois M, Greene WC. Studies of ebola virus glycoprotein-mediated entry and fusion by using pseudotyped human immunodeficiency virus type 1 virions: involvement of cytoskeletal proteins and enhancement by tumor necrosis factor alpha. *J Virol.* 2005;79(2):918-26. Epub 2004/12/23. doi: 10.1128/JVI.79.2.918-926.2005. PubMed PMID: 15613320; PubMed Central PMCID: PMCPMC538559.
 63. Burke E, Mahoney NM, Almo SC, Barik S. Profilin is required for optimal actin-dependent transcription of respiratory syncytial virus genome RNA. *J Virol.* 2000;74(2):669-75. Epub 2000/01/07. doi: 10.1128/jvi.74.2.669-675.2000. PubMed PMID: 10623728; PubMed Central PMCID: PMCPMC111586.
 64. Gupta S, De BP, Drazba JA, Banerjee AK. Involvement of actin microfilaments in the replication of human parainfluenza virus type 3. *J Virol.* 1998;72(4):2655-62. Epub 1998/04/03. doi: 10.1128/JVI.72.4.2655-2662.1998. PubMed PMID: 9525582; PubMed Central PMCID: PMCPMC109707.
 65. Forest T, Barnard S, Baines JD. Active intranuclear movement of herpesvirus capsids. *Nat Cell Biol.* 2005;7(4):429-31. Epub 2005/04/02. doi: 10.1038/ncb1243. PubMed PMID: 15803134.
 66. Poole E, Strappe P, Mok HP, Hicks R, Lever AM. HIV-1 Gag-RNA interaction occurs at a perinuclear/centrosomal site; analysis by confocal microscopy and

- FRET. *Traffic*. 2005;6(9):741-55. Epub 2005/08/17. doi: 10.1111/j.1600-0854.2005.00312.x. PubMed PMID: 16101678.
67. Rietdorf J, Ploubidou A, Reckmann I, Holmstrom A, Frischknecht F, Zettl M, et al. Kinesin-dependent movement on microtubules precedes actin-based motility of vaccinia virus. *Nat Cell Biol*. 2001;3(11):992-1000. Epub 2001/11/21. doi: 10.1038/ncb1101-992. PubMed PMID: 11715020.
 68. Nawaz-ul-Rehman MS, Prasanth KR, Xu K, Sasvari Z, Kovalev N, de Castro Martin IF, et al. Viral Replication Protein Inhibits Cellular Cofilin Actin Depolymerization Factor to Regulate the Actin Network and Promote Viral Replicase Assembly. *PLoS Pathog*. 2016;12(2):e1005440. Epub 2016/02/11. doi: 10.1371/journal.ppat.1005440. PubMed PMID: 26863541; PubMed Central PMCID: PMC4749184.
 69. Prasanth KR, Kovalev N, de Castro Martin IF, Baker J, Nagy PD. Screening a yeast library of temperature-sensitive mutants reveals a role for actin in tombusvirus RNA recombination. *Virology*. 2016;489:233-42. Epub 2016/01/17. doi: 10.1016/j.virol.2015.12.007. PubMed PMID: 26773384.
 70. Calil IP, Fontes EPB. Plant immunity against viruses: antiviral immune receptors in focus. *Ann Bot*. 2017;119(5):711-23. Epub 2016/10/27. doi: 10.1093/aob/mcw200. PubMed PMID: 27780814; PubMed Central PMCID: PMC4749184.
 71. Zheng YH, Jeang KT, Tokunaga K. Host restriction factors in retroviral infection: promises in virus-host interaction. *Retrovirology*. 2012;9:112. Epub 2012/12/21. doi: 10.1186/1742-4690-9-112. PubMed PMID: 23254112; PubMed Central PMCID: PMC3549941.
 72. Zhou LY, Zhang LL. Host restriction factors for hepatitis C virus. *World J Gastroenterol*. 2016;22(4):1477-86. Epub 2016/01/29. doi: 10.3748/wjg.v22.i4.1477. PubMed PMID: 26819515; PubMed Central PMCID: PMC4721981.
 73. Villalon-Letelier F, Brooks AG, Saunders PM, Londrigan SL, Reading PC. Host Cell Restriction Factors that Limit Influenza A Infection. *Viruses*. 2017;9(12). Epub 2017/12/08. doi: 10.3390/v9120376. PubMed PMID: 29215570; PubMed Central PMCID: PMC5744151.
 74. Colomer-Lluch M, Ruiz A, Moris A, Prado JG. Restriction Factors: From Intrinsic Viral Restriction to Shaping Cellular Immunity Against HIV-1. *Front Immunol*. 2018;9:2876. Epub 2018/12/24. doi: 10.3389/fimmu.2018.02876. PubMed PMID: 30574147; PubMed Central PMCID: PMC6291751.
 75. Sasvari Z, Alatraste Gonzalez P, Nagy PD. Tombusvirus-yeast interactions identify conserved cell-intrinsic viral restriction factors. *Front Plant Sci*. 2014;5:383. Epub 2014/08/27. doi: 10.3389/fpls.2014.00383. PubMed PMID: 25157258; PubMed Central PMCID: PMC4127529.
 76. Bamberg JR, Wiggan OP. ADF/cofilin and actin dynamics in disease. *Trends Cell Biol*. 2002;12(12):598-605. Epub 2002/12/24. doi: 10.1016/s0962-8924(02)02404-2. PubMed PMID: 12495849.
 77. Bamberg JR, Bernstein BW. Roles of ADF/cofilin in actin polymerization and beyond. *F1000 Biol Rep*. 2010;2:62. Epub 2010/12/22. doi: 10.3410/B2-62. PubMed PMID: 21173851; PubMed Central PMCID: PMC2990448.

78. Bernstein BW, Bamburg JR. ADF/cofilin: a functional node in cell biology. *Trends Cell Biol.* 2010;20(4):187-95. Epub 2010/02/06. doi: 10.1016/j.tcb.2010.01.001. PubMed PMID: 20133134; PubMed Central PMCID: PMCPMC2849908.
79. Pogany J, Panavas T, Serviene E, Nawaz-ul-Rehman MS, P DN. A high-throughput approach for studying virus replication in yeast. *Curr Protoc Microbiol.* 2010;Chapter 16:Unit16J 1. Epub 2010/11/06. doi: 10.1002/9780471729259.mc16j01s19. PubMed PMID: 21053256.
80. Nagy PD, Pogany J. Yeast as a model host to dissect functions of viral and host factors in tombusvirus replication. *Virology.* 2006;344(1):211-20. Epub 2005/12/21. doi: 10.1016/j.virol.2005.09.017. PubMed PMID: 16364751.
81. Nagy PD. Yeast as a model host to explore plant virus-host interactions. *Annu Rev Phytopathol.* 2008;46:217-42. Epub 2008/04/22. doi: 10.1146/annurev.phyto.121407.093958. PubMed PMID: 18422427.
82. Li Z, Barajas D, Panavas T, Herbst DA, Nagy PD. Cdc34p ubiquitin-conjugating enzyme is a component of the tombusvirus replicase complex and ubiquitinates p33 replication protein. *J Virol.* 2008;82(14):6911-26. Epub 2008/05/09. doi: 10.1128/JVI.00702-08. PubMed PMID: 18463149; PubMed Central PMCID: PMCPMC2446948.
83. Mendu V, Chiu M, Barajas D, Li Z, Nagy PD. Cpr1 cyclophilin and Ess1 parvulin prolyl isomerases interact with the tombusvirus replication protein and inhibit viral replication in yeast model host. *Virology.* 2010;406(2):342-51. Epub 2010/08/17. doi: 10.1016/j.virol.2010.07.022. PubMed PMID: 20709345.
84. Li Z, Pogany J, Panavas T, Xu K, Esposito AM, Kinzy TG, et al. Translation elongation factor 1A is a component of the tombusvirus replicase complex and affects the stability of the p33 replication co-factor. *Virology.* 2009;385(1):245-60. Epub 2009/01/10. doi: 10.1016/j.virol.2008.11.041. PubMed PMID: 19131084; PubMed Central PMCID: PMCPMC2785496.
85. Gancarz BL, Hao L, He Q, Newton MA, Ahlquist P. Systematic identification of novel, essential host genes affecting bromovirus RNA replication. *PLoS One.* 2011;6(8):e23988. Epub 2011/09/15. doi: 10.1371/journal.pone.0023988. PubMed PMID: 21915247; PubMed Central PMCID: PMCPMC3161824.
86. Li J, Fuchs S, Zhang J, Wellford S, Schuldiner M, Wang X. An unrecognized function for COPII components in recruiting the viral replication protein BMV 1a to the perinuclear ER. *J Cell Sci.* 2016;129(19):3597-608. Epub 2016/08/20. doi: 10.1242/jcs.190082. PubMed PMID: 27539921.
87. Zhu J, Gopinath K, Murali A, Yi G, Hayward SD, Zhu H, et al. RNA-binding proteins that inhibit RNA virus infection. *Proc Natl Acad Sci U S A.* 2007;104(9):3129-34. Epub 2007/03/16. doi: 10.1073/pnas.0611617104. PubMed PMID: 17360619; PubMed Central PMCID: PMCPMC1805585.
88. Wu CY, Nagy PD. Blocking tombusvirus replication through the antiviral functions of DDX17-like RH30 DEAD-box helicase. *PLoS Pathog.* 2019;15(5):e1007771. Epub 2019/05/29. doi: 10.1371/journal.ppat.1007771. PubMed PMID: 31136641; PubMed Central PMCID: PMCPMC6555533.
89. Nagy PD. Host protein chaperones, RNA helicases and the ubiquitin network highlight the arms race for resources between tombusviruses and their hosts. *Adv*

- Virus Res. 2020;107:133-58. Epub 2020/07/28. doi: 10.1016/bs.aivir.2020.06.006. PubMed PMID: 32711728; PubMed Central PMCID: PMCPMC7342006.
90. Uetz P, Giot L, Cagney G, Mansfield TA, Judson RS, Knight JR, et al. A comprehensive analysis of protein-protein interactions in *Saccharomyces cerevisiae*. *Nature*. 2000;403(6770):623-7. Epub 2000/02/25. doi: 10.1038/35001009. PubMed PMID: 10688190.
 91. Ito T, Chiba T, Ozawa R, Yoshida M, Hattori M, Sakaki Y. A comprehensive two-hybrid analysis to explore the yeast protein interactome. *Proc Natl Acad Sci U S A*. 2001;98(8):4569-74. Epub 2001/04/03. doi: 10.1073/pnas.061034498. PubMed PMID: 11283351; PubMed Central PMCID: PMCPMC31875.
 92. Krogan NJ, Cagney G, Yu H, Zhong G, Guo X, Ignatchenko A, et al. Global landscape of protein complexes in the yeast *Saccharomyces cerevisiae*. *Nature*. 2006;440(7084):637-43. Epub 2006/03/24. doi: 10.1038/nature04670. PubMed PMID: 16554755.
 93. Gavin AC, Aloy P, Grandi P, Krause R, Boesche M, Marzioch M, et al. Proteome survey reveals modularity of the yeast cell machinery. *Nature*. 2006;440(7084):631-6. Epub 2006/01/24. doi: 10.1038/nature04532. PubMed PMID: 16429126.
 94. Raman K. Construction and analysis of protein-protein interaction networks. *Autom Exp*. 2010;2(1):2. Epub 2010/03/26. doi: 10.1186/1759-4499-2-2. PubMed PMID: 20334628; PubMed Central PMCID: PMCPMC2834675.
 95. Hakes L, Pinney JW, Robertson DL, Lovell SC. Protein-protein interaction networks and biology--what's the connection? *Nat Biotechnol*. 2008;26(1):69-72. Epub 2008/01/10. doi: 10.1038/nbt0108-69. PubMed PMID: 18183023.
 96. Xia J, Benner MJ, Hancock RE. NetworkAnalyst--integrative approaches for protein-protein interaction network analysis and visual exploration. *Nucleic Acids Res*. 2014;42(Web Server issue):W167-74. Epub 2014/05/28. doi: 10.1093/nar/gku443. PubMed PMID: 24861621; PubMed Central PMCID: PMCPMC4086107.
 97. Koh GC, Porras P, Aranda B, Hermjakob H, Orchard SE. Analyzing protein-protein interaction networks. *J Proteome Res*. 2012;11(4):2014-31. Epub 2012/03/06. doi: 10.1021/pr201211w. PubMed PMID: 22385417.
 98. De Las Rivas J, Fontanillo C. Protein-protein interactions essentials: key concepts to building and analyzing interactome networks. *PLoS Comput Biol*. 2010;6(6):e1000807. Epub 2010/07/01. doi: 10.1371/journal.pcbi.1000807. PubMed PMID: 20589078; PubMed Central PMCID: PMCPMC2891586.
 99. Serva S, Nagy PD. Proteomics analysis of the tombusvirus replicase: Hsp70 molecular chaperone is associated with the replicase and enhances viral RNA replication. *J Virol*. 2006;80(5):2162-9. Epub 2006/02/14. doi: 10.1128/JVI.80.5.2162-2169.2006. PubMed PMID: 16474124; PubMed Central PMCID: PMCPMC1395393.
 100. Cherry JM, Hong EL, Amundsen C, Balakrishnan R, Binkley G, Chan ET, et al. *Saccharomyces Genome Database: the genomics resource of budding yeast*. *Nucleic Acids Res*. 2012;40(Database issue):D700-5. Epub 2011/11/24. doi: 10.1093/nar/gkr1029. PubMed PMID: 22110037; PubMed Central PMCID: PMCPMC3245034.

101. Oughtred R, Rust J, Chang C, Breitkreutz BJ, Stark C, Willems A, et al. The BioGRID database: A comprehensive biomedical resource of curated protein, genetic, and chemical interactions. *Protein Sci.* 2021;30(1):187-200. Epub 2020/10/19. doi: 10.1002/pro.3978. PubMed PMID: 33070389; PubMed Central PMCID: PMC7737760.
102. Shannon P, Markiel A, Ozier O, Baliga NS, Wang JT, Ramage D, et al. Cytoscape: a software environment for integrated models of biomolecular interaction networks. *Genome Res.* 2003;13(11):2498-504. Epub 2003/11/05. doi: 10.1101/gr.1239303. PubMed PMID: 14597658; PubMed Central PMCID: PMC403769.
103. Costanzo M, VanderSluis B, Koch EN, Baryshnikova A, Pons C, Tan G, et al. A global genetic interaction network maps a wiring diagram of cellular function. *Science.* 2016;353(6306). Epub 2016/10/07. doi: 10.1126/science.aaf1420. PubMed PMID: 27708008; PubMed Central PMCID: PMC45661885.
104. Cheng CP, Serviene E, Nagy PD. Suppression of viral RNA recombination by a host exoribonuclease. *J Virol.* 2006;80(6):2631-40. Epub 2006/02/28. doi: 10.1128/JVI.80.6.2631-2640.2006. PubMed PMID: 16501073; PubMed Central PMCID: PMC1395426.
105. Catania S, Allshire RC. Anarchic centromeres: deciphering order from apparent chaos. *Curr Opin Cell Biol.* 2014;26:41-50. Epub 2014/02/18. doi: 10.1016/j.ceb.2013.09.004. PubMed PMID: 24529245; PubMed Central PMCID: PMC3978670.
106. Zeitlin SG. Centromeres: the wild west of the post-genomic age. *Epigenetics.* 2010;5(1):34-40. Epub 2010/01/23. doi: 10.4161/epi.5.1.10629. PubMed PMID: 20093854.
107. Belov GA, van Kuppeveld FJ. (+)RNA viruses rewire cellular pathways to build replication organelles. *Curr Opin Virol.* 2012;2(6):740-7. Epub 2012/10/06. doi: 10.1016/j.coviro.2012.09.006. PubMed PMID: 23036609; PubMed Central PMCID: PMC37102821.
108. Neufeldt CJ, Cortese M, Acosta EG, Bartenschlager R. Rewiring cellular networks by members of the Flaviviridae family. *Nat Rev Microbiol.* 2018;16(3):125-42. Epub 2018/02/13. doi: 10.1038/nrmicro.2017.170. PubMed PMID: 29430005; PubMed Central PMCID: PMC57097628.
109. Shulla A, Randall G. (+) RNA virus replication compartments: a safe home for (most) viral replication. *Curr Opin Microbiol.* 2016;32:82-8. Epub 2016/06/03. doi: 10.1016/j.mib.2016.05.003. PubMed PMID: 27253151; PubMed Central PMCID: PMC4983521.
110. Li Z, Nagy PD. Diverse roles of host RNA binding proteins in RNA virus replication. *RNA Biol.* 2011;8(2):305-15. Epub 2011/04/21. doi: 10.4161/rna.8.2.15391. PubMed PMID: 21505273; PubMed Central PMCID: PMC3230553.
111. Nagy PD, Pogany J. Global genomics and proteomics approaches to identify host factors as targets to induce resistance against Tomato bushy stunt virus. *Adv Virus Res.* 2010;76:123-77. Epub 2010/10/23. doi: 10.1016/S0065-3527(10)76004-8. PubMed PMID: 20965073; PubMed Central PMCID: PMC3173251.
112. Nagy PD, Wang RY, Pogany J, Hafren A, Makinen K. Emerging picture of host chaperone and cyclophilin roles in RNA virus replication. *Virology.*

- 2011;411(2):374-82. Epub 2011/02/08. doi: 10.1016/j.virol.2010.12.061. PubMed PMID: 21295323.
113. Nagy PD. Exploitation of a surrogate host, *Saccharomyces cerevisiae*, to identify cellular targets and develop novel antiviral approaches. *Curr Opin Virol.* 2017;26:132-40. Epub 2017/08/27. doi: 10.1016/j.coviro.2017.07.031. PubMed PMID: 28843111.
 114. Pogany J, Nagy PD. Activation of Tomato Bushy Stunt Virus RNA-Dependent RNA Polymerase by Cellular Heat Shock Protein 70 Is Enhanced by Phospholipids In Vitro. *J Virol.* 2015;89(10):5714-23. Epub 2015/03/13. doi: 10.1128/JVI.03711-14. PubMed PMID: 25762742; PubMed Central PMCID: PMC4442504.
 115. Inaba JI, Xu K, Kovalev N, Ramanathan H, Roy CR, Lindenbach BD, et al. Screening *Legionella* effectors for antiviral effects reveals Rab1 GTPase as a proviral factor coopted for tombusvirus replication. *Proc Natl Acad Sci U S A.* 2019;116(43):21739-47. Epub 2019/10/09. doi: 10.1073/pnas.1911108116. PubMed PMID: 31591191; PubMed Central PMCID: PMC6815150.
 116. Sasvari Z, Kovalev N, Gonzalez PA, Xu K, Nagy PD. Assembly-hub function of ER-localized SNARE proteins in biogenesis of tombusvirus replication compartment. *PLoS Pathog.* 2018;14(5):e1007028. Epub 2018/05/11. doi: 10.1371/journal.ppat.1007028. PubMed PMID: 29746582; PubMed Central PMCID: PMC5963807.
 117. Sasvari Z, Lin W, Inaba JI, Xu K, Kovalev N, Nagy PD. Co-opted Cellular Sac1 Lipid Phosphatase and PI(4)P Phosphoinositide Are Key Host Factors during the Biogenesis of the Tombusvirus Replication Compartment. *J Virol.* 2020;94(12). Epub 2020/04/10. doi: 10.1128/JVI.01979-19. PubMed PMID: 32269127; PubMed Central PMCID: PMC7307105.
 118. Nagy PD, Pogany J, Lin JY. How yeast can be used as a genetic platform to explore virus-host interactions: from 'omics' to functional studies. *Trends Microbiol.* 2014;22(6):309-16. Epub 2014/03/22. doi: 10.1016/j.tim.2014.02.003. PubMed PMID: 24647076.
 119. Huang TS, Nagy PD. Direct inhibition of tombusvirus plus-strand RNA synthesis by a dominant negative mutant of a host metabolic enzyme, glyceraldehyde-3-phosphate dehydrogenase, in yeast and plants. *J Virol.* 2011;85(17):9090-102. Epub 2011/06/24. doi: 10.1128/JVI.00666-11. PubMed PMID: 21697488; PubMed Central PMCID: PMC3165801.
 120. Sasvari Z, Izotova L, Kinzy TG, Nagy PD. Synergistic roles of eukaryotic translation elongation factors 1Bgamma and 1A in stimulation of tombusvirus minus-strand synthesis. *PLoS Pathog.* 2011;7(12):e1002438. Epub 2011/12/24. doi: 10.1371/journal.ppat.1002438. PubMed PMID: 22194687; PubMed Central PMCID: PMC3240602.
 121. Wang RY, Nagy PD. Tomato bushy stunt virus co-opts the RNA-binding function of a host metabolic enzyme for viral genomic RNA synthesis. *Cell Host Microbe.* 2008;3(3):178-87. Epub 2008/03/11. doi: 10.1016/j.chom.2008.02.005. PubMed PMID: 18329617.
 122. Pogany J, Stork J, Li Z, Nagy PD. In vitro assembly of the Tomato bushy stunt virus replicase requires the host Heat shock protein 70. *Proc Natl Acad Sci U S A.*

- 2008;105(50):19956-61. Epub 2008/12/09. doi: 10.1073/pnas.0810851105. PubMed PMID: 19060219; PubMed Central PMCID: PMCPMC2604936.
123. Wang RY, Stork J, Nagy PD. A key role for heat shock protein 70 in the localization and insertion of tombusvirus replication proteins to intracellular membranes. *J Virol.* 2009;83(7):3276-87. Epub 2009/01/21. doi: 10.1128/JVI.02313-08. PubMed PMID: 19153242; PubMed Central PMCID: PMCPMC2655559.
 124. Barajas D, Martin IF, Pogany J, Risco C, Nagy PD. Noncanonical role for the host Vps4 AAA+ ATPase ESCRT protein in the formation of Tomato bushy stunt virus replicase. *PLoS Pathog.* 2014;10(4):e1004087. Epub 2014/04/26. doi: 10.1371/journal.ppat.1004087. PubMed PMID: 24763736; PubMed Central PMCID: PMCPMC3999190.
 125. Chuang C, Barajas D, Qin J, Nagy PD. Inactivation of the host lipin gene accelerates RNA virus replication through viral exploitation of the expanded endoplasmic reticulum membrane. *PLoS Pathog.* 2014;10(2):e1003944. Epub 2014/03/04. doi: 10.1371/journal.ppat.1003944. PubMed PMID: 24586157; PubMed Central PMCID: PMCPMC3930575.
 126. Sharma M, Sasvari Z, Nagy PD. Inhibition of sterol biosynthesis reduces tombusvirus replication in yeast and plants. *J Virol.* 2010;84(5):2270-81. Epub 2009/12/18. doi: 10.1128/JVI.02003-09. PubMed PMID: 20015981; PubMed Central PMCID: PMCPMC2820916.
 127. Sharma M, Sasvari Z, Nagy PD. Inhibition of phospholipid biosynthesis decreases the activity of the tombusvirus replicase and alters the subcellular localization of replication proteins. *Virology.* 2011;415(2):141-52. Epub 2011/05/13. doi: 10.1016/j.virol.2011.04.008. PubMed PMID: 21561636; PubMed Central PMCID: PMCPMC3107895.
 128. Xu K, Nagy PD. RNA virus replication depends on enrichment of phosphatidylethanolamine at replication sites in subcellular membranes. *Proc Natl Acad Sci U S A.* 2015;112(14):E1782-91. Epub 2015/03/27. doi: 10.1073/pnas.1418971112. PubMed PMID: 25810252; PubMed Central PMCID: PMCPMC4394249.
 129. Pitzalis N, Heinlein M. The roles of membranes and associated cytoskeleton in plant virus replication and cell-to-cell movement. *J Exp Bot.* 2017;69(1):117-32. Epub 2017/10/17. doi: 10.1093/jxb/erx334. PubMed PMID: 29036578.
 130. Schneider R, Persson S. Connecting two arrays: the emerging role of actin-microtubule cross-linking motor proteins. *Front Plant Sci.* 2015;6:415. Epub 2015/06/18. doi: 10.3389/fpls.2015.00415. PubMed PMID: 26082793; PubMed Central PMCID: PMCPMC4451249.
 131. Petrasek J, Schwarzerova K. Actin and microtubule cytoskeleton interactions. *Curr Opin Plant Biol.* 2009;12(6):728-34. Epub 2009/10/27. doi: 10.1016/j.pbi.2009.09.010. PubMed PMID: 19854097.
 132. Becker BE, Cassimeris L. Cytoskeleton: microtubules born on the run. *Curr Biol.* 2005;15(14):R551-4. Epub 2005/07/30. doi: 10.1016/j.cub.2005.07.006. PubMed PMID: 16051163.
 133. Roll-Mecak A. Intrinsically disordered tubulin tails: complex tuners of microtubule functions? *Semin Cell Dev Biol.* 2015;37:11-9. Epub 2014/10/14. doi:

- 10.1016/j.semcdb.2014.09.026. PubMed PMID: 25307498; PubMed Central PMCID: PMCPMC7060838.
134. Frederick RL, Shaw JM. Moving mitochondria: establishing distribution of an essential organelle. *Traffic*. 2007;8(12):1668-75. Epub 2007/10/20. doi: 10.1111/j.1600-0854.2007.00644.x. PubMed PMID: 17944806; PubMed Central PMCID: PMCPMC3739988.
 135. Horio T, Murata T. The role of dynamic instability in microtubule organization. *Front Plant Sci*. 2014;5:511. Epub 2014/10/24. doi: 10.3389/fpls.2014.00511. PubMed PMID: 25339962; PubMed Central PMCID: PMCPMC4188131.
 136. Bratman SV, Chang F. Mechanisms for maintaining microtubule bundles. *Trends Cell Biol*. 2008;18(12):580-6. Epub 2008/10/28. doi: 10.1016/j.tcb.2008.09.004. PubMed PMID: 18951798.
 137. Howard J, Hyman AA. Microtubule polymerases and depolymerases. *Curr Opin Cell Biol*. 2007;19(1):31-5. Epub 2006/12/23. doi: 10.1016/j.ceb.2006.12.009. PubMed PMID: 17184986.
 138. Zhao J, Lendahl U, Nister M. Regulation of mitochondrial dynamics: convergences and divergences between yeast and vertebrates. *Cell Mol Life Sci*. 2013;70(6):951-76. Epub 2012/07/19. doi: 10.1007/s00018-012-1066-6. PubMed PMID: 22806564; PubMed Central PMCID: PMCPMC3578726.
 139. Li Z, Vizeacoumar FJ, Bahr S, Li J, Warringer J, Vizeacoumar FS, et al. Systematic exploration of essential yeast gene function with temperature-sensitive mutants. *Nat Biotechnol*. 2011;29(4):361-7. Epub 2011/03/29. doi: 10.1038/nbt.1832. PubMed PMID: 21441928; PubMed Central PMCID: PMCPMC3286520.
 140. Gupta ML, Jr., Bode CJ, Dougherty CA, Marquez RT, Himes RH. Mutagenesis of beta-tubulin cysteine residues in *Saccharomyces cerevisiae*: mutation of cysteine 354 results in cold-stable microtubules. *Cell Motil Cytoskeleton*. 2001;49(2):67-77. Epub 2001/07/10. doi: 10.1002/cm.1021. PubMed PMID: 11443737.
 141. Gupta ML, Jr., Bode CJ, Thrower DA, Pearson CG, Suprenant KA, Bloom KS, et al. beta-Tubulin C354 mutations that severely decrease microtubule dynamics do not prevent nuclear migration in yeast. *Mol Biol Cell*. 2002;13(8):2919-32. Epub 2002/08/16. doi: 10.1091/mbc.e02-01-0003. PubMed PMID: 12181356; PubMed Central PMCID: PMCPMC117952.
 142. Beh CT, Cool L, Phillips J, Rine J. Overlapping functions of the yeast oxysterol-binding protein homologues. *Genetics*. 2001;157(3):1117-40. Epub 2001/03/10. PubMed PMID: 11238399; PubMed Central PMCID: PMCPMC1461579.
 143. Janke C, Magiera MM, Rathfelder N, Taxis C, Reber S, Maekawa H, et al. A versatile toolbox for PCR-based tagging of yeast genes: new fluorescent proteins, more markers and promoter substitution cassettes. *Yeast*. 2004;21(11):947-62. Epub 2004/08/31. doi: 10.1002/yea.1142. PubMed PMID: 15334558.
 144. Kovalev N, Nagy PD. Cyclophilin A binds to the viral RNA and replication proteins, resulting in inhibition of tombusviral replicase assembly. *J Virol*. 2013;87(24):13330-42. Epub 2013/10/04. doi: 10.1128/JVI.02101-13. PubMed PMID: 24089553; PubMed Central PMCID: PMCPMC3838255.
 145. Sasvari Z, Gonzalez PA, Rachubinski RA, Nagy PD. Tombusvirus replication depends on Sec39p endoplasmic reticulum-associated transport protein. *Virology*.

- 2013;447(1-2):21-31. Epub 2013/11/12. doi: 10.1016/j.virol.2013.07.039. PubMed PMID: 24210096.
146. Chakrabarty R, Banerjee R, Chung SM, Farman M, Citovsky V, Hogenhout SA, et al. PSITE vectors for stable integration or transient expression of autofluorescent protein fusions in plants: probing *Nicotiana benthamiana*-virus interactions. *Mol Plant Microbe Interact*. 2007;20(7):740-50. Epub 2007/07/03. doi: 10.1094/MPMI-20-7-0740. PubMed PMID: 17601162.
 147. Dinesh-Kumar SP, Anandalakshmi R, Marathe R, Schiff M, Liu Y. Virus-induced gene silencing. *Methods Mol Biol*. 2003;236:287-94. Epub 2003/09/23. doi: 10.1385/1-59259-413-1:287. PubMed PMID: 14501071.
 148. Gietz RD, Woods RA. Transformation of yeast by lithium acetate/single-stranded carrier DNA/polyethylene glycol method. *Methods Enzymol*. 2002;350:87-96. Epub 2002/06/21. doi: 10.1016/s0076-6879(02)50957-5. PubMed PMID: 12073338.
 149. Barajas D, Li Z, Nagy PD. The Nedd4-type Rsp5p ubiquitin ligase inhibits tombusvirus replication by regulating degradation of the p92 replication protein and decreasing the activity of the tombusvirus replicase. *J Virol*. 2009;83(22):11751-64. Epub 2009/09/18. doi: 10.1128/JVI.00789-09. PubMed PMID: 19759160; PubMed Central PMCID: PMCPMC2772669.
 150. Panaviene Z, Baker JM, Nagy PD. The overlapping RNA-binding domains of p33 and p92 replicase proteins are essential for tombusvirus replication. *Virology*. 2003;308(1):191-205. Epub 2003/04/23. doi: 10.1016/s0042-6822(02)00132-0. PubMed PMID: 12706102.
 151. Nagy PD, Pogany J, Simon AE. In vivo and in vitro characterization of an RNA replication enhancer in a satellite RNA associated with turnip crinkle virus. *Virology*. 2001;288(2):315-24. Epub 2001/10/17. doi: 10.1006/viro.2001.1099. PubMed PMID: 11601903.
 152. Kong Q, Wang J, Simon AE. Satellite RNA-mediated resistance to turnip crinkle virus in *Arabidopsis* involves a reduction in virus movement. *Plant Cell*. 1997;9(11):2051-63. Epub 1997/12/24. doi: 10.1105/tpc.9.11.2051. PubMed PMID: 9401127; PubMed Central PMCID: PMCPMC157057.
 153. Kovalev N, Pogany J, Nagy PD. A Co-Opted DEAD-Box RNA helicase enhances tombusvirus plus-strand synthesis. *PLoS Pathog*. 2012;8(2):e1002537. Epub 2012/02/24. doi: 10.1371/journal.ppat.1002537. PubMed PMID: 22359508; PubMed Central PMCID: PMCPMC3280988.
 154. Jaag HM, Nagy PD. Silencing of *Nicotiana benthamiana* Xrn4p exoribonuclease promotes tombusvirus RNA accumulation and recombination. *Virology*. 2009;386(2):344-52. Epub 2009/02/24. doi: 10.1016/j.virol.2009.01.015. PubMed PMID: 19232421.
 155. Martin K, Kopperud K, Chakrabarty R, Banerjee R, Brooks R, Goodin MM. Transient expression in *Nicotiana benthamiana* fluorescent marker lines provides enhanced definition of protein localization, movement and interactions in planta. *Plant J*. 2009;59(1):150-62. Epub 2009/03/25. doi: 10.1111/j.1365-313X.2009.03850.x. PubMed PMID: 19309457.
 156. Kost B, Spielhofer P, Chua NH. A GFP-mouse talin fusion protein labels plant actin filaments in vivo and visualizes the actin cytoskeleton in growing pollen tubes.

- Plant J. 1998;16(3):393-401. Epub 1999/01/09. doi: 10.1046/j.1365-313x.1998.00304.x. PubMed PMID: 9881160.
157. Lopez-Fanarraga M, Avila J, Guasch A, Coll M, Zabala JC. Review: postchaperonin tubulin folding cofactors and their role in microtubule dynamics. *J Struct Biol.* 2001;135(2):219-29. Epub 2001/10/03. doi: 10.1006/jsbi.2001.4386. PubMed PMID: 11580271.
158. Weber-Lotfi F, Dietrich A, Russo M, Rubino L. Mitochondrial targeting and membrane anchoring of a viral replicase in plant and yeast cells. *J Virol.* 2002;76(20):10485-96. Epub 2002/09/20. doi: 10.1128/jvi.76.20.10485-10496.2002. PubMed PMID: 12239325; PubMed Central PMCID: PMC136569.
159. Vasquez RJ, Howell B, Yvon AM, Wadsworth P, Cassimeris L. Nanomolar concentrations of nocodazole alter microtubule dynamic instability in vivo and in vitro. *Mol Biol Cell.* 1997;8(6):973-85. Epub 1997/06/01. doi: 10.1091/mbc.8.6.973. PubMed PMID: 9201709; PubMed Central PMCID: PMC1305707.
160. Diffley JF, Bousset K, Labib K, Noton EA, Santocanale C, Tercero JA. Coping with and recovering from hydroxyurea-induced replication fork arrest in budding yeast. *Cold Spring Harb Symp Quant Biol.* 2000;65:333-42. Epub 2003/05/23. doi: 10.1101/sqb.2000.65.333. PubMed PMID: 12760047.
161. Morejohn LC, Bureau TE, Mole-Bajer J, Bajer AS, Fosket DE. Oryzalin, a dinitroaniline herbicide, binds to plant tubulin and inhibits microtubule polymerization in vitro. *Planta.* 1987;172(2):252-64. Epub 1987/10/01. doi: 10.1007/BF00394595. PubMed PMID: 24225878.
162. Langhans M, Niemes S, Pimpl P, Robinson DG. Oryzalin bodies: in addition to its anti-microtubule properties, the dinitroaniline herbicide oryzalin causes nodulation of the endoplasmic reticulum. *Protoplasma.* 2009;236(1-4):73-84. Epub 2009/06/27. doi: 10.1007/s00709-009-0059-2. PubMed PMID: 19557498.
163. McCartney AW, Greenwood JS, Fabian MR, White KA, Mullen RT. Localization of the tomato bushy stunt virus replication protein p33 reveals a peroxisome-to-endoplasmic reticulum sorting pathway. *Plant Cell.* 2005;17(12):3513-31. Epub 2005/11/15. doi: 10.1105/tpc.105.036350. PubMed PMID: 16284309; PubMed Central PMCID: PMC1315385.
164. Pathak KB, Sasvari Z, Nagy PD. The host Pex19p plays a role in peroxisomal localization of tombusvirus replication proteins. *Virology.* 2008;379(2):294-305. Epub 2008/08/08. doi: 10.1016/j.virol.2008.06.044. PubMed PMID: 18684480.
165. Lin JY, Mendu V, Pogany J, Qin J, Nagy PD. The TPR domain in the host Cyp40-like cyclophilin binds to the viral replication protein and inhibits the assembly of the tombusviral replicase. *PLoS Pathog.* 2012;8(2):e1002491. Epub 2012/02/22. doi: 10.1371/journal.ppat.1002491. PubMed PMID: 22346747; PubMed Central PMCID: PMC3276564.
166. Dogterom M, Koenderink GH. Actin-microtubule crosstalk in cell biology. *Nat Rev Mol Cell Biol.* 2019;20(1):38-54. Epub 2018/10/17. doi: 10.1038/s41580-018-0067-1. PubMed PMID: 30323238.
167. Takeuchi M, Karahara I, Kajimura N, Takaoka A, Murata K, Misaki K, et al. Single microfilaments mediate the early steps of microtubule bundling during preprophase

- band formation in onion cotyledon epidermal cells. *Mol Biol Cell*. 2016;27(11):1809-20. Epub 2016/04/08. doi: 10.1091/mbc.E15-12-0820. PubMed PMID: 27053663; PubMed Central PMCID: PMC4884071.
168. Kovalev N, Pogany J, Nagy PD. Reconstitution of an RNA Virus Replicase in Artificial Giant Unilamellar Vesicles Supports Full Replication and Provides Protection for the Double-Stranded RNA Replication Intermediate. *J Virol*. 2020;94(18). Epub 2020/07/10. doi: 10.1128/JVI.00267-20. PubMed PMID: 32641477; PubMed Central PMCID: PMC7459549.
 169. Xu K, Nagy PD. Sterol Binding by the Tombusviral Replication Proteins Is Essential for Replication in Yeast and Plants. *J Virol*. 2017;91(7). Epub 2017/01/20. doi: 10.1128/JVI.01984-16. PubMed PMID: 28100609; PubMed Central PMCID: PMC5355592.
 170. Mesmin B, Bigay J, Moser von Filseck J, Lacas-Gervais S, Drin G, Antonny B. A four-step cycle driven by PI(4)P hydrolysis directs sterol/PI(4)P exchange by the ER-Golgi tether OSBP. *Cell*. 2013;155(4):830-43. Epub 2013/11/12. doi: 10.1016/j.cell.2013.09.056. PubMed PMID: 24209621.
 171. Stefan CJ, Manford AG, Baird D, Yamada-Hanff J, Mao Y, Emr SD. Osh proteins regulate phosphoinositide metabolism at ER-plasma membrane contact sites. *Cell*. 2011;144(3):389-401. Epub 2011/02/08. doi: 10.1016/j.cell.2010.12.034. PubMed PMID: 21295699.
 172. Wang P, Hawkins TJ, Richardson C, Cummins I, Deeks MJ, Sparkes I, et al. The plant cytoskeleton, NET3C, and VAP27 mediate the link between the plasma membrane and endoplasmic reticulum. *Curr Biol*. 2014;24(12):1397-405. Epub 2014/06/10. doi: 10.1016/j.cub.2014.05.003. PubMed PMID: 24909329.
 173. Imura Y, Molho M, Chuang C, Nagy PD. Cellular Ubc2/Rad6 E2 ubiquitin-conjugating enzyme facilitates tombusvirus replication in yeast and plants. *Virology*. 2015;484:265-75. Epub 2015/07/03. doi: 10.1016/j.virol.2015.05.022. PubMed PMID: 26135843.
 174. de Wilde AH, Snijder EJ, Kikkert M, van Hemert MJ. Host Factors in Coronavirus Replication. *Curr Top Microbiol Immunol*. 2018;419:1-42. Epub 2017/06/24. doi: 10.1007/82_2017_25. PubMed PMID: 28643204; PubMed Central PMCID: PMC7119980.
 175. Sanfacon H. Plant Translation Factors and Virus Resistance. *Viruses*. 2015;7(7):3392-419. Epub 2015/06/27. doi: 10.3390/v7072778. PubMed PMID: 26114476; PubMed Central PMCID: PMC4517107.
 176. Shulla A, Randall G. Hepatitis C virus-host interactions, replication, and viral assembly. *Curr Opin Virol*. 2012;2(6):725-32. Epub 2012/10/23. doi: 10.1016/j.coviro.2012.09.013. PubMed PMID: 23083892; PubMed Central PMCID: PMC3508086.
 177. Lin W, Liu Y, Molho M, Zhang S, Wang L, Xie L, et al. Co-opting the fermentation pathway for tombusvirus replication: Compartmentalization of cellular metabolic pathways for rapid ATP generation. *PLoS Pathog*. 2019;15(10):e1008092. Epub 2019/10/28. doi: 10.1371/journal.ppat.1008092. PubMed PMID: 31648290; PubMed Central PMCID: PMC6830812.
 178. Wieland G, Orthaus S, Ohndorf S, Diekmann S, Hemmerich P. Functional complementation of human centromere protein A (CENP-A) by Cse4p from

- Saccharomyces cerevisiae*. *Mol Cell Biol*. 2004;24(15):6620-30. Epub 2004/07/16. doi: 10.1128/MCB.24.15.6620-6630.2004. PubMed PMID: 15254229; PubMed Central PMCID: PMC444843.
179. Quenet D, Dalal Y. A long non-coding RNA is required for targeting centromeric protein A to the human centromere. *Elife*. 2014;3:e03254. Epub 2014/08/15. doi: 10.7554/eLife.03254. PubMed PMID: 25117489; PubMed Central PMCID: PMC4145801.
 180. Earnshaw WC. Discovering centromere proteins: from cold white hands to the A, B, C of CENPs. *Nat Rev Mol Cell Biol*. 2015;16(7):443-9. Epub 2015/05/21. doi: 10.1038/nrm4001. PubMed PMID: 25991376.
 181. Stellfox ME, Bailey AO, Foltz DR. Putting CENP-A in its place. *Cell Mol Life Sci*. 2013;70(3):387-406. Epub 2012/06/26. doi: 10.1007/s00018-012-1048-8. PubMed PMID: 22729156; PubMed Central PMCID: PMC4084702.
 182. Chuang C, Prasanth KR, Nagy PD. Coordinated function of cellular DEAD-box helicases in suppression of viral RNA recombination and maintenance of viral genome integrity. *PLoS Pathog*. 2015;11(2):e1004680. Epub 2015/02/19. doi: 10.1371/journal.ppat.1004680. PubMed PMID: 25693185; PubMed Central PMCID: PMC4333740.
 183. Ranjitkar P, Press MO, Yi X, Baker R, MacCoss MJ, Biggins S. An E3 ubiquitin ligase prevents ectopic localization of the centromeric histone H3 variant via the centromere targeting domain. *Mol Cell*. 2010;40(3):455-64. Epub 2010/11/13. doi: 10.1016/j.molcel.2010.09.025. PubMed PMID: 21070971; PubMed Central PMCID: PMC2995698.
 184. Goodin MM, Dietzgen RG, Schichnes D, Ruzin S, Jackson AO. pGD vectors: versatile tools for the expression of green and red fluorescent protein fusions in agroinfiltrated plant leaves. *Plant J*. 2002;31(3):375-83. Epub 2002/08/08. doi: 10.1046/j.1365-313x.2002.01360.x. PubMed PMID: 12164816.
 185. Chuang C, Prasanth KR, Nagy PD. The Glycolytic Pyruvate Kinase Is Recruited Directly into the Viral Replicase Complex to Generate ATP for RNA Synthesis. *Cell Host Microbe*. 2017;22(5):639-52 e7. Epub 2017/11/07. doi: 10.1016/j.chom.2017.10.004. PubMed PMID: 29107644.
 186. Rajendran KS, Nagy PD. Characterization of the RNA-binding domains in the replicase proteins of tomato bushy stunt virus. *J Virol*. 2003;77(17):9244-58. Epub 2003/08/14. doi: 10.1128/jvi.77.17.9244-9258.2003. PubMed PMID: 12915540; PubMed Central PMCID: PMC4187376.
 187. Imamura H, Nhat KP, Togawa H, Saito K, Iino R, Kato-Yamada Y, et al. Visualization of ATP levels inside single living cells with fluorescence resonance energy transfer-based genetically encoded indicators. *Proc Natl Acad Sci U S A*. 2009;106(37):15651-6. Epub 2009/09/02. doi: 10.1073/pnas.0904764106. PubMed PMID: 19720993; PubMed Central PMCID: PMC2735558.
 188. Stoler S, Keith KC, Curnick KE, Fitzgerald-Hayes M. A mutation in CSE4, an essential gene encoding a novel chromatin-associated protein in yeast, causes chromosome nondisjunction and cell cycle arrest at mitosis. *Genes Dev*. 1995;9(5):573-86. Epub 1995/03/01. doi: 10.1101/gad.9.5.573. PubMed PMID: 7698647.

189. Pogany J, Fabian MR, White KA, Nagy PD. A replication silencer element in a plus-strand RNA virus. *EMBO J.* 2003;22(20):5602-11. Epub 2003/10/09. doi: 10.1093/emboj/cdg523. PubMed PMID: 14532132; PubMed Central PMCID: PMCPMC213777.
190. Pathak KB, Pogany J, Nagy PD. Non-template functions of the viral RNA in plant RNA virus replication. *Curr Opin Virol.* 2011;1(5):332-8. Epub 2012/03/24. doi: 10.1016/j.coviro.2011.09.011. PubMed PMID: 22440835.
191. Morey L, Barnes K, Chen Y, Fitzgerald-Hayes M, Baker RE. The histone fold domain of Cse4 is sufficient for CEN targeting and propagation of active centromeres in budding yeast. *Eukaryot Cell.* 2004;3(6):1533-43. Epub 2004/12/14. doi: 10.1128/EC.3.6.1533-1543.2004. PubMed PMID: 15590827; PubMed Central PMCID: PMCPMC539035.
192. Lefrancois P, Euskirchen GM, Auerbach RK, Rozowsky J, Gibson T, Yellman CM, et al. Efficient yeast ChIP-Seq using multiplex short-read DNA sequencing. *BMC Genomics.* 2009;10:37. Epub 2009/01/23. doi: 10.1186/1471-2164-10-37. PubMed PMID: 19159457; PubMed Central PMCID: PMCPMC2656530.
193. Athwal RK, Walkiewicz MP, Baek S, Fu S, Bui M, Camps J, et al. CENP-A nucleosomes localize to transcription factor hotspots and subtelomeric sites in human cancer cells. *Epigenetics Chromatin.* 2015;8:2. Epub 2015/03/20. doi: 10.1186/1756-8935-8-2. PubMed PMID: 25788983; PubMed Central PMCID: PMCPMC4363203.
194. Hildebrand EM, Biggins S. Regulation of Budding Yeast CENP-A levels Prevents Misincorporation at Promoter Nucleosomes and Transcriptional Defects. *PLoS Genet.* 2016;12(3):e1005930. Epub 2016/03/18. doi: 10.1371/journal.pgen.1005930. PubMed PMID: 26982580; PubMed Central PMCID: PMCPMC4794243.
195. Prasanth KR, Chuang C, Nagy PD. Co-opting ATP-generating glycolytic enzyme PGK1 phosphoglycerate kinase facilitates the assembly of viral replicase complexes. *PLoS Pathog.* 2017;13(10):e1006689. Epub 2017/10/24. doi: 10.1371/journal.ppat.1006689. PubMed PMID: 29059239; PubMed Central PMCID: PMCPMC5695612.
196. Kovalev N, de Castro Martin IF, Pogany J, Barajas D, Pathak K, Risco C, et al. Role of Viral RNA and Co-opted Cellular ESCRT-I and ESCRT-III Factors in Formation of Tombusvirus Spherules Harboring the Tombusvirus Replicase. *J Virol.* 2016;90(7):3611-26. Epub 2016/01/23. doi: 10.1128/JVI.02775-15. PubMed PMID: 26792735; PubMed Central PMCID: PMCPMC4794697.
197. Liu L, Li Y, Zhang S, Yu D, Zhu M. Hepatitis B virus X protein mutant upregulates CENP-A expression in hepatoma cells. *Oncol Rep.* 2012;27(1):168-73. Epub 2011/10/01. doi: 10.3892/or.2011.1478. PubMed PMID: 21956590.
198. Himoto T, Tanaka N, Saito A, Muro Y, Sugiura K, Tani J, et al. Diversity of humoral responses to the centromere proteins among HCV-related chronic liver disease, PBC and AIH patients. *Clin Res Hepatol Gastroenterol.* 2015;39(2):222-9. Epub 2014/09/16. doi: 10.1016/j.clinre.2014.08.004. PubMed PMID: 25220385.
199. Qin S, Liu Y, Tempel W, Eram MS, Bian C, Liu K, et al. Structural basis for histone mimicry and hijacking of host proteins by influenza virus protein NS1. *Nat*

- Commun. 2014;5:3952. Epub 2014/05/24. doi: 10.1038/ncomms4952. PubMed PMID: 24853335.
200. Randall RE, Goodbourn S. Interferons and viruses: an interplay between induction, signalling, antiviral responses and virus countermeasures. *J Gen Virol.* 2008;89(Pt 1):1-47. Epub 2007/12/20. doi: 10.1099/vir.0.83391-0. PubMed PMID: 18089727.
201. Mandadi KK, Scholthof KB. Plant immune responses against viruses: how does a virus cause disease? *Plant Cell.* 2013;25(5):1489-505. Epub 2013/05/28. doi: 10.1105/tpc.113.111658. PubMed PMID: 23709626; PubMed Central PMCID: PMC3694688.

VITA

PAULINA ALATRISTE GONZÁLEZ

Education

2009 — 2013, B.S. in Genomic Sciences, National Autonomous University of Mexico, Cuernavaca, Morelos, Mexico

Awards and distinctions

2020 — Gabriela Jiskrova Award. UK Graduate Student Congress.

2020 — Recognition of Special Distinction, National Association of Graduate-Professional Students. For recognition of leadership and professional excellence in the service of graduate and professional students.

2019 — I.E Melhus Student Symposium Award. APS Foundation and I.E Melhus Graduate Student Symposium Fund.

2016 — Milt Zaitlin Student Travel Award. ASV Plant Virology Club.

2016 — Graduate Student Travel Award. UK Graduate School.

2011 — Gold Medal in iGEM Jamboree, North America Competition. “Hydrobium etli Project”. UNAM-Genomics Team, UNAM.

Publications

1. Sasvari, Z., Kovalev, N., **Alatrisme Gonzalez, P.**, Xu, K., Nagy, P.D. (2018). Assembly-hub function of ER-localized SNARE proteins in biogenesis of tombusvirus replication compartment. *PLoS Pathogens*. 14(5).
2. Tian, M., Sasvari, Z., **Alatrisme Gonzalez, P.**, Friso, G., Rowland, E., et al. (2015). Salicylic acid inhibits the replication of Tomato Bushy Stunt Virus by directly targeting a host component in the replication complex. *Mol. Plant Microbe Interact*. 28:379–86.
3. Li, Z., **Alatrisme Gonzalez, P.**, Sasvari, Z., Goss Kinzy, T. and Nagy, P.D. (2014). Methylation of translation elongation factor 1A by the METTL10-like See1 methyltransferase facilitates tombusvirus replication in yeast and plants. *Virology*. 448:43-54.
4. Sasvari, Z.*, **Alatrisme Gonzalez, P.*** and Nagy, P. (2014). Tombusvirus-Yeast Interactions Identify Conserved Cell-Intrinsic Viral Restriction Factors. *Front. Plant Sc*. 383:1-14. *authors contributed equally

5. Sasvari, Z., **Alariste Gonzalez, P.**, Rachubinski, R.A., and Nagy, P.D. (2013). Tombusvirus replication depends on Sec39p endoplasmic reticulum-associated transport protein. *Virology*. 447:21-31.